CONSTRUCTION MATERIALS CONSULTANTS, INC.

# Investigation of Pyrrhotite-Related Deterioration In Residential Concrete Foundations In Mansfield, Connecticut

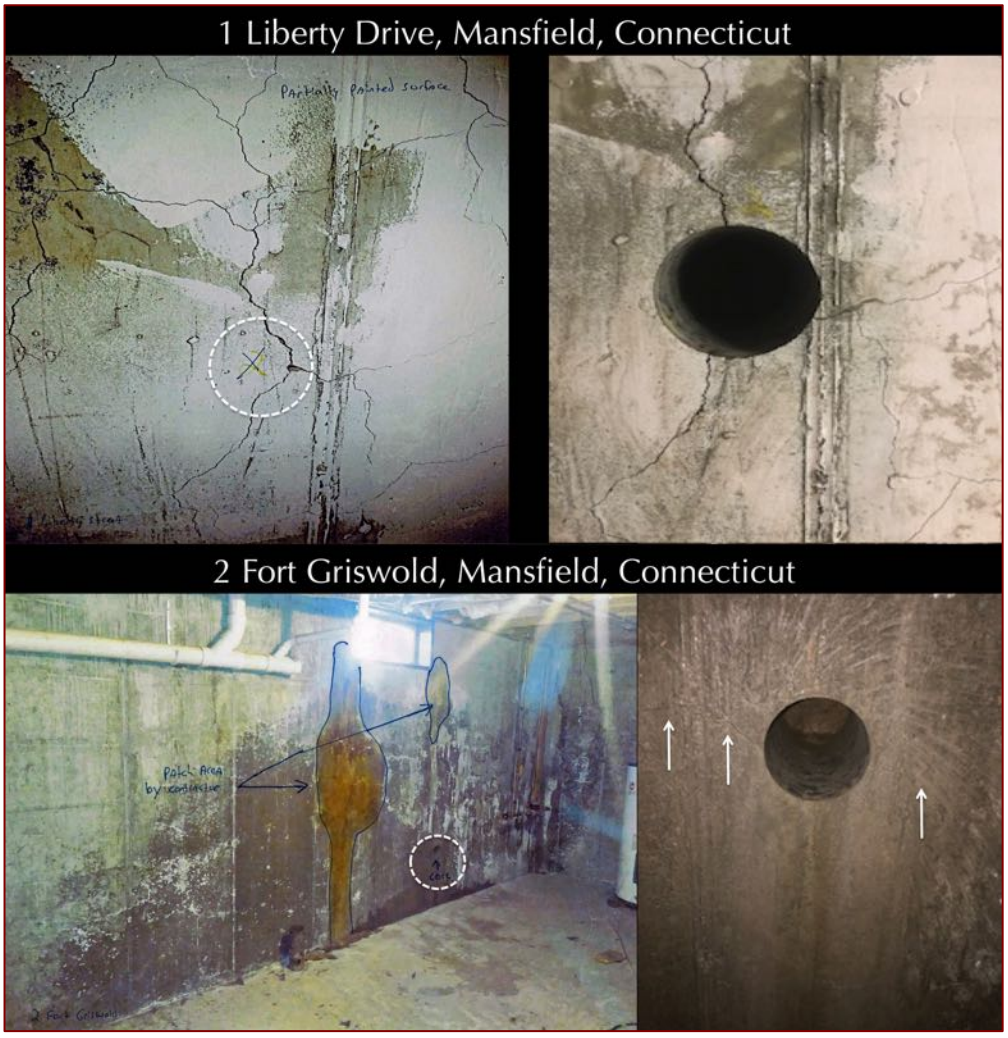


Villages At Freedom Green Condominium Association, Inc.
1 Liberty Drive and 2 Fort Griswold
Mansfield, Connecticut

May 31, 2019
CMC 0419120

## TABLE OF CONTENTS

## EXECUTIVE SUMMARY

Widespread outbreak of deterioration of many residential concrete foundations due to oxidation of an iron sulfide mineral 'pyrrhotite' in the quarried aggregate stones has occurred in the state of Connecticut with many thousands of homes being affected. Pyrrhotite (from Greek *pyrrhos* i.e. flame-colored or redness) commonly occurs in many mafic igneous, sedimentary, and metamorphic rocks, or in high temperature hydrothermal and replacement veins as a minor accessory mineral having a chemical formula of $Fe_{1-x}S$, where x varies from 0 to 0.125. It is commonly associated with pyrite ($FeS_2$) but is distinguished by its bronze rather than brass color of pyrite, its lower hardness, decomposition in HCl (Deer et al., 2008), lower S/Fe ratio, and weakly magnetic nature. All these features along with X-ray diffraction of rocks containing both iron sulfide minerals help to determine the pyrrhotite content, whereas XRF analysis of rocks determine the sulfur (as $SO_3$) content from all iron sulfide minerals. Currently, much of the information available on pyrrhotite-related concrete deterioration in northeastern Connecticut is limited to news media but the cause of deterioration has been attributed by an investigation conducted at the University of Connecticut (Wille and Zhong, 2016) and Jana (2017, 2018, 2019) as oxidation of pyrrhotite present in the coarse aggregate in the presence of moisture and oxygen in concrete. Manifestation of the damage has taken as much as 10 to 20 years. Typical visual deterioration is in the form of map cracking, some causing deformation of the wall, reddish-brown discoloration as rust stains, whitish formation of sodium sulfate salts (thenardite and mirabilite) in the vicinity of surface cracking, and in some severe cases crumbling of concrete. Most of the damage to date has been linked to aggregates supplied from one square-shaped quarry (Becker's quarry) in Willington, CT that sits in a weathered hydrothermal vein of metamorphic rocks containing significant pyrrhotite mineralization. The geology in the vicinity of the quarry is made up of metamorphic rocks predominately from two to three formations consisting predominantly of foliated schists and gneissic rock, granofels, and foliated quartz diorite. Quartz, plagioclase or oligoclase are primary minerals with micas, and noted are garnet and pyrrhotite as common accessory minerals. Most findings of concrete deterioration around the world due to pyrrhotite oxidation, including the ones in northeastern Connecticut (e.g., Moum and Rosenqvist 1959 from Norway, Tagnit-Hamou, et.al. 2005 and Rodrigues et al. 2012 from Canada, Oliveira, et al. 2014 from Spain, and Wille and Zhong, 2016 and Jana 2017, 2018, 2019 from USA) indicated the following two-stage mechanisms of distress due to: (a) primary expansions associated with oxidation of pyrrhotite in the presence of oxygen, moisture, and high pH in concrete to form ferric oxy-hydroxides, e.g., ferrihydrite [$Fe(OH)_3$] causing cracking of the unsound aggregates, followed by (b) secondary expansions from internal sulfate attacks by the sulfates released from pyrrhotite oxidation to cement hydration and carbonation products forming secondary ettringite and thaumasite, respectively causing further cracking in the paste. The former expansion is contributed from the pyrrhotite-bearing aggregates, whereas, the latter expansion is contributed from internal sulfate attacks within the confined spaces of the released sulfate-contaminated hydrated cement paste.

In light of this known problem of pyrrhotite in concrete aggregate from around the world, and particularly from the Becker's quarry in CT, and the resulting distress in many residential foundations in northeastern Connecticut, two concrete cores were collected from cracked foundation walls at 1 Liberty Drive and 2 Fort Griswold in Mansfield, Connecticut i.e. within the known area of 'pyrrhotite epidemic.' The cores were provided with the concern of: (a) whether or not the distressed concrete foundations contain pyrrhotite in their aggregate, and, if detected, (b) if pyrrhotite has played the role for cracking of concrete foundation, as in the case of other residential foundations from eastern Connecticut that have shown widespread cracking from pyrrhotite oxidation and resultant sulfate attacks in concretes.

Field photographs of the subject foundation walls showed extensive cracking either as a network of closed polygonal-shaped cracks at 1 Liberty Drive or parallel cracks often with intersecting ones at 2 Fort Griswold. Concrete cores were drilled over visible cracks on the foundation walls through the entire wall thickness. Laboratory investigations were conducted to determine the possible presence of pyrrhotite in concrete, and, its potentially deleterious role in concrete deterioration, if any. Pyrrhotite's possible presence along with overall condition of concretes and aggregates were examined by detailed petrographic examinations (optical microscopy) *a la* ASTM C 856, whereas possible roles of pyrrhotite, its potential oxidation products and sulfate levels, and microstructures of deteriorated concrete around pyrrhotite-bearing aggregates are examined by scanning electron microscopy and energy-dispersive X-ray microanalysis (SEM-EDS) of multiple thin sections of concretes (*a la* ASTM C 1723), X-ray diffraction (XRD) and X-ray fluorescence (XRF) of multiple pyrrhotite-bearing coarse aggregate particles extracted

from the concretes, and ion chromatography (IC *a la* ASTM D 4327) of extracted aggregate particles digested in a strong oxidant of 35% hydrogen peroxide solution in an accelerated oxidation test, then diluted in distilled water to determine levels of sulfates released by these aggregates in relation to a control aggregate without any iron sulfide mineral. Detection of pyrrhotite by optical microscopy, SEM-EDS, and XRD, along with detection of its oxidation products by SEM-EDS and XRD, reaction microstructures and evidence of distress by SEM-EDS, sulfate contamination of paste by SEM-EDS, and measurement of release of sulfate levels by IC provide a good assessment of potential role of pyrrhotite in causing oxidation-related cracking in the foundation walls.

Petrographic examinations have determined the concretes in both foundations to be compositionally similar having similar crushed gneiss coarse aggregates, which is a testament of their possible derivation from the same mix/supplier. Furthermore, the observed concrete compositions are similar to the other distressed concretes from eastern CT that were reportedly provided by JJ Mottes. The unsound pyrrhotite-bearing aggregates in the other distressed foundations were known to have been quarried from a hydrothermal vein in Becker's quarry situated in Willington, CT that has extensive pyrrhotite crystallization. Concretes in both cores are made using: (a) crushed gneiss coarse aggregates having nominal maximum sizes of $^{3}/_{4}$ in. (19 mm), (b) natural siliceous sand fine aggregates having nominal maximum sizes of $^{3}/_{8}$ in. (9.5 mm) and containing major amounts of quartz and quartzite, and subordinate amounts of feldspar, mica, ferruginous rock, and mafic minerals; (c) hardened pastes of Portland cement as the sole cementitious components having cement contents similar in both cores and estimated to be 6 to $6^{1}/_{2}$ bags per cubic yard, water-cement ratios (*w/c*) similar within the bodies in both cores, estimated to be 0.45 to 0.50, and (d) air contents estimated to be 6 to 8 percent; concretes in both cores are air-entrained. Overall compositions of concretes, including the crushed gneiss coarse aggregate particles present in the examined concretes are similar to concretes (containing similar crushed gneiss coarse aggregates) from other distressed foundations from eastern Connecticut that were examined by this laboratory and confirmed pyrrhotite-oxidation-related cracking.

Similar to other pyrrhotite-related cracking of residential foundations, along with numerous visible cracks, petrographic examinations of both cores have detected numerous microcracks in the foundation walls similar to the microcracks found in other distressed walls from the neighborhood that are diagnosed to be due to deleterious chemical reactions from pyrrhotite-oxidation. Extensive cracking of cores, especially the one from 1 Liberty Drive are not only evident when received, but also during subsequent examinations of lapped and saw-cut cross sections, especially after impregnating the cross sections with a fluorescent dye-mixed epoxy and viewed in ultraviolet light where many microcracks are readily revealed due to penetration of fluorescent epoxy into the cracks and then become highlighted in UV light. Many unsound crushed gneiss coarse aggregate particles in both cores showed internal cracking, many of which are due to oxidation of pyrrhotite in crushed gneiss coarse aggregates causing internal fracturing, parallel fine microcracking and disintegration of oxidized pyrrhotite grains, along with development of veins of oxidized iron within pyrrhotite matrix that are highlighted in Fe-O maps and corresponding depletions in S-maps of oxidized veins in SEM studies.

Petrographic examinations detected mixtures of three different color tones of gravel and crushed gravel coarse aggregate particles in the cores: (a) dominant dark gray to black gneiss consisting of parallel alignment of quartz, albite feldspar, biotite mica, and occasional pyrope garnet porphyroblasts, anhedral to subhedral equigranular to gneissose arrangement of minerals; (b) subordinate light to medium brown granite gneiss of quartz, albite feldspar, garnet, biotite mica and occasional pyroxene (augite) grains; and (c) minor white granite gneiss with quartzo-feldspathic minerals and black specs of mica flakes in parallel alternate (gneissose) arrangements. Brown and dark gray gneiss contain more iron sulfide and iron oxide minerals than the minor white granite gneiss. All particles are angular, dense, hard, and medium to dark gray to brown, gneissose-textured, equidimensional to elongated, variably altered, uncoated, and variably cracked. Coarse aggregate particles are well-graded and well-distributed. There is no evidence of alkali-aggregate reactions of coarse aggregates in concretes.

Similar to the predominant dark gray to brown pyrrhotite-bearing gneiss that have caused pyrrhotite oxidation and subsequent distress in other case studies, present study from both foundations also showed more dark gray to brown unsound pyrrhotite-bearing garnetiferous quartzo-feldspathic gneiss compared to lighter colored (white with black specs of mica) granite gneiss to contain disseminated unsound pyrrhotite to cause distress. Unlike other studies, however, pastes in the present concrete cores are free of any sulfate contamination released from pyrrhotite

oxidation. However, both cores showed profuse development of secondary ettringite in cracks, microcracks, voids, and pore spaces in paste due to the presence of moisture and sulfate from pyrrhotite oxidation during service.

XRD analyses of ten different dark gray and brown coarse aggregate particles extracted from the cores as well as XRD analysis of the bulk concretes of both cores showed mineralogical similarities to cores from many other distressed foundations, including the absence of any detectable pyrrhotite in XRD (despite its detection in optical microscopy and SEM-EDS) but the presence of ferrihydrite type iron hydroxide phase. Pyrrhotite grains were oxidized to ferrihydrite to be detected in XRD, however the amount of pyrrhotite and its oxidation product ferrihydrite may not have been enough to cause sufficient release of sulfates to cause sulfate contamination of paste except forming profuse secondary ettringite in voids, cracks, and porous areas of paste. XRF studies of dark gray and brown crushed gneiss coarse aggregates showed sulfate contents, probably due to variable pyrrhotite contents in these particles but the bulk concrete showed noticeable sulfate (as $SO_3$) in both cores, which is discussed later. Despite the absence of sulfate contamination in the paste to be noted in SEM-EDS studies and absence of detectable pyrrhotite in the concretes or extracted aggregates from XRD studies, the overall sulfate (as $SO_3$) contents of concretes in both foundations are very high, e.g., 2.37 percent in the core from 1 Liberty Drive and 2.74 percent in the core from 2 Fort Griswold. These concrete sulfate (as $SO_3$) contents are notably higher than sulfate contents typically found in a normal Portland cement concrete, e.g., 0.45 percent sulfate (as $SO_3$) with 3 percent sulfate (as $SO_3$) in Portland cement and 15 percent Portland cement by mass in concrete.

Microcracking within many pyrrhotite-bearing crushed gneiss coarse aggregates occurs due to pyrrhotite oxidation, which is often associated with reddish-brown oxidation products of pyrrhotite, and microcracks often extend from unsound aggregates to paste – this is the first microstructural evidence of distress due to primary expansion of unsound aggregate *per se* that are distinct in numerous photomicrographs of thin sections of concretes from other residential foundations of eastern Connecticut studied as well as in the present study. Detailed examinations of crushed gneiss coarse aggregate particles in the present cores, both from stereomicroscopical examination of lapped cross sections and petrographic microscopical examination of thin sections, have detected widespread occurrences of similar microcracking and associated reddish-brown oxidation product of pyrrhotite from oxidation and related distress to cause visible microcracking in concretes.

Petrographic examinations of distressed residential foundations in the present study as well as from other distressed homes of eastern Connecticut have also detected abundant secondary ettringite crystallization lining or filling many air voids and occasionally lining some microcracks that are indicative of prolonged presence of moisture in concretes during service, which is an essential pre-requisite for pyrrhotite oxidation. Presence of moisture also indicates availability of sulfates to be released from pyrrhotite-oxidation and for subsequent ettringite crystallization, which, however, may or may not have necessarily derived from pyrrhotite oxidation since ettringite-filled air-voids are a very common microstructural feature in a concrete exposed to moisture without even any iron sulfide contaminant. Any Portland cement concrete exposed to moisture during service forms secondary ettringite deposits lining and filling air voids. To establish the source of secondary ettringite i.e. from Portland cement's sulfate and/or from oxidation of pyrrhotite-bearing aggregates require determination of sulfate levels in concrete i.e. if the level is higher than that expected from a typical Portland cement concrete where sulfate (as $SO_3$) content in cement is around 3 weight percent i.e. giving about 0.45 percent sulfate in concrete for a usual cement content of 15 percent by mass of a normal weight concrete. Excess sulfate in concrete above 0.45 percent from cement's contribution would then correspond to the pyrrhotite-aggregate source if no other sulfate source were present. To determine the sulfate ($SO_3$) level of bulk concrete, thin slices of concretes were sectioned through the entire lengths of the cores traversing the full thickness of the foundation walls and pulverized for XRF analysis, which, as mentioned, showed 2.37 percent in the core from 1 Liberty Drive and 2.74 percent in the core from 2 Fort Griswold, which are significantly higher than the sulfates normally contributed from Portland cement. Clearly, the observed sulfate contents of present concretes indicate a sulfate source other than Portland cement, which is determined to be numerous disseminated pyrrhotite inclusions in coarse aggregates. Consistent with above observation, petrographic examinations of paste in the present cores detected potentially deleterious secondary ettringite, as found in other distressed foundations, indicating again that moisture, the essential ingredient for release of sulfate from pyrrhotite to the paste was present for the present concretes during service in the respective foundations.

Therefore, similar to other pyrrhotite-oxidation-related cracking in residential foundations from eastern Connecticut, examined cores have shown microstructural evidence of (a) primary expansion of concrete due to oxidation of pyrrhotite in crushed gneiss coarse aggregate to cause cracking within the unsound aggregate particles or their extension into paste, and (b) secondary expansion of paste due to formation of poorly crystalline (perhaps also colloidal formed) secondary ettringite in relatively confined areas in paste along with voids, cracks and porous areas causing further expansion and associated cracking.

In accelerated pyrrhotite oxidation test, multiple crushed gneiss coarse aggregate particles were extracted from the cores, cleaned of adhered paste remains, crushed, then immersed in a 35% hydrogen peroxide (strong oxidant) solution for 10 days. Sulfates released from aggregates to the filtrates were measured (as $SO_4^{-2}$) in an anion exchange chromatograph. All particles showed noticeable release of sulfates from aggregates and concretes as opposed to no sulfate release from a control gneiss aggregate containing no pyrrhotite indicating the potential for continued sulfate release in the field during service in prolonged presence of moisture.

Case studies on pyrrhotite-oxidation-related distress of concrete foundations from eastern Connecticut by the present laboratory have confirmed and provided clear mechanisms of the common consensus that the observed cracking and reported crumbling of many concrete foundation walls in eastern Connecticut are due to: (a) oxidation of pyrrhotite in crushed garnetiferous quartzo-feldspathic gneiss coarse aggregate particles *in the presence of oxygen and moisture during service in concrete* with the formation of ferrihydrite causing expansion of the unsound aggregates and formation of cracks from unsound aggregates to paste, which was then followed by (b) additional expansion in the paste from reactions between sulfates released from pyrrhotite oxidation and cement hydration products (internal sulfate attack) and formation of poorly crystalline or perhaps colloidal ettringite within the confined spaces in paste. The present examined concrete cores provided similar evidence of pyrrhotite-oxidation-related distress and its manifestation as cracking indicating moisture, the essential ingredient for pyrrhotite-oxidation and subsequent internal sulfate attack of concrete, was present in foundation walls during service.

Visible and invisible cracking in the present foundations and evidence of pyrrhotite-oxidation-related distress confirms: (a) source of coarse aggregates of present concretes possibly from the Becker's quarry, which has produced unsound aggregates for other distressed foundations, and (b) presence of moisture in these foundations during service. Perhaps slow uptake of moisture through the wall from the ground could have initiated pyrrhotite oxidation and resultant cracking, which is similar in other residential foundations of eastern Connecticut that have shown distress after 10 to 20 years of construction, the time period within which the present foundations reportedly fall.

In summary: concretes from two foundations at 1 Liberty Drive and 2 Fort Griswold have not only confirmed the presence of disseminated pyrrhotite inclusions in crushed gneiss coarse aggregates but also evidence of pyrrhotite-oxidation-related cracking. Crushed gneiss coarse aggregates are similar to the ones from other distressed foundations in having a greater proportion of dark gray and brown granite gneiss than the white gneiss where the former two gneiss types contained noticeable disseminated pyrrhotite inclusions as in other pyrrhotite-bearing dark gray and brown gneiss quarried from the hydrothermal vein of pyrrhotite crystallization in the Becker's quarry in Willington, CT that has provided the unsound aggregate for other distressed foundations. Extensive macro and micro cracking in foundations are testament of deleterious pyrrhotite oxidation. Very high sulfate (as $SO_3$) contents of concretes (as high as 2.7% $SO_3$) compared to 0.45% $SO_3$ in normal Portland cement concretes indicates additional sulfate sources beside Portland cement, which is confirmed to be from pyrrhotite in aggregates. XRD studies did not detect pyrrhotite in concretes or extracted coarse aggregates but the oxidation product ferrihydrite is detected, which is in conformance to optical microscopy, SEM-EDs and other studies. SEM-EDS studies have failed to detect any sulfate contamination in the paste, which occurs from sulfates released from pyrrhotite oxidation. However, optical microscopy and SEM-EDS studies both detected many deleterious secondary ettringite formation in paste, voids, and cracks, which (along with high total sulfate in concretes) are testament of additional sulfate sources beyond cement, from pyrrhotite with expansion and cracking from pyrrhotite oxidation. Ion chromatography of crushed gneiss coarse aggregates extracted from concretes showed potential release of sulfate in a highly oxidizing solution of hydrogen peroxide, indicating a similar potential release of sulfate in the field in prolonged oxidizing condition from the presence of moisture. This indicates role of prolonged presence of moisture and moisture penetration through existing cracks in foundations to sustain pyrrhotite oxidation and continued distress.

## INTRODUCTION

Reported herein are the results of detailed laboratory studies of two hardened concrete cores reportedly retrieved from concrete foundation walls in Freedom Green Condominium Complex from residences at 1 Liberty Drive and 2 Fort Griswold in Mansfield, Connecticut. Both foundation walls have shown numerous visible cracks as seen in Figures 1 and 2. Due to the proximity of the condominium in an area that is known to show cracking in foundation walls from the presence of an iron sulfide mineral, pyrrhotite, in coarse aggregate, the purpose of this investigation is to examine the cores for the possible presence of pyrrhotite, and pyrrhotite-related distress in concrete. Since both cores were retrieved from over visible cracks in the respective foundation walls as seen in Figures 1 and 2, the cause(s) of cracking, e.g., whether due to oxidation of pyrrhotite was also investigated.

## BACKGROUND INFORMATION

The subject residences in the condominium were reportedly constructed in 1990s, which falls within the time period when many other residential foundations constructed across eastern Connecticut have shown pyrrhotite-oxidation-related distress in concrete, especially during the paste 5 years. It has been reported that pyrrhotite in concrete has been identified in a different building within the same condo association.

## FIELD PHOTOGRAPHS

Figure 1 shows the visibly cracked foundation wall at 1 Liberty Drive where a network of closed polygonal-shaped cracks are seen. Also show in Figure 1 is the location at the intersection of radial cracks from where the core for the present study was retrieved. The core was taken from a center position of the wall about halfway above the floor.

Figure 2 shows the visibly cracked foundation wall at 2 Fort Griswold where many parallel and intersecting cracks are seen as opposed to closed polygonal-shaped cracks found in the foundation wall at 1 Liberty Drive. Extent of cracking is reported to be more at the 1 Liberty Drive foundation than the 2 Fort Griswold foundation. Field photos in Figure 2 shows an area on the wall that has received repair patch. The core was taken from near the floor over a visible crack on the wall.

Therefore, both cores were taken from over visible cracks on the walls. When received, both cores show maximum cracking in the interior portion than the two opposite ends indicating similar cracking in the walls mostly concentrated within the interior of the walls than the end surfaces.


Figure 1: Field photographs of concrete foundation at 1 Liberty Drive showing extensive cracking of the foundation wall, overall closed polygonal-shaped pattern of many visible cracks, and location of the core for the present study retrieved from over visible radial cracks. Notice extension of the crack across the wall thickness at the core hole in the bottom photos, which is more clearly shown in the photos of the core when received in the laboratory.

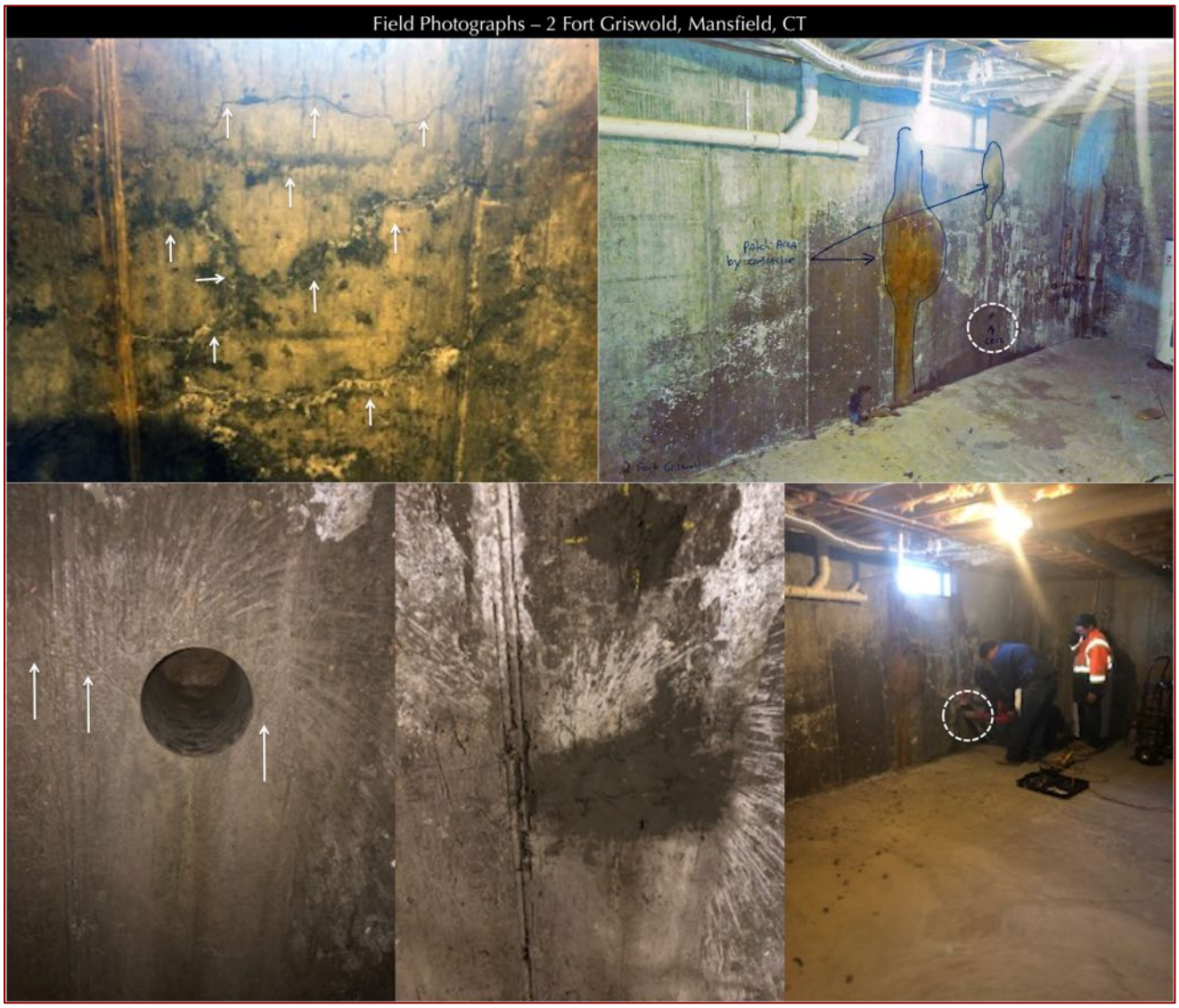


Figure 2: Field photographs of concrete foundation at 2 Fort Griswold showing extensive cracking of the foundation wall and location of the core for the present study retrieved from over a visible crack.

## PURPOSES OF PRESENT INVESTIGATION

Based on the background information provided, the purposes of the present investigation are to determine:

a. Compositions, qualities, and overall conditions of concrete in the walls as represented by the cores; and particularly
b. Detection of any possible physical or chemical deterioration of concrete that may have contributed to the observed cracking of the foundation walls; and,
c. Detection of unsound pyrrhotite grains in concrete aggregates, and, if present whether or not pyrrhotite grains have caused the visible cracking in the foundation walls due to its known deleterious effects on durability of concrete from other studies in the region.

## METHODOLOGIES

### OPTICAL MICROSCOPY (FOR OVERALL CONDITION OF CONCRETE AND AGGREGATES)

The cores were tested and examined by following the methods of ASTM C 856 "Standard Practice for Petrographic Examination of Hardened Concrete." Details of petrographic examinations and sample preparation are described in Jana (2006). The steps of petrographic examinations include (Jana 2006):

i. Visual examinations of the cores, as received to trace all visible cracks, if any;
ii. Low-power stereomicroscopical examinations of as-received, saw-cut and freshly fractured sections, and lapped cross sections of cores for evaluation of concrete composition, condition, extent of cracking (if any), detection of iron sulfide minerals, etc.;
iii. Low-power stereomicroscopical examinations of air contents and air-void systems of concretes as well as detection of iron sulfide minerals (amount and distribution) in the lapped cross sections;
iv. Examinations of oil immersion mounts in a petrographic microscope for mineralogical compositions of specific areas of interest;
v. Examinations of un-treated and fluorescent-dye-mixed (to highlight open spaces, cracks, etc.) epoxy-impregnated treated lapped cross sections of concretes in a stereomicroscope for detailed compositional and microstructural analyses;
vi. Examinations of fluorescent dye-mixed (to highlight open spaces, cracks, etc.) epoxy-impregnated large area (50 mm × 75 mm) thin sections of concretes in a stereomicroscope and in a petrographic microscope for detailed compositional and microstructural analyses;
vii. Photographing samples as received, and during preparation with a digital camera and a flatbed scanner;
viii. Photomicrographs of full-length lapped cross sections and thin sections of cores taken with stereomicroscope and petrographic microscope, respectively to provide detailed compositional, microstructural, and mineralogical information of concrete;
ix. Detailed compositional, mineralogical, and microstructural examinations of concretes in a petrographic microscope from thin sections;
x. Selection of areas of interest in the thin sections for subsequent examinations in scanning electron microscope;
xi. A Nikon Eclipse 600 POL petrographic microscope attached to a Jenoptik Progres GRYPHAX high-resolution digital camera were used for petrographic examinations and collecting photomicrographs of thin sections of concretes (Figure 3). A Nikon SMZ-10A stereomicroscope (Figure 3) and an Olympus SZH stereo zoom microscope (equipped with transmitted polarizing light facilities) were used for examinations of fresh fractured and lapped sections and transmitted-light examinations of thin sections, respectively.


Figure 3: Optical Microscopy: Left - A Nikon Eclipse E600 POL polarizing (petrographic) microscope at left with reflected, transmitted, polarized-light, and fluorescent-light capabilities; Middle – An Olympus SZH reflected/transmitted/polarized-light Stereozoom microscope; and Right – A Nikon SMZ-10A Stereozoom microscope. All microscopes are equipped with Jenoptik Gryphax and Lumenera Infinity digital cameras.

## X-RAY DIFFRACTION (FOR MINERALOGY OF UNSOUND AGGREGATE, IDENTIFICATION OF IRON SULFIDE PHASES & THEIR OXIDATION PRODUCTS)

A few crushed stone coarse aggregate particles containing metallic-lustered iron sulfide minerals (as detected from the cores as received, and from lapped cross sections) were extracted from the cores, pulverized, and used for X-ray diffraction to determine the iron sulfide species (e.g., pyrite, pyrrhotite) present in the aggregates.


Figure 4: XRD: Siemens D5000 X-ray diffractometer and MDI Jade search/match software used for determination of mineralogical compositions of extracted concrete aggregates. Left to right: Rocklab pulverizer for initial grinding of aggregate with anhydrous alcohol; McCrone micronizing mill for final grinding; Spex 25-ton press for pellet preparation; Siemens D5000 X-ray diffractometer; and custom-made sample holder to place a 32-mm diameter pellet on sample stage.

A Rocklab pulverizer was used to grind the extracted aggregate particles down to finer than 100 microns. Usually, a few drops of anhydrous alcohol are added to reduce decomposition of any hydrous phases from the heat generated from grinding. Approximately 10 grams of sample was ground first in the Rockland pulverizer, from which about 8.0 grams of sample was selected, mixed with three binder tablets (total binder weight of 0.6 grams, for a fixed binder proportion of 7.5%), the mixture is then further ground in Rocklab pulverizer and in a McCrone micronizing mill down to finer than 44 micron size. Approximately 7.0 grams of binder-mixed pulverized sample thus prepared was weighed into a stainless steel die to prepare the sample pellet. A 25-ton Spex X-press was used to prepare 32 mm pellet from the pulverized sample. The same pellet is used for XRD to determine the mineralogy and XRF to determine the chemical composition.

X-ray diffraction was carried out in a Siemens D5000 Powder diffractometer (θ-2θ goniometer, Figure 4) employing a long line focus Cu X-ray tube, divergent and anti-scatter slits fixed at 1 mm, a receiving slit (0.6 mm), diffracted and incident beam Soller slits (0.04 rad), a curved graphite diffracted beam monochromator, and a sealed proportional counter. Generator settings used are 40 kV and 30mA. Sample was placed in a custom-made circular sample holder and excited with the copper radiation of 1.54 angstroms. Tests were scanned at 2θ from 4° to 64° with a step of 0.02° 2θ integrated at 1 sec. step$^{-1}$ dwell time.

The resulting diffraction patterns were collected by DataScan 4 software of Materials Data, Inc. (MDI), analyzed by Jade software of MDI with ICDD PDF-4 (Minerals 2017) diffraction data. Phase identification, and quantitative analyses were carried out with MDI's Search/Match, Easy Quant, and Rietveld modules, respectively.

## SCANNING ELECTRON MICROSCOPY AND ENERGY-DISPERSIVE X-RAY SPECTROSCOPY (SEM-EDS) (FOR MICROSTRUCTURE & COMPOSITION OF DETERIORATED CONCRETE & UNSOUND AGGREGATE)

Products of oxidation of iron sulfide minerals, if present, and associated possible secondary ettringite/thaumasite reaction products and reaction microstructures were examined in detail by SEM-EDS. Procedures for SEM examinations are described in ASTM C 1723.

Polished and gold-palladium coated thin sections of cores already examined by optical microscopy were selected for SEM-EDS studies and examined in a Cambridge CamScan Series II scanning electron microscope equipped with a backscatter detector, a secondary electron detector, and x-ray fluorescence spectrometer (Figure 5) to observe pyrrhotite or other potentially unsound constituents in concretes and aggregates and their effect on the performance and durability of concretes, as well as evidence of internal sulfate attacks and secondary ettringite formation in the paste from released sulfates.


Figure 5: SEM-EDS: Cambridge CamScan Series II Scanning Electron Microscope and 4Pi Revolution software, backscatter detector, secondary electron detector, and energy-dispersive X-ray fluorescence spectrometer used for microstructural and microchemical analyses of concretes and aggregates.

## ENERGY-DISPERSIVE X-RAY FLUORESCENCE SPECTROSCOPY (ED-XRF) (FOR OXIDE COMPOSITION & SULFUR ($SO_3$) LEVEL OF UNSOUND AGGREGATE & CONCRETE)

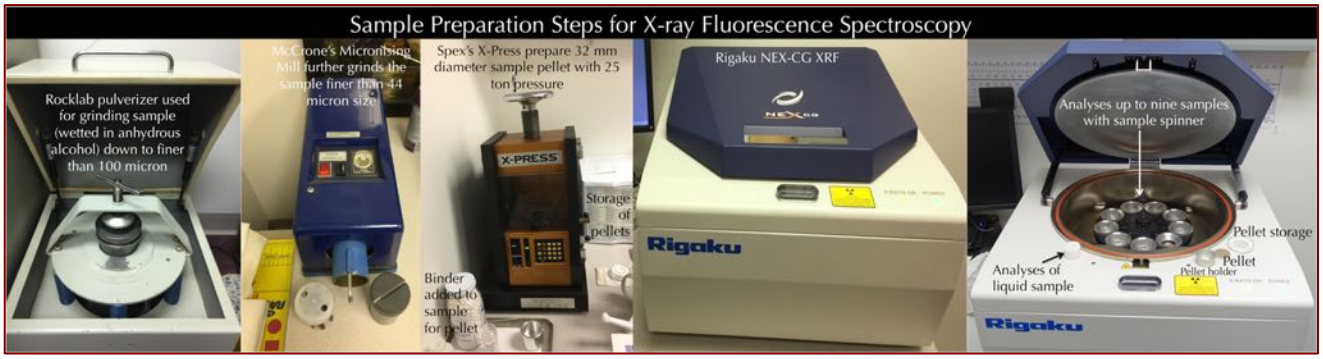


Figure 6: XRF: Rigaku NEX-CG bench-top ED-XRF unit used for bulk chemical compositions of aggregates.

An energy-dispersive bench-top X-ray fluorescence unit from Rigaku Americas Corporation (NEX-CG, Figure 6) was used for determination of bulk chemical (oxide) compositions and sulfur (as $SO_3$) contents of unsound aggregate

particles, and concretes from both cores. The instrument is calibrated by using various certified (CCRL, NIST, GSA, and Brammer) reference standards of rocks. The sample pellet prepared for X-ray diffraction is used for X-ray fluorescence studies as well. The main focus of this analysis was to determine the sulfur contents (as $SO_3$) in the aggregate particles as well as sulfate contents (as $SO_3$) in concretes.

## ION CHROMATOGRAPHY (FOR RELEASED SULFATES FROM UNSOUND AGGREGATES)

In order to investigate sulfate-leaching capacity of pyrrhotite in coarse aggregates to cause internal sulfate attack in paste, aliquots of pulverized pyrrhotite-bearing coarse aggregate particles extracted from the cores and studied for XRD and XRF were digested in a hydrogen peroxide (35%) solution for ten days for accelerated oxidation, then filtered through 2.5-micron and 0.2-micron micro-filter papers under vacuum. The filtrates were then diluted to 100 mL with distilled water to be analyzed by Metrohm's 861 Advanced Ion Chromatograph (Figure 7) for determination of released sulfates from oxidation of sulfides.

Procedures followed in Ion chromatography are described in ASTM D 4327 "Standard Test Method for Anions in Water by Chemically Suppressed Ion Chromatography." The IC was calibrated against six (6) different custom-made Metrohm anion standard solutions having sulfate from 0.1-ppm to 100-ppm levels.

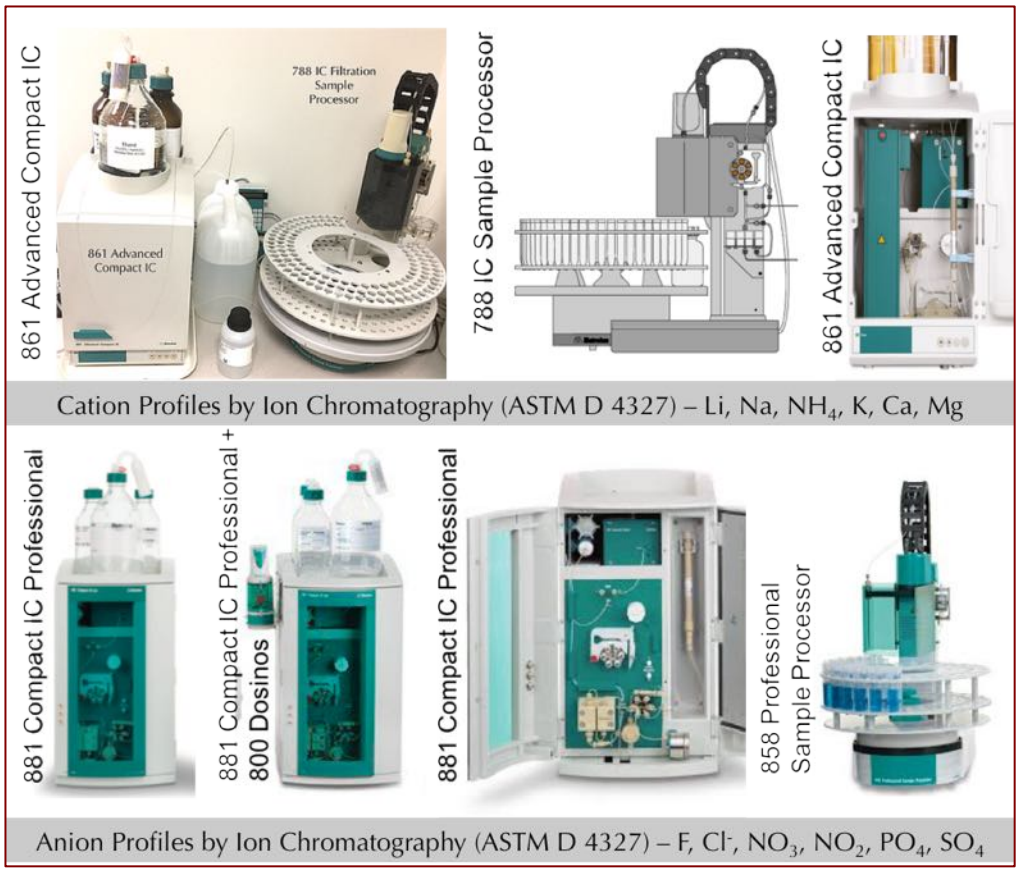


Figure 7: Set ups of Metrohm ion chromatography units for analysis of water-soluble anions in concretes and concrete aggregates. Cations were not measured.

## SAMPLES

### PHOTOGRAPHS, IDENTIFICATION, INTEGRITY, AND DIMENSIONS

Figures 8 and 9 show the cores from the foundation walls of 1 Liberty Drive and 2 Fort Griswold, respectively, as received. Since the cores were retrieved from over visible cracks in the walls, the cracks show full-depth extensions in the cores from the interior to the opposite exterior ends mostly concentrated within the bodies of the cores than at the ends. The cores are $10^{1}/_{4}$ in. (260 mm) and 10 in. (250 mm) in total lengths representing thicknesses of foundation walls at 1 Liberty Drive and 2 Fort Griswold, respectively, and $3^{1}/_{2}$ in. (95 mm) in nominal diameters.

### END SURFACES

Both cores show visible cracks on their ends representing interior exposed surfaces of foundation walls, and absence of cracking on the opposite ends, which are the exterior surfaces of walls.

### CRACKING & OTHER VISIBLE DISTRESS

Both cores were taken from over visible cracks on the interior surfaces of foundation walls hence showed cracking at their interior surface ends, but more cracking in the interior bodies and lack of cracking at the opposite exterior surface ends of walls. Cracks are oriented perpendicular to the interior exposed surfaces and extended to distances of 1.5 in. from the interior surfaces in both cores, and then many parallel cracks through the entire length of the cores mostly concentrated in the interior bodies. Cracks have transected and circumscribed the coarse and fine aggregate particles along their paths. There are no joints or large voids present in the cores.

### EMBEDDED ITEMS

There is no evidence of any fibers, wire mesh, reinforcing steel or other embedded items found in the cores.

### TESTING STRATEGY

After detailed photographs and preliminary descriptions, the cores were sectioned longitudinally into multiple slabs by using an oil-cooled diamond saw. Slabs thus sectioned were used for various purposes, e.g. (1) preparation of lapped cross sections for observations in a stereo-zoom microscope by successively grinding the slabs in water-cooled metal and resin-bonded diamond lapping disc, (3) impregnating a slab with fluorescent epoxy to examine a lapped section in ultraviolet light for voids, pore spaces, and microcracks in concrete, (4) trimming a slab for preparation of thin sections for observations in a petrographic microscope and scanning electron microscope, (5) pulverizing a slab and its aggregates for chemical analysis by X-ray fluorescence, and mineralogical analysis by X-ray diffraction, and (6) ion chromatography of aggregates for sulfate-leaching capability.


Figure 8: Shown are: (a) the black formed exterior surface of the foundation wall on the core end in the top left photo, (b) smooth, flat, gray formed interior surface of the foundation wall with visible cracks on the core end in the top right photo, and cylindrical side views of the core from 1 Liberty Drive (rest photos), as received, showing full-depth extension of numerous visible cracks due to retrieval of the core from over visible cracks on the wall. Visible cracks on cylindrical surface of core are highlighted, which are mostly concentrated in the interior of the core (wall) than the interior or exterior ends.


Figure 9: Shown are: (a) the formed exterior surface of the foundation wall on the core end in the top right photo, (b) smooth, flat, gray formed interior surface of the foundation wall with visible cracks on the core end in the top left photo, and cylindrical side views of the core from 2 Fort Griswold (rest photos), as received, showing full-depth extension of numerous visible cracks due to retrieval of the core from over visible cracks on the wall. Visible cracks on cylindrical surface of core are highlighted, which are mostly concentrated in the interior of the core (wall) than the interior or exterior ends. Interior wall has a vertical crack extended to a distance of 1.5 in. inside the core. Notice this core from 2 Fort Griswold residence has less visible cracks in the interior than that from 1 Liberty Drive.

## LABORATORY STUDIES

### SAW-CUT CROSS SECTIONS


Figure 10: Multiple saw-cut cross sections of the core from 1 Liberty Drive showing: (a) full-depth extension of visible cracks that are highlighted in red (mostly concentrated in the inside of the core); (b) beige discoloration of paste at the interior end of the wall (at the top) and also at the exterior end (bottom) that are marked with black dashed lines at the top, where beige discoloration is due to atmospheric carbonation of concrete during service, mostly occurred along the interior wall surface (to a distance of 20 to 25 mm) than from the exterior end (only 5 mm). Notice a vertical crack from the interior end (at the top) extended to a distance of 1.5 in.

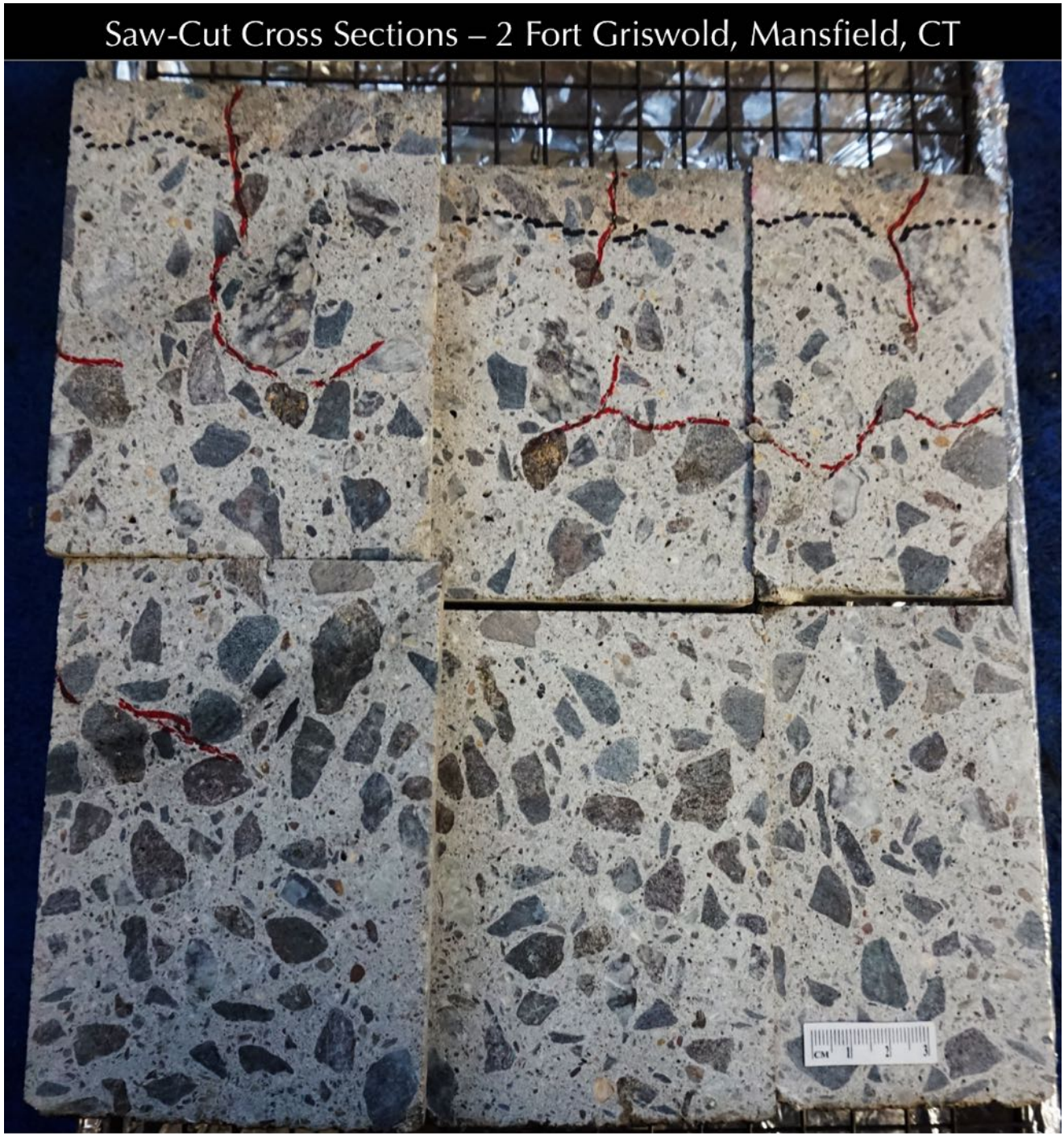


Figure 11: Multiple saw-cut cross sections of the core from 2 Fort Griswold showing: (a) full-depth extension of visible cracks that are highlighted in red (mostly concentrated in the inside of the core); (b) beige discoloration of paste at the interior end of the wall (at the top) and also at the exterior end (bottom) that are marked with black dashed lines at the top, where beige discoloration is due to atmospheric carbonation of concrete during service, mostly occurred along the interior wall surface (to a distance of 20 to 25 mm) than from the exterior end (only 5 mm). Notice a vertical crack from the interior end (at the top) extended to a distance of 1.5 in. Notice this core from 2 Fort Griswold residence has less visible cracks in the interior than that from 1 Liberty Drive.

## LAPPED CROSS SECTIONS

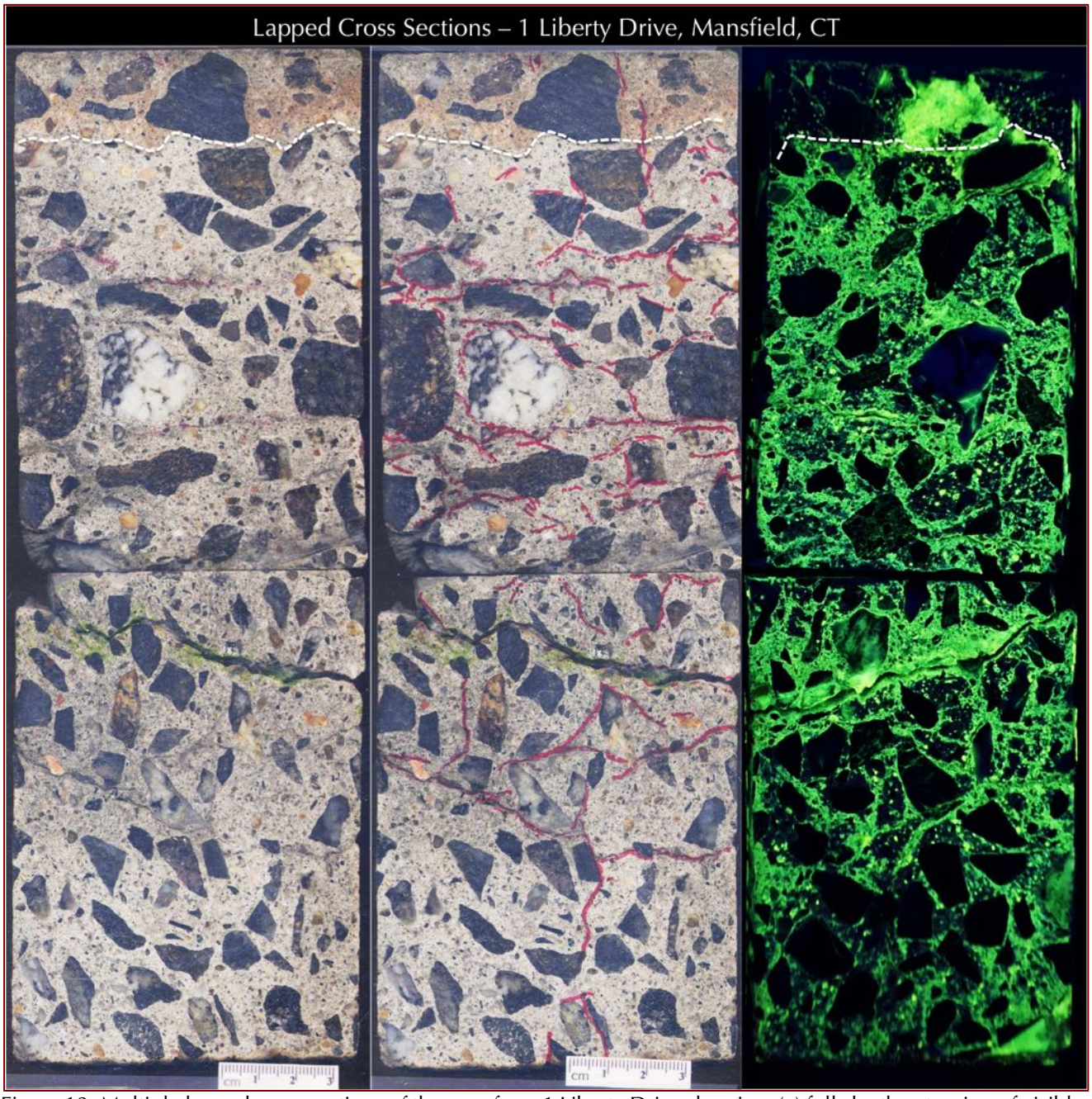


Figure 12: Multiple lapped cross sections of the core from 1 Liberty Drive showing: (a) full-depth extension of visible cracks that are highlighted in red in the middle column (mostly concentrated in the inside of the core); (b) beige discoloration of paste at the interior end of the wall (at the top) and also at the exterior end (bottom) that are marked with white dashed lines at the top, where beige discoloration is due to atmospheric carbonation of concrete during service, mostly occurred along the interior wall surface (to a distance of 20 to 25 mm) than from the exterior end (only 5 mm). Notice a vertical crack from the interior end (at the top) extended to a distance of 1.5 in. Right column shows fluorescent dye-mixed epoxy-impregnated lapped cross section viewed in an ultraviolet light where all visible and invisible cracks as well as porous areas of paste and voids are highlighted whereas dense aggregates appeared dark. Carbonated concrete at the interior end (at the top above white dashed line) remained dark in fluorescent light due to densification of paste by carbonation.

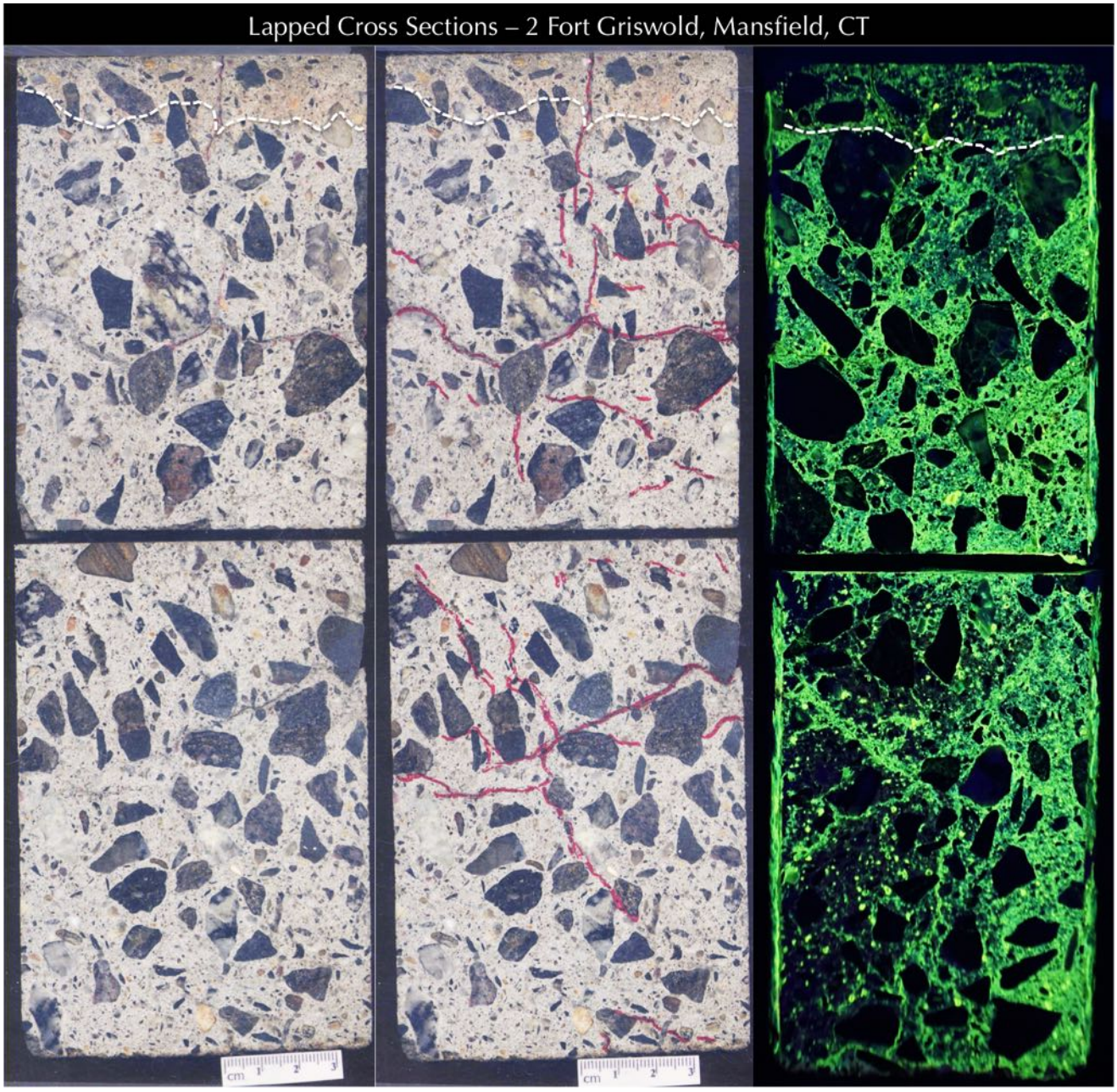


Figure 13: Multiple lapped cross sections of the core from 2 Fort Griswold showing: (a) full-depth extension of visible cracks that are highlighted in red in the middle column (mostly concentrated in the inside of the core); (b) beige discoloration of paste at the interior end of the wall (at the top) and also at the exterior end (bottom) that are marked with white dashed lines at the top, where beige discoloration is due to atmospheric carbonation of concrete during service, mostly occurred along the interior wall surface (to a distance of 20 to 25 mm) than from the exterior end (only 5 mm). Notice a vertical crack from the interior end (at the top) extended to a distance of 1.5 in. Right column shows fluorescent dye-mixed epoxy-impregnated lapped cross section viewed in an ultraviolet light where all visible and invisible cracks as well as porous areas of paste and voids are highlighted whereas dense aggregates appeared dark. Carbonated concrete at the interior end (at the top above white dashed line) remained dark in fluorescent light due to densification of paste by carbonation.

## IRON SULFIDE MINERALS IN CRUSHED GNEISS COARSE AGGREGATE IN LAPPED CROSS SECTIONS

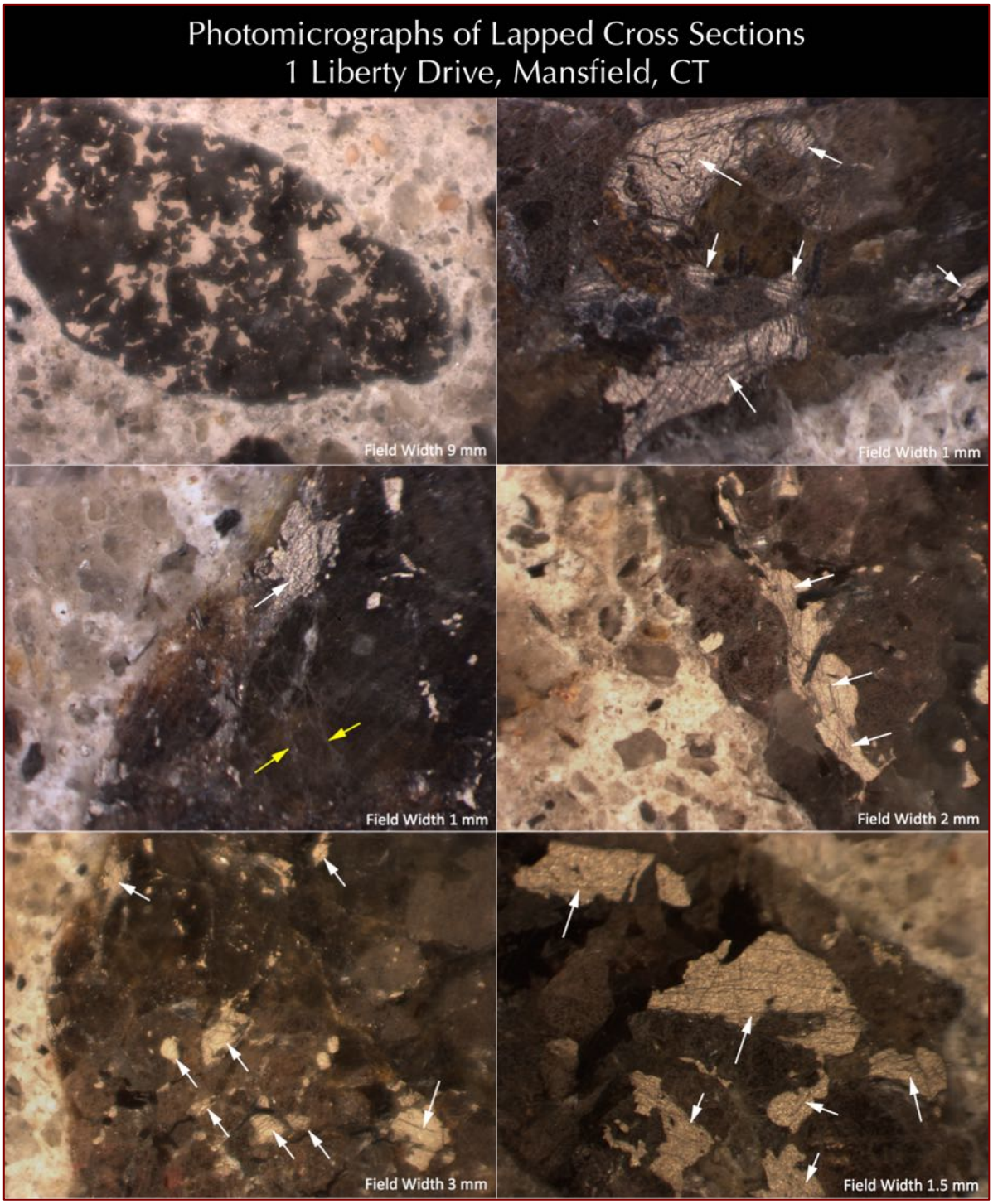


Figure 14: Photomicrographs of lapped cross sections of core from 1 Liberty Drive showing disseminated iron sulfide (pyrrhotite) and oxidized iron sulfide grains scattered throughout the crushed gneiss coarse aggregate particles many of which are marked with arrows. Oxidation causes development of fine parallel striations within pyrrhotite as seen in the top and bottom right photos, which are later in subseqeunt SEM-EDS studies found to be oxidized iron veins within pyrrhotite. Expansions due to oxidation causes formation of fine hairline cracks within pyrrhotite.

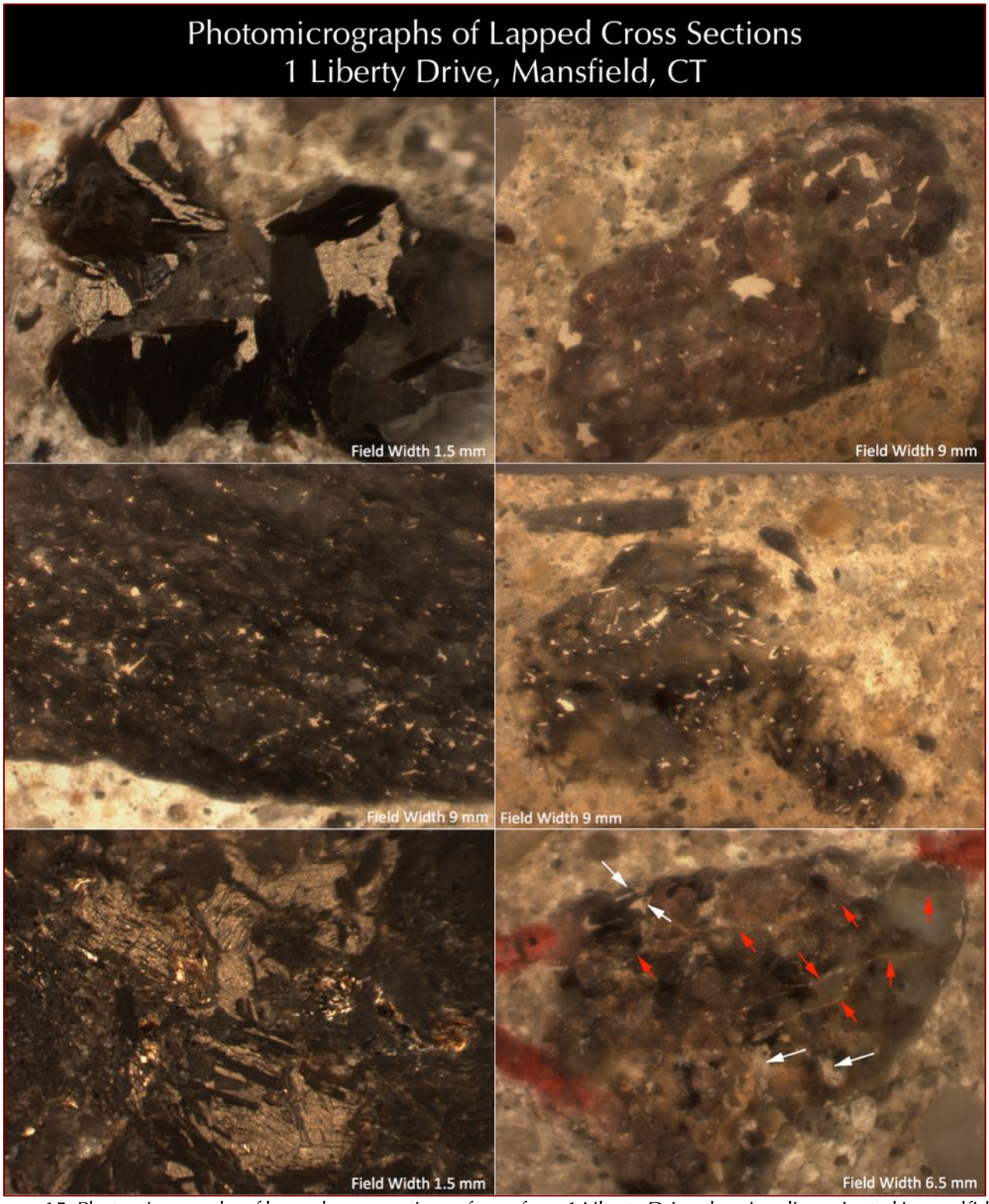


Figure 15: Photomicrographs of lapped cross sections of core from 1 Liberty Drive showing disseminated iron sulfide (pyrrhotite) and oxidized iron sulfide grains scattered throughout the crushed gneiss coarse aggregate particles many of which are marked with arrows. Oxidation causes development of fine parallel striations within pyrrhotite as seen in the top and bottom left photos, which are later in subseqeunt SEM-EDS studies found to be oxidized iron veins within pyrrhotite. Expansions due to oxidation causes formation of fine hairline cracks within pyrrhotite some of which are marked in red arrows in the bottom right photo.

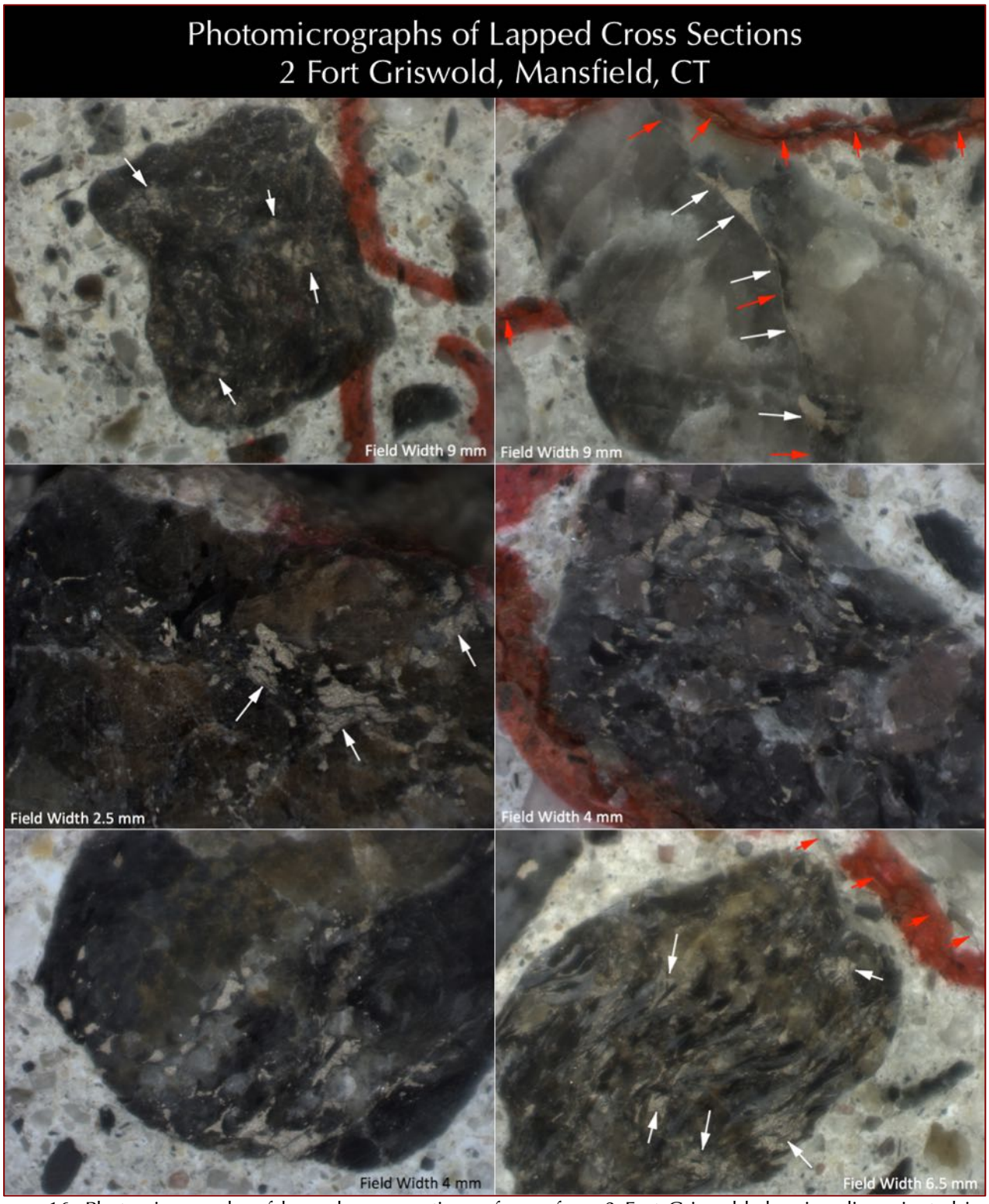


Figure 16: Photomicrographs of lapped cross sections of core from 2 Fort Griswold showing disseminated iron sulfide (pyrrhotite) and oxidized iron sulfide grains scattered throughout the crushed gneiss coarse aggregate particles many of which are marked with arrows. Oxidation causes development of fine parallel striations within pyrrhotite as seen in the middle left and bottom right photos, which are later in subseqeunt SEM-EDS studies found to be oxidized iron veins within pyrrhotite. Expansions due to oxidation causes formation of fine hairline cracks within pyrrhotite.

## PHOTOMICROGRAPHS OF LAPPED CROSS SECTIONS

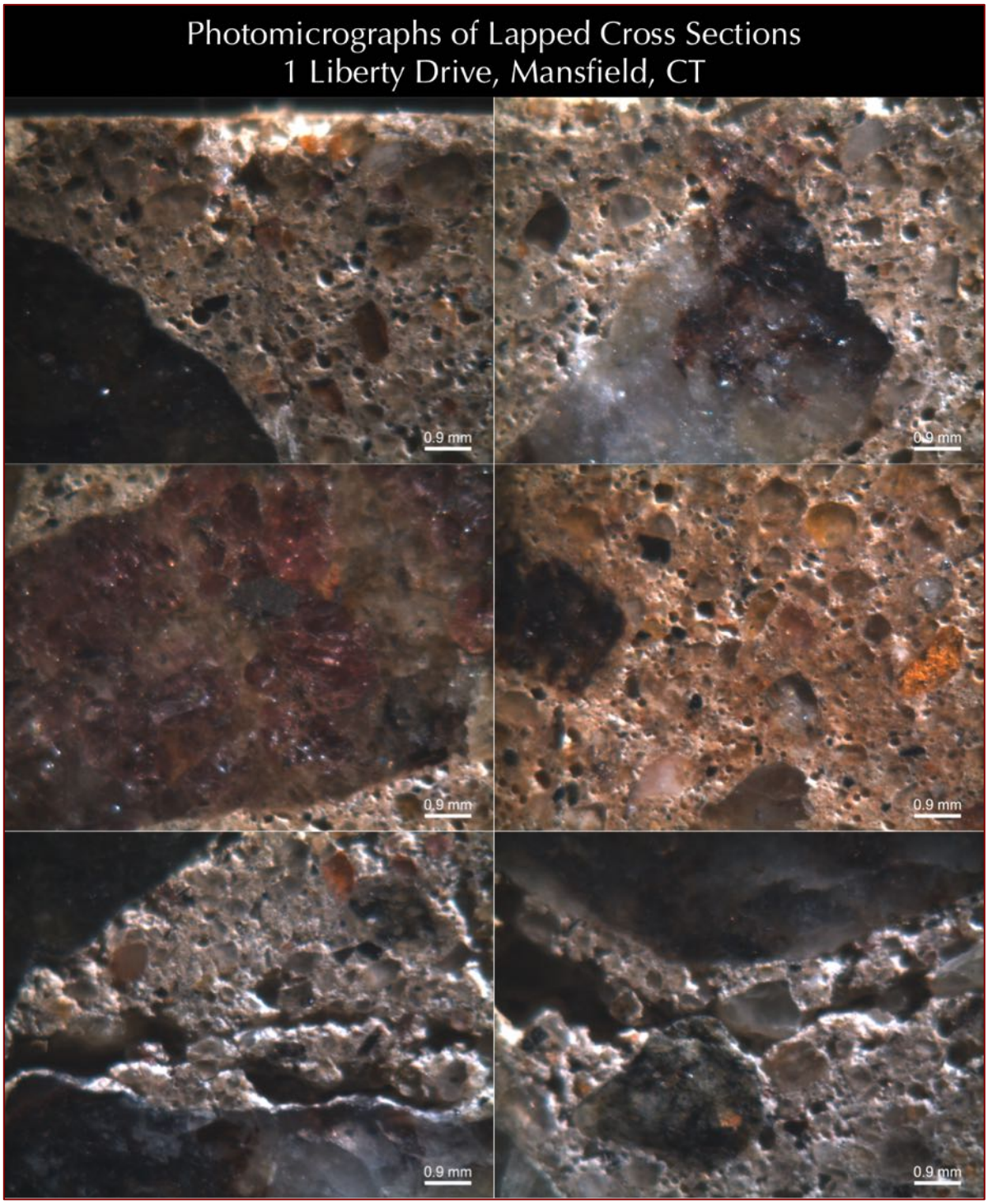


Figure 17: Photomicrographs of lapped cross section of core from 1 Liberty Drive showing crushed gneiss coarse aggregate particles, e.g., white granite gneiss with black specs of mica in parallel (gneissose) arrangements, light to medium brown granite gneiss, and dark gray to black gneiss. Notice air-entrained nature of concrete having many fine, discrete spherical and near-spherical entrained air voids of sizes 1 mm or less. Carbonation of paste has caused beige discoloration from the normal gray color tone of non-carbonated paste. Notice cracking in interior concrete in the bottom row.

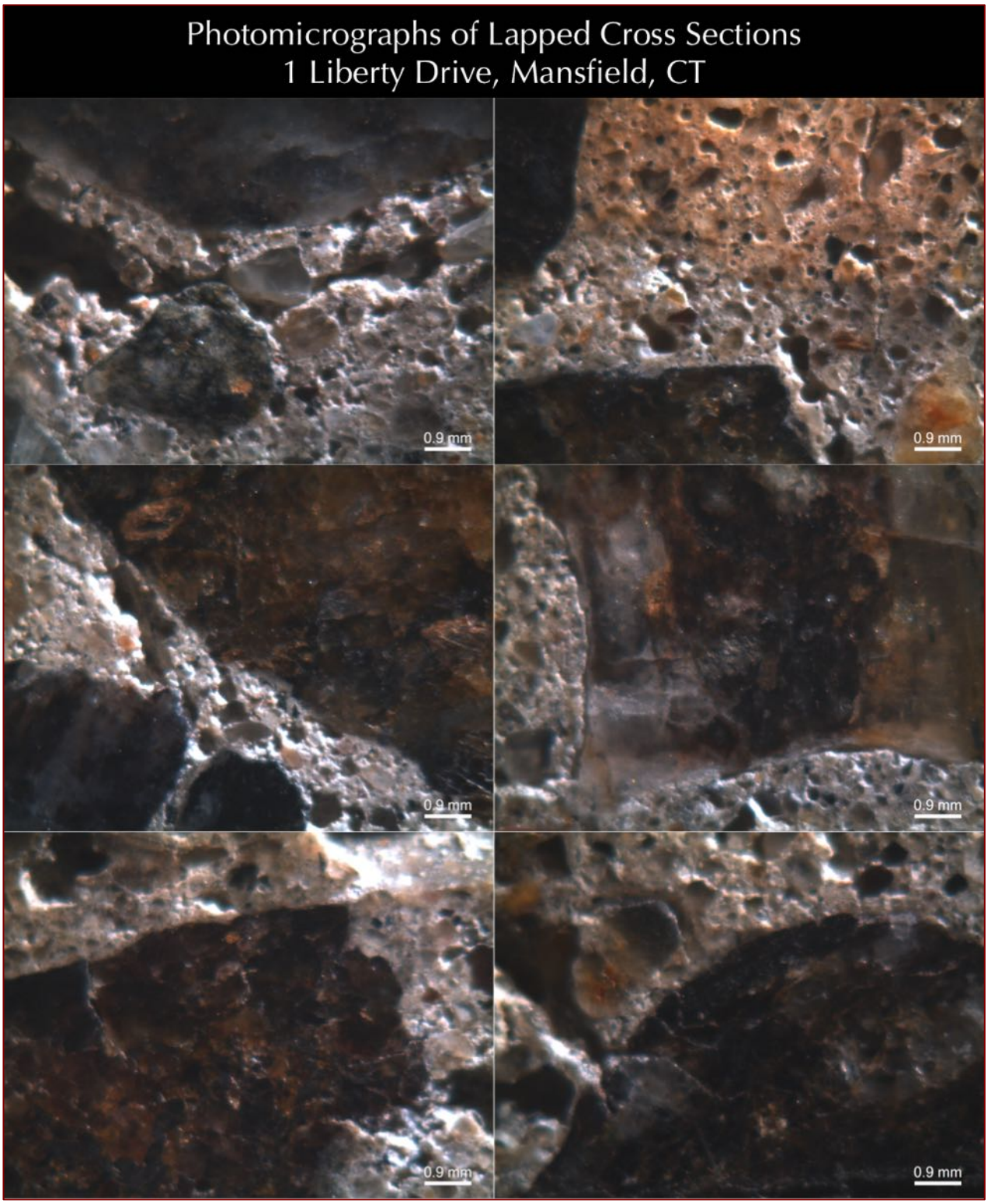


Figure 18: Photomicrographs of lapped cross section of core from 1 Liberty Drive showing crushed gneiss coarse aggregate particles, e.g., white granite gneiss with black specs of mica in parallel (gneissose) arrangements, light to medium brown granite gneiss, and dark gray to black gneiss. Notice air-entrained nature of concrete having many fine, discrete spherical and near-spherical entrained air voids of sizes 1 mm or less. Carbonation of paste has caused beige discoloration from the normal gray color tone of non-carbonated paste. Notice cracking in interior concrete.

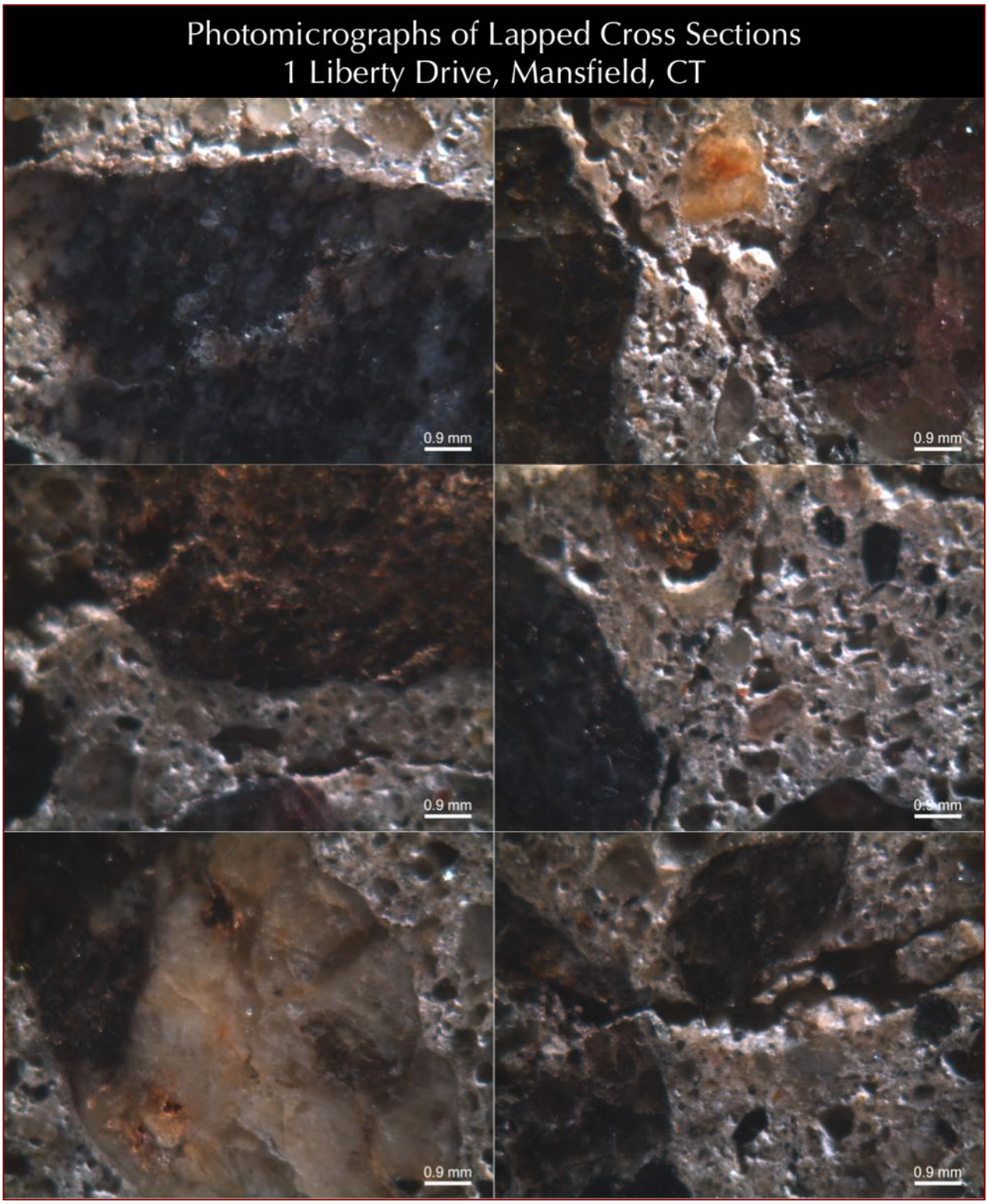


Figure 19: Photomicrographs of lapped cross section of core from 1 Liberty Drive showing crushed gneiss coarse aggregate particles, e.g., white granite gneiss with black specs of mica in parallel (gneissose) arrangements, light to medium brown granite gneiss, and dark gray to black gneiss. Notice air-entrained nature of concrete having many fine, discrete spherical and near-spherical entrained air voids of sizes 1 mm or less. Notice cracking in interior concrete.

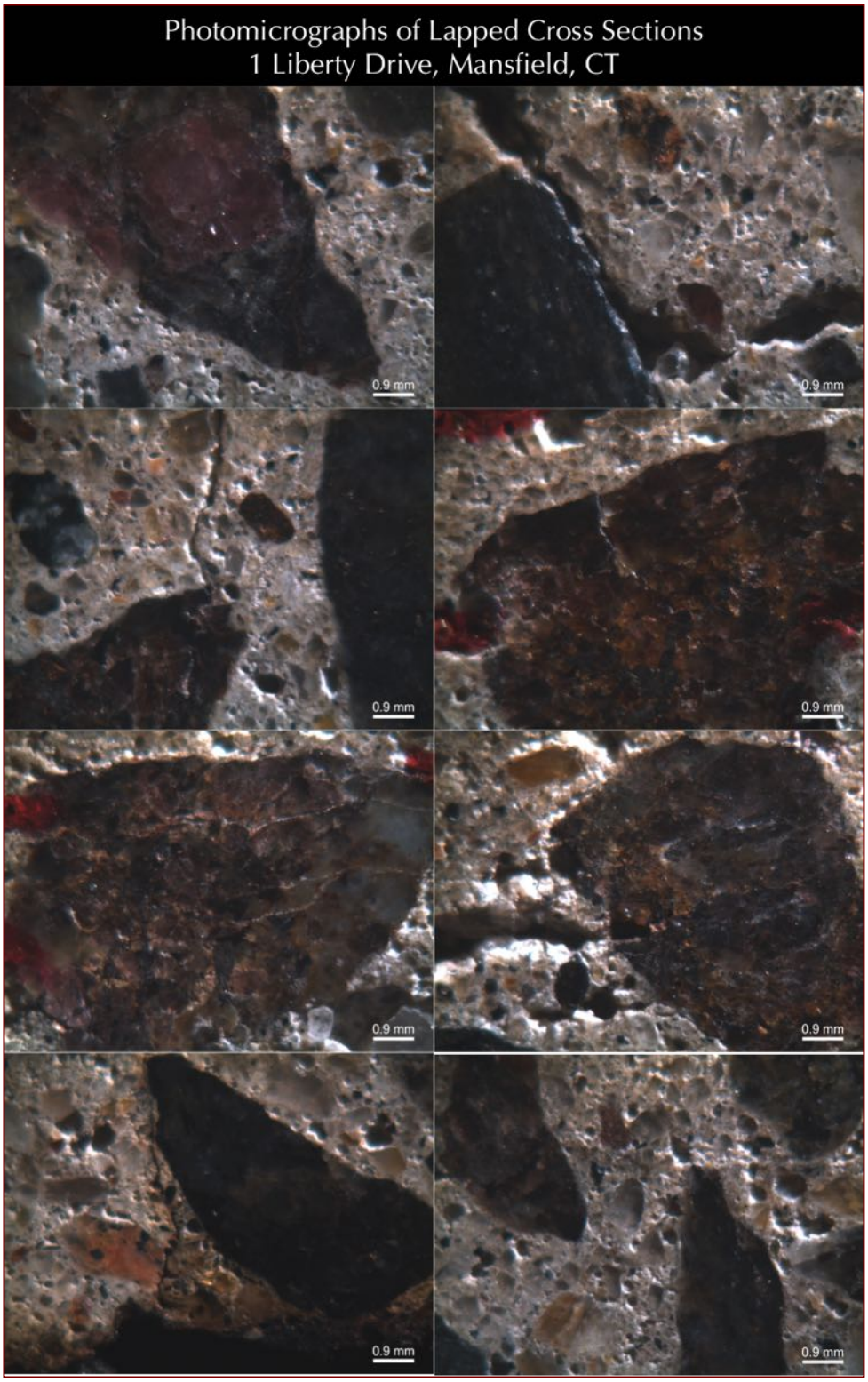


Figure 20: Photomicrographs of lapped cross section of core from 1 Liberty Drive showing crushed gneiss coarse aggregate particles, e.g., white granite gneiss with black specs of mica in parallel (gneissose) arrangements, light to medium brown granite gneiss, and dark gray to black gneiss. Notice air-entrained nature of concrete having many fine, discrete spherical and near-spherical entrained air voids of sizes 1 mm or less. Notice cracking in interior concrete.

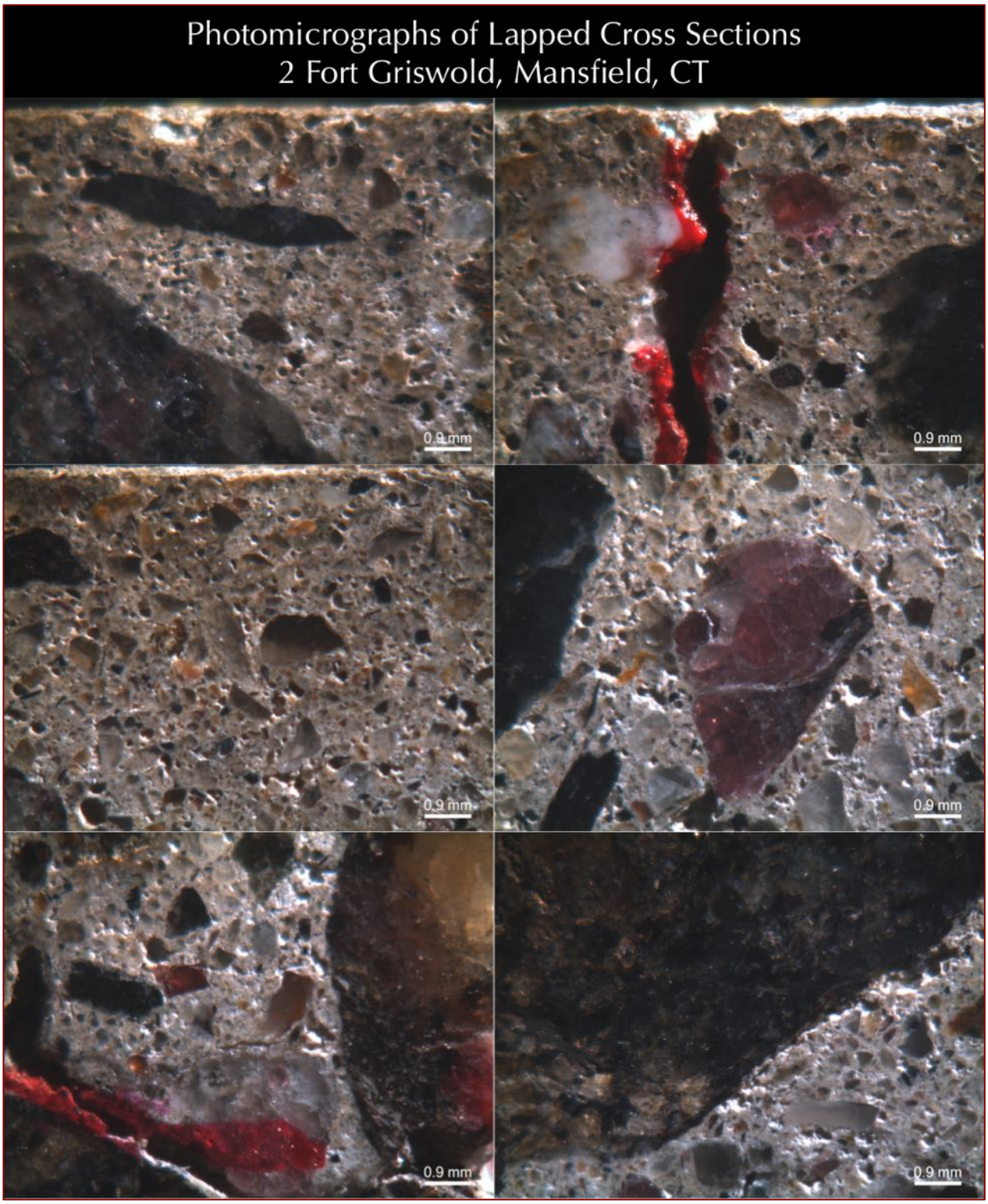


Figure 21: Photomicrographs of lapped cross section of core from 2 Fort Griswold showing crushed gneiss coarse aggregate particles, e.g., white granite gneiss with black specs of mica in parallel (gneissose) arrangements, light to medium brown granite gneiss, and dark gray to black gneiss. Notice air-entrained nature of concrete having many fine, discrete spherical and near-spherical entrained air voids of sizes 1 mm or less. Notice cracking in interior concrete.

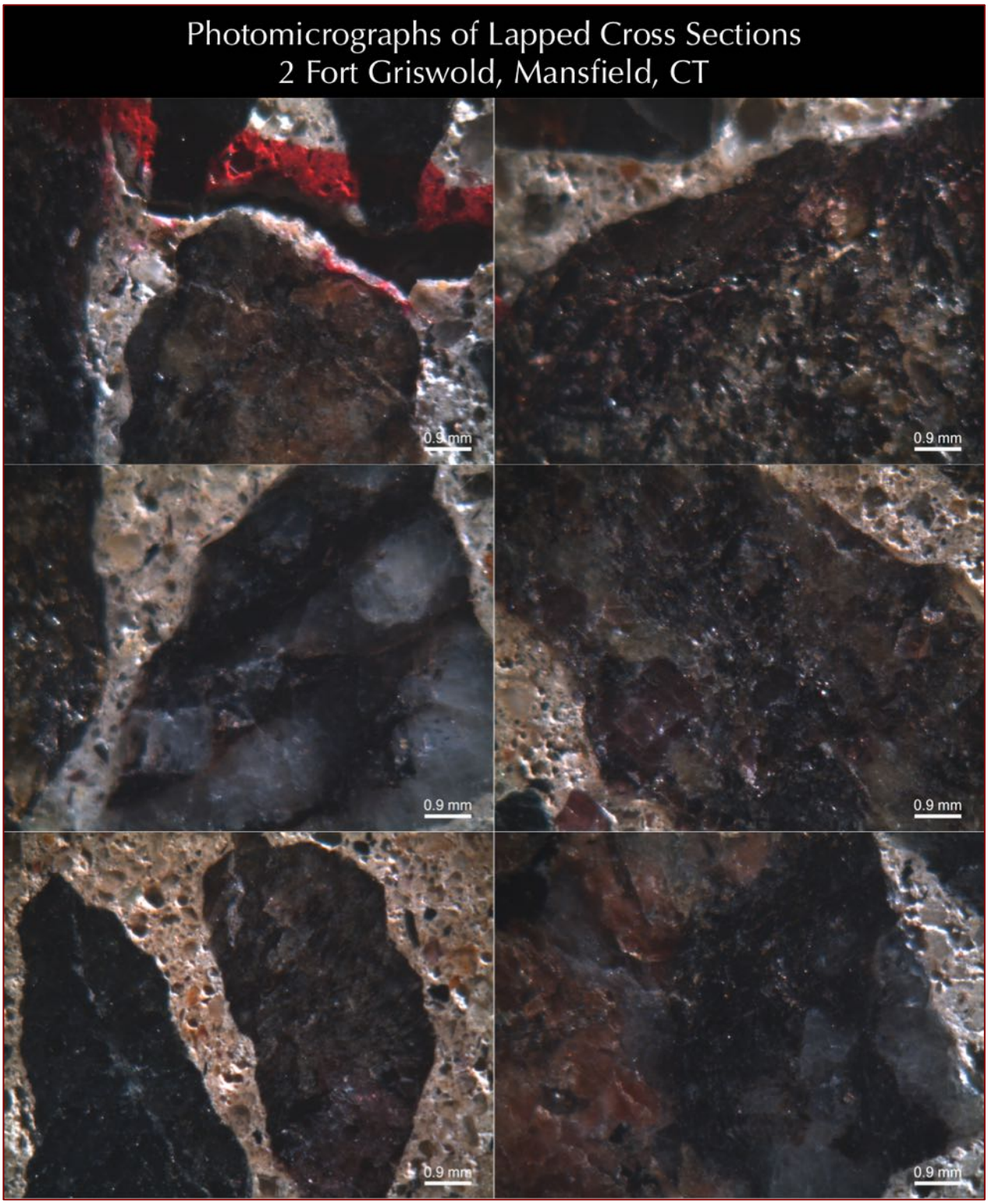


Figure 22: Photomicrographs of lapped cross section of core from 2 Fort Griswold showing crushed gneiss coarse aggregate particles, e.g., white granite gneiss with black specs of mica in parallel (gneissose) arrangements, light to medium brown granite gneiss, and dark gray to black gneiss. Notice air-entrained nature of concrete having many fine, discrete spherical and near-spherical entrained air voids of sizes 1 mm or less. Notice cracking in interior concrete. Carbonation of paste has caused beige discoloration from the normal gray color tone of non-carbonated paste.

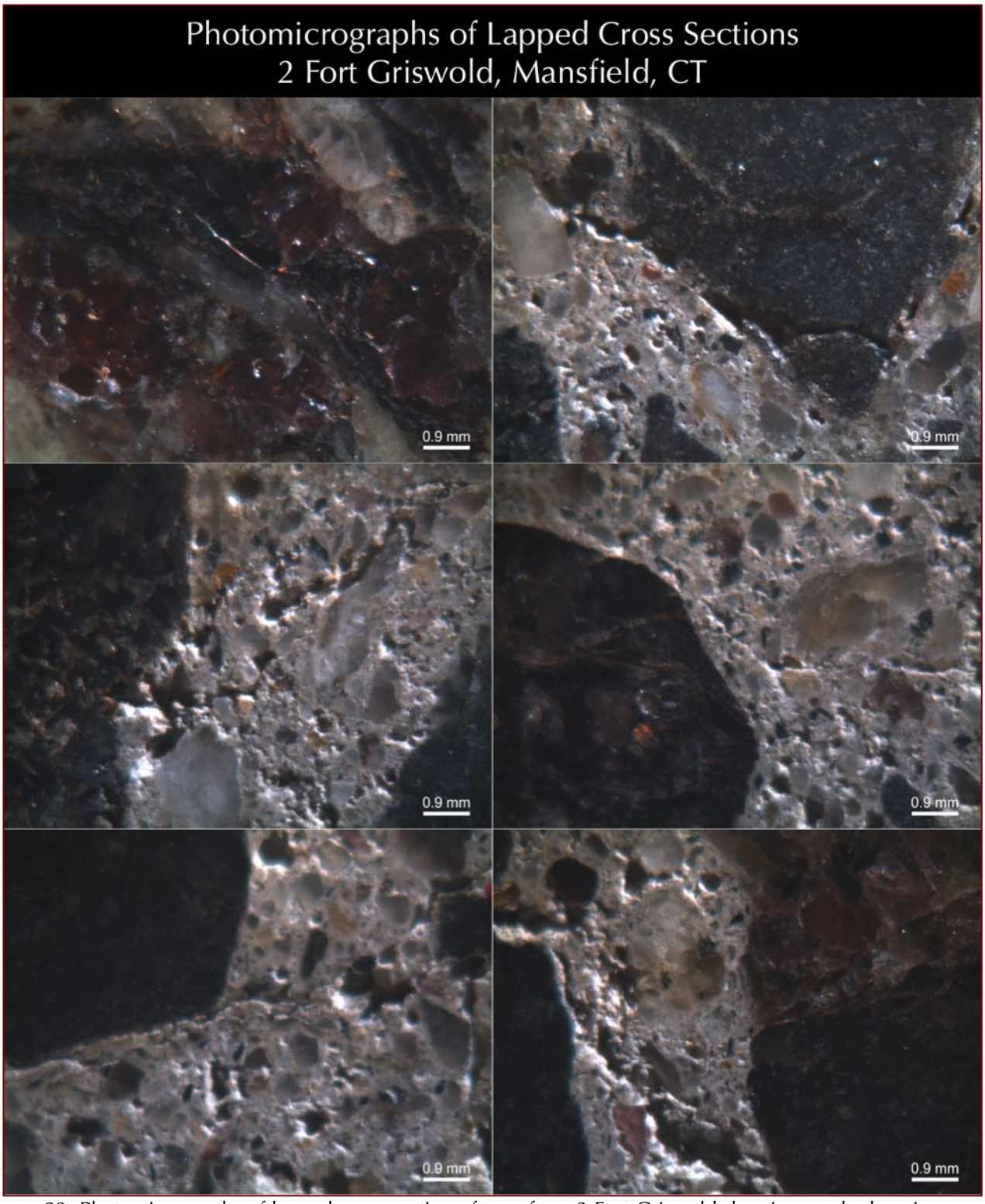


Figure 23: Photomicrographs of lapped cross section of core from 2 Fort Griswold showing crushed gneiss coarse aggregate particles, e.g., white granite gneiss with black specs of mica in parallel (gneissose) arrangements, light to medium brown granite gneiss, and dark gray to black gneiss. Notice air-entrained nature of concrete having many fine, discrete spherical and near-spherical entrained air voids of sizes 1 mm or less. Notice cracking in interior concrete.

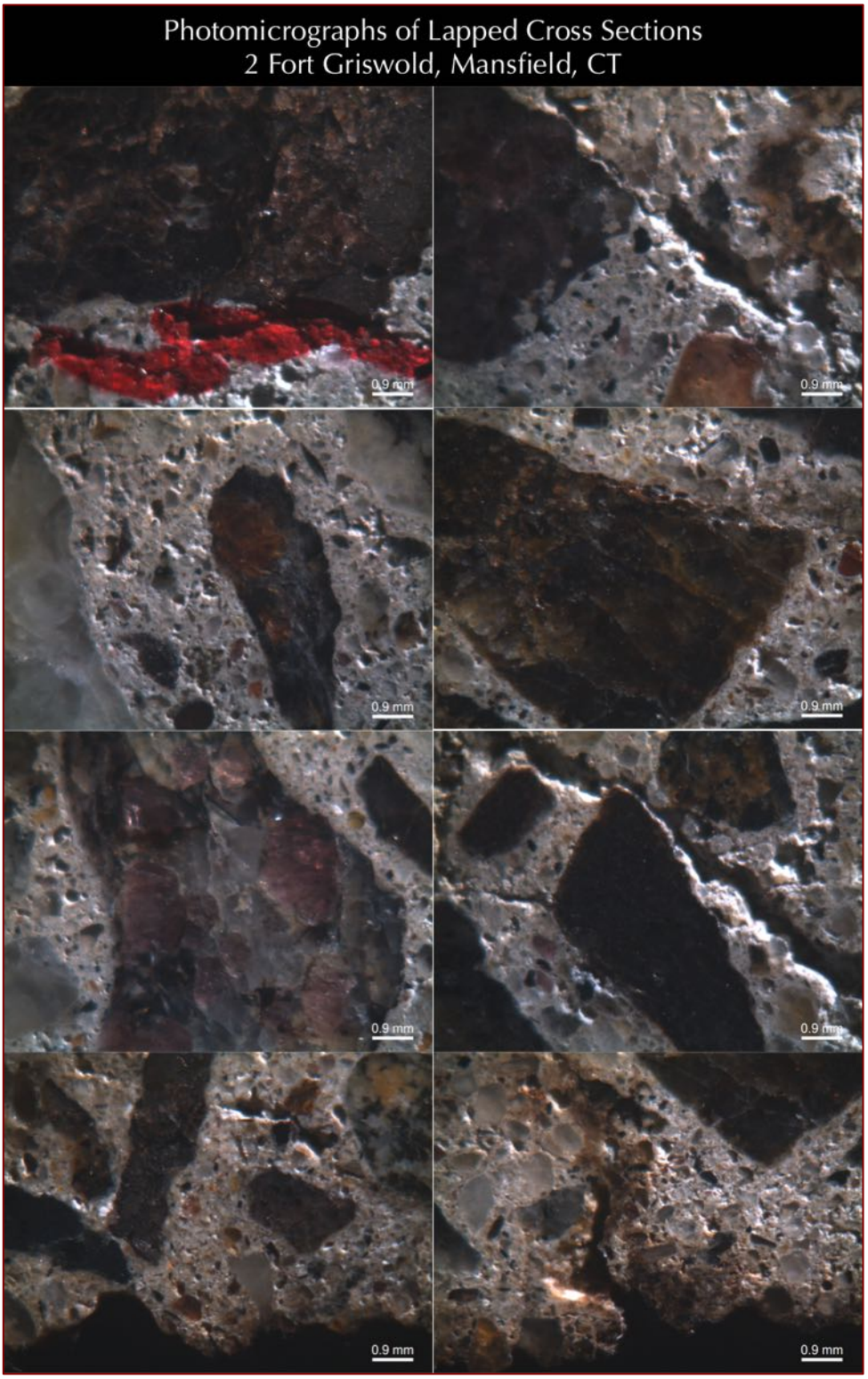


Figure 24: Photomicrographs of lapped cross section of core from 2 Fort Griswold showing crushed gneiss coarse aggregate particles, e.g., white granite gneiss with black specs of mica in parallel (gneissose) arrangements, light to medium brown granite gneiss, and dark gray to black gneiss. Notice air-entrained nature of concrete having many fine, discrete spherical and near-spherical entrained air voids of sizes 1 mm or less. Notice cracking in interior concrete.

## THIN SECTIONS

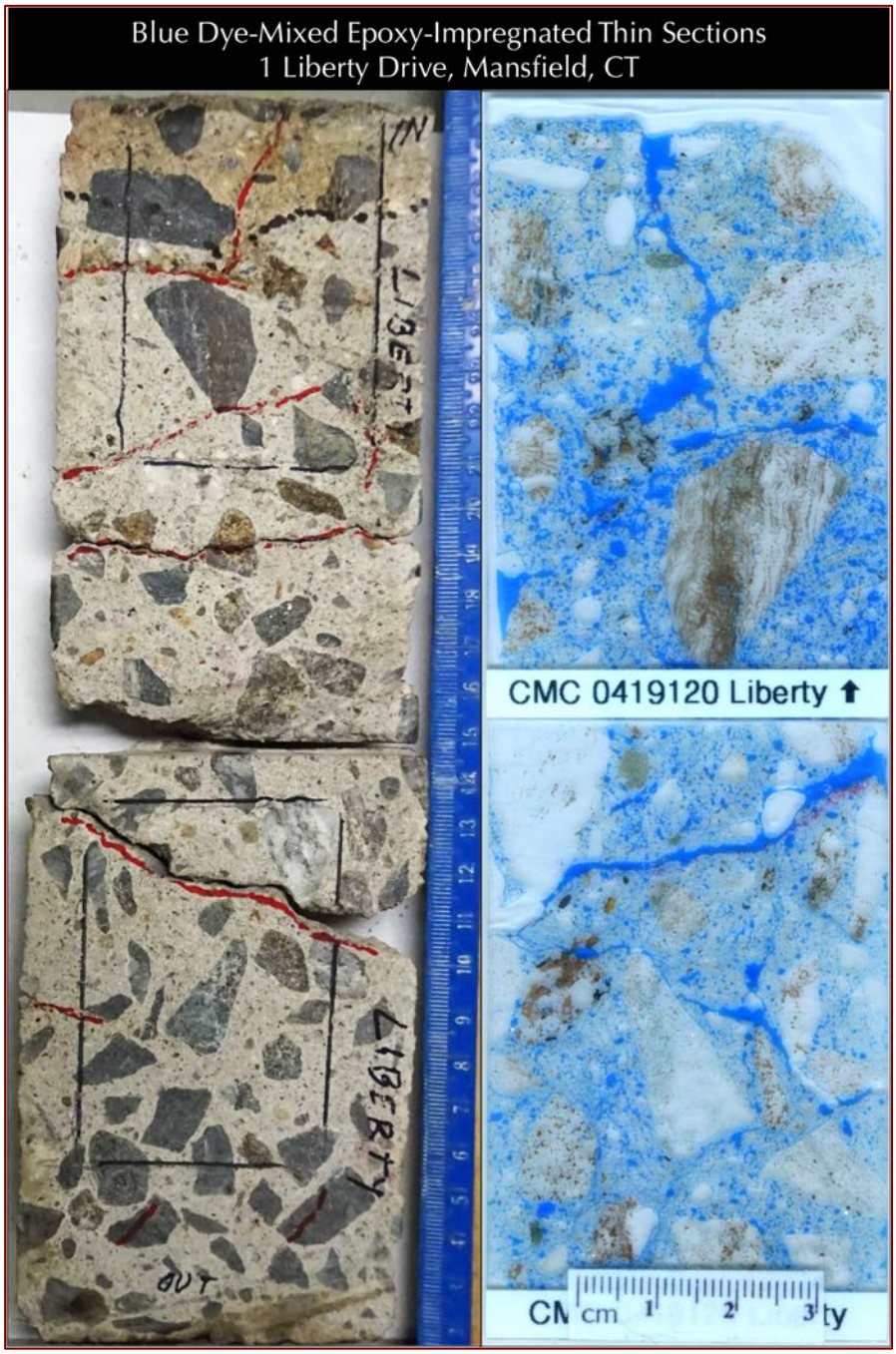


Figure 25: Blue dye-mixed epoxy-impregnated thin sections (30 micron thickness, right) and corresponding saw-cut sections (left) having rectangular marked portions selected for trrimming and thin section preparation for the core from 1 Liberty Drive. Thin sections were examined: (a) in a stereozoom microscope, in transmited and reflected-light modes to highlight pores, air voids, and cracks, (b) in a petrographic microscope to examine various microstructural features at higher magnifications than that from stereomicroscope, and (c) finally in a scanning electron microscope with attached energy-dispersive X-ray spectrometer to examine specific areas of interests for microstructural and microchemical analyses selected from optical microsocpy (after coating the sections with a thin conductive gold film). Visible and invisible cracks, porous areas of paste, and air voids are highlighted by blue dyed epoxy. Coarse aggregate particles are dense gneiss, hence did not absorb blue epoxy.

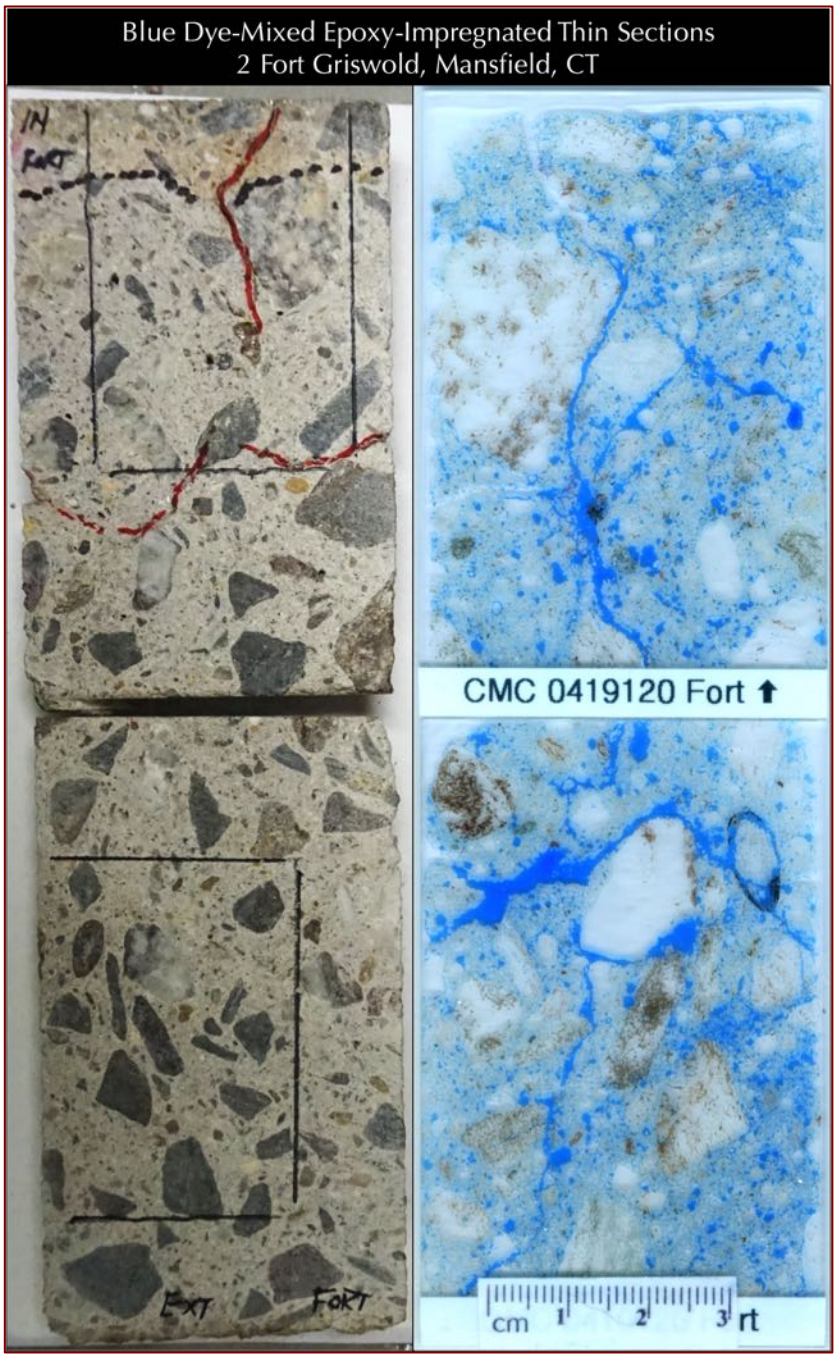


Figure 26: Blue dye-mixed epoxy-impregnated thin sections (30 micron thickness, right) and corresponding saw-cut sections (left) having rectangular marked portions selected for trrimming and thin section preparation for the core from 2 Fort Griswold. Thin sections were examined: (a) in a stereozoom microscope, in transmited and reflected-light modes to highlight pores, air voids, and cracks, (b) in a petrographic microscope to examine various microstructural features at higher magnifications than that from stereomicroscope, and (c) finally in a scanning electron microscope with attached energy-dispersive X-ray spectrometer to examine specific areas of interest for microstructural and microchemical analyses selected from optical microsocpy (after coating the sections with a thin conductive gold film). Visible and invisible cracks, porous areas of paste, and air voids are highlighted by blue dyed epoxy. Coarse aggregate particles are dense gneiss, hence did not absorb blue epoxy.

## PHOTOMICROGRAPHS OF THIN SECTIONS

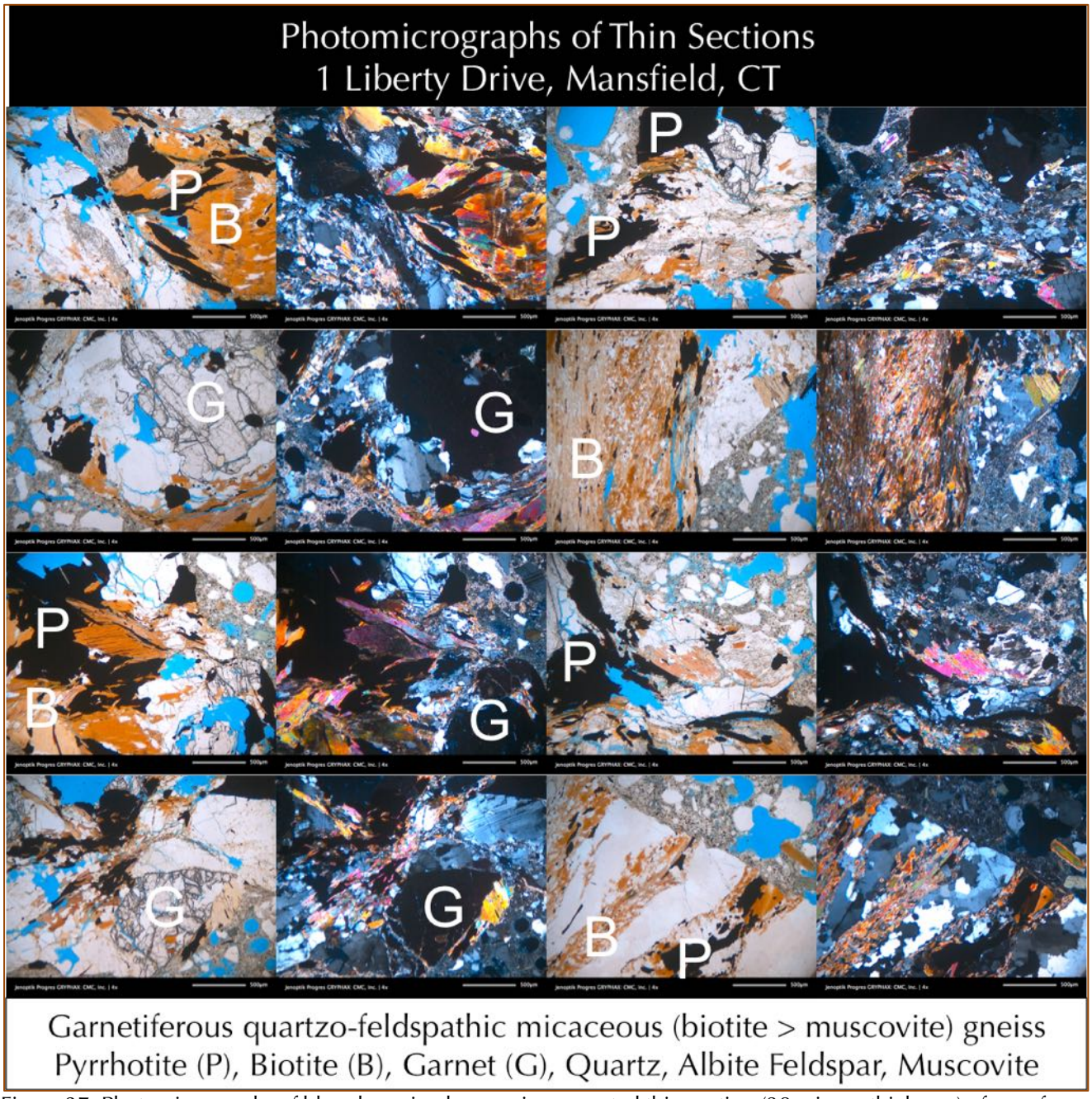


Figure 27: Photomicrographs of blue dye-mixed epoxy-impregnated thin section (30 micron thickness) of core from 1 Liberty Drive showing: (a) crushed gneiss coarse aggregate particles having anhedral to subhedral porphyroblasts of garnet (marked as 'G') and alternating bands of light-colored quartzo-feldspathic and dark brown colored pleochroic biotite (marked as 'B') and light-colored muscovite/chlorite micaceous minerals defining the gneissose texture common in these crushed gneiss coarse aggregate particles, and (b) dark opaque iron sulfide and iron oxide minerals (marked as 'P') scattered throughout the grains in fine disseminated forms. Right column photomicrographs in the 2nd and 4th columns were taken in crossed-polarized light modes and left columns in corresponding 1st and 3rd columns were taken in plane polarized modes with a petrographic microscope.

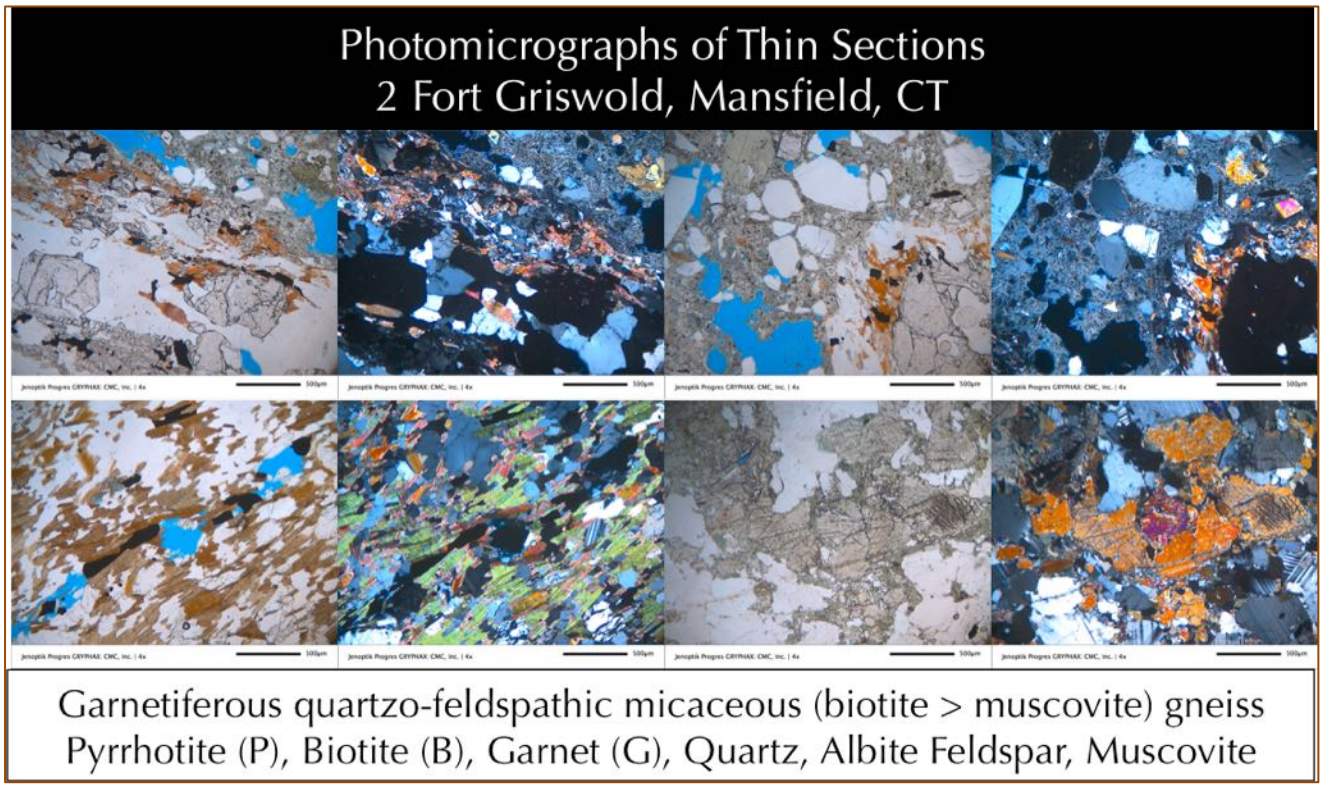


Figure 28: Photomicrographs of blue dye-mixed epoxy-impregnated thin section (30 micron thickness) of core from 2 Fort Griswold showing: (a) crushed gneiss coarse aggregate particles having anhedral to subhedral porphyroblasts of garnet and alternating bands of light-colored quartzo-feldspathic and dark brown colored pleochroic biotite and light-colored muscovite/chlorite micaceous minerals defining the gneissose texture common in these crushed gneiss coarse aggregate particles, and (b) dark opaque iron sulfide and iron oxide minerals scattered throughout the grains in fine disseminated forms. Right column photomicrographs in the 2nd and 4th columns were taken in crossed-polarized light modes and left columns in corresponding 1st and 3rd columns were taken in plane polarized modes with a petrographic microscope. Notice some clinopyroxene grains in coarse aggregate in the bottom photos in 3rd and 4th columns. Notice parallel alignment of fine lath-shaped biotite mica in the bottom 1st and 2nd column photos, which define the gneissose texture of crushed gneiss coarse aggregate. The top photos in the 1st and 2nd columns show plane and crossed polarized light photos of garnet porphyroblasts in parallel alignment to micaceous layers of gneiss.

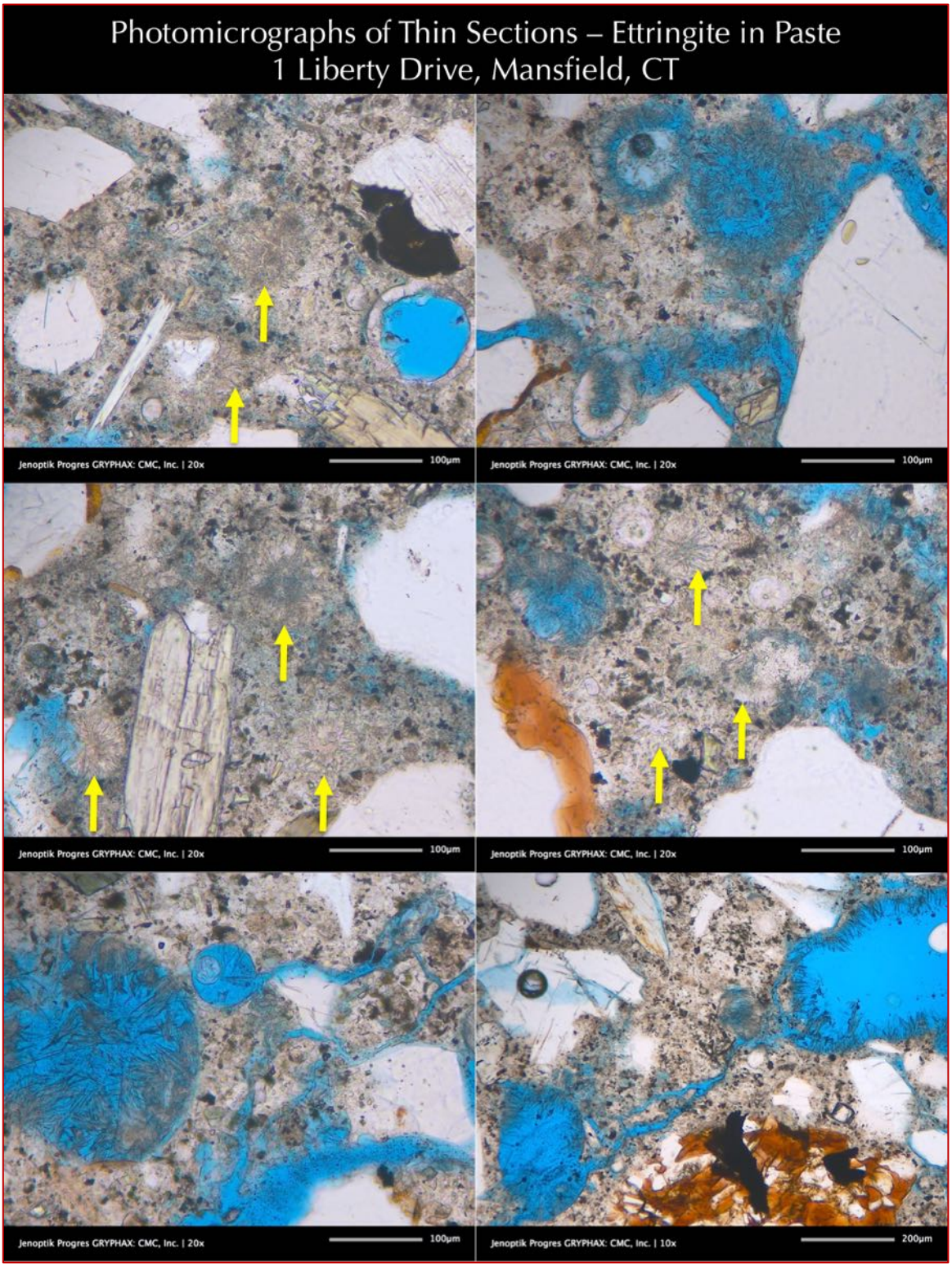


Figure 29: Photomicrographs of blue dye-mixed epoxy-impregnated thin section (30 micron thickness) of core from 1 Liberty Drive showing the mortar fraction of concrete away from crushed gneiss coarse aggregate particles. Notice many fine, fibrous and acicular secondary ettringite deposits lining the walls of coarse voids as well as filling the smaller voids, secondary ettringite in cracks, and also in confined areas in paste (many are marked with arrows).

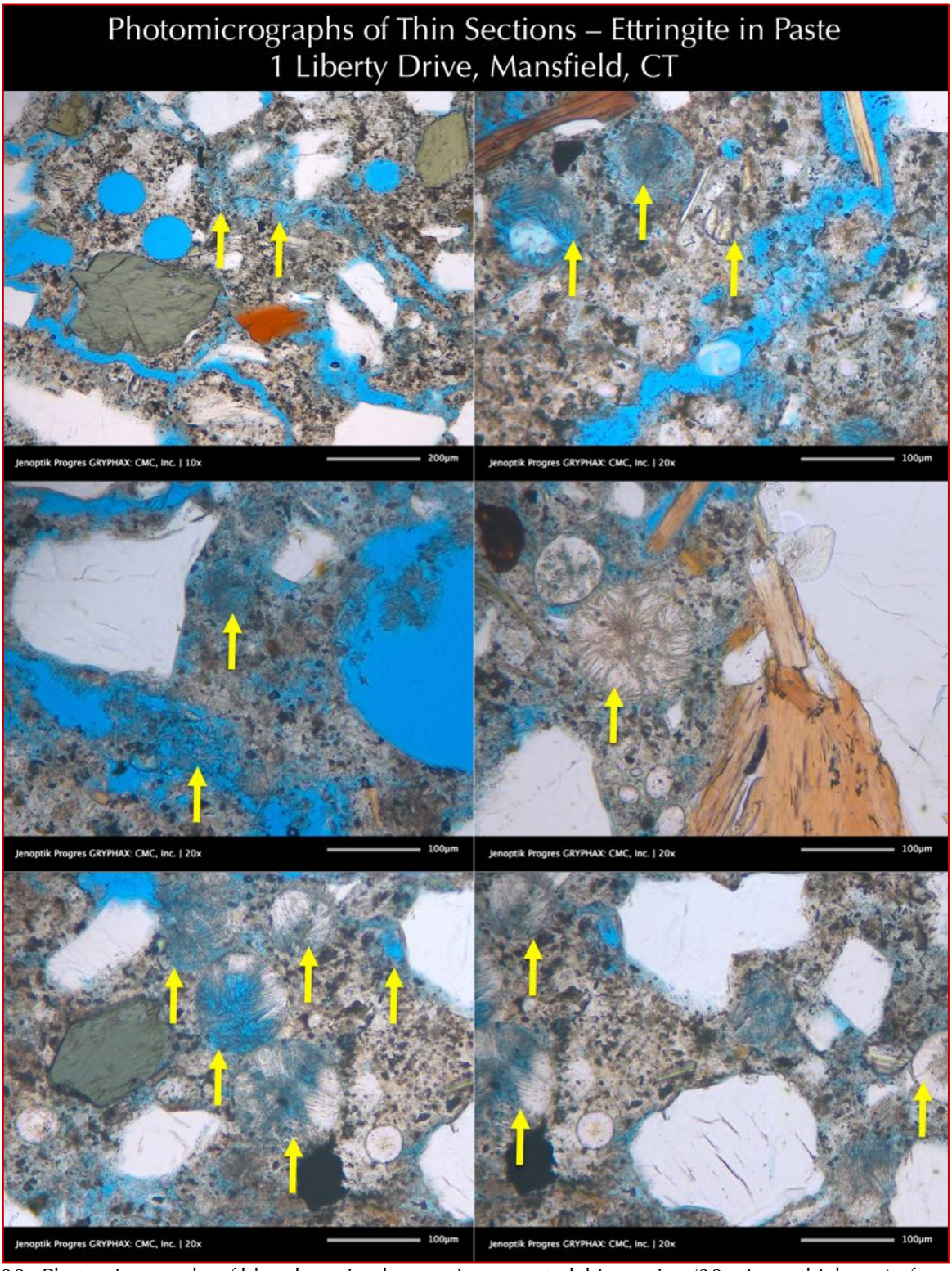


Figure 30: Photomicrographs of blue dye-mixed epoxy-impregnated thin section (30 micron thickness) of core from 1 Liberty Drive showing the mortar fraction of concrete away from crushed gneiss coarse aggregate particles. Notice many fine, fibrous and acicular secondary ettringite deposits lining the walls of coarse voids as well as filling the smaller voids, and secondary ettringite in cracks (many are marked with arrows).

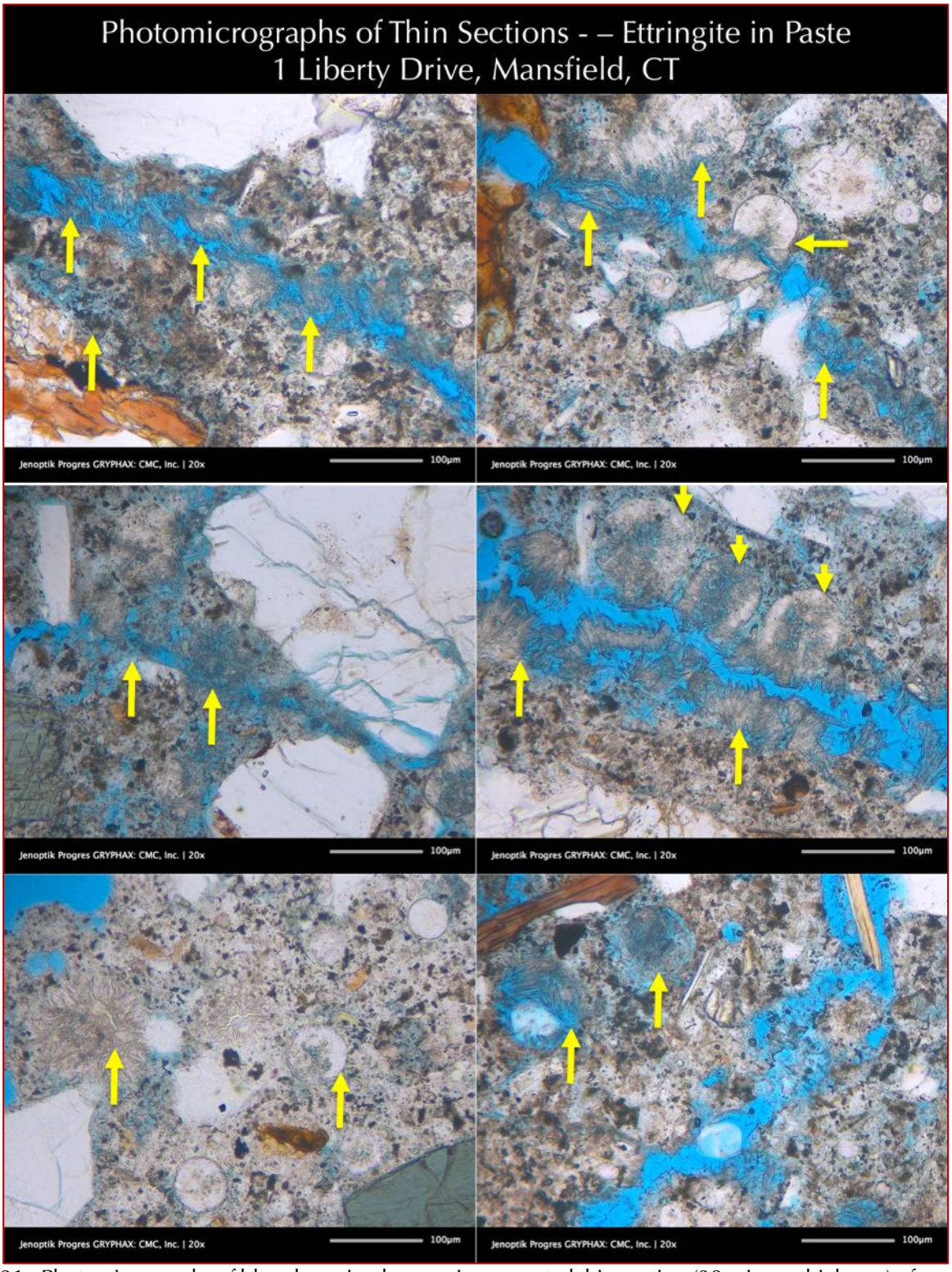


Figure 31: Photomicrographs of blue dye-mixed epoxy-impregnated thin section (30 micron thickness) of core from 1 Liberty Drive showing the mortar fraction of concrete away from crushed gneiss coarse aggregate particles. Notice many fine, fibrous and acicular secondary ettringite deposits lining the walls of coarse voids as well as filling the smaller voids, and secondary ettringite in cracks (many are marked with arrows).

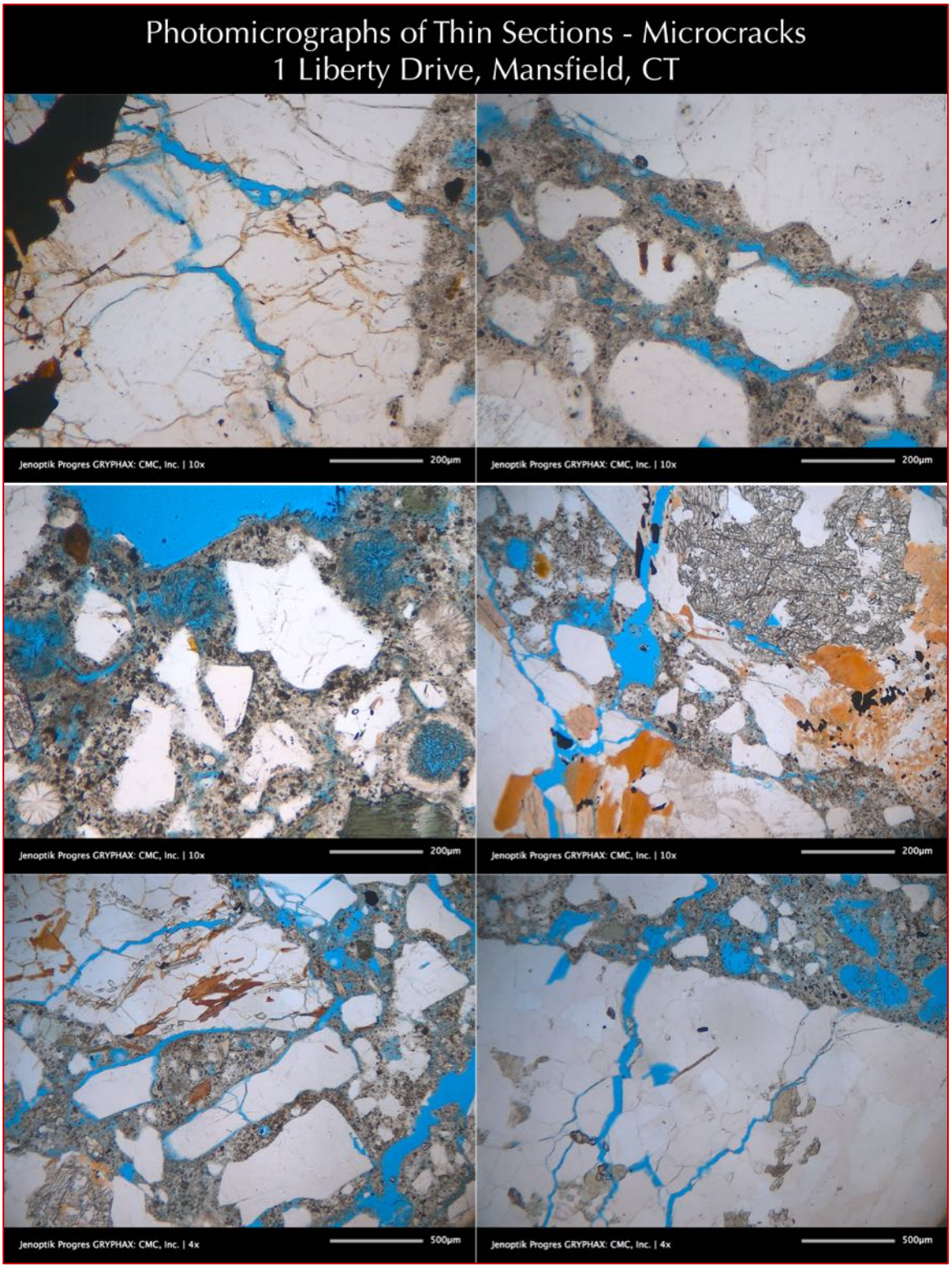


Figure 32 Photomicrographs of blue dye-mixed epoxy-impregnated thin section (30 micron thickness) of core from 1 Liberty Drive showing the mortar fraction of concrete away from crushed gneiss coarse aggregate particles. Notice many fine, fibrous and acicular secondary ettringite deposits lining the walls of coarse voids as well as filling the smaller voids, secondary ettringite in cracks, and also in confined areas in paste. Notice extensive cracking in concrete through aggregates and paste.

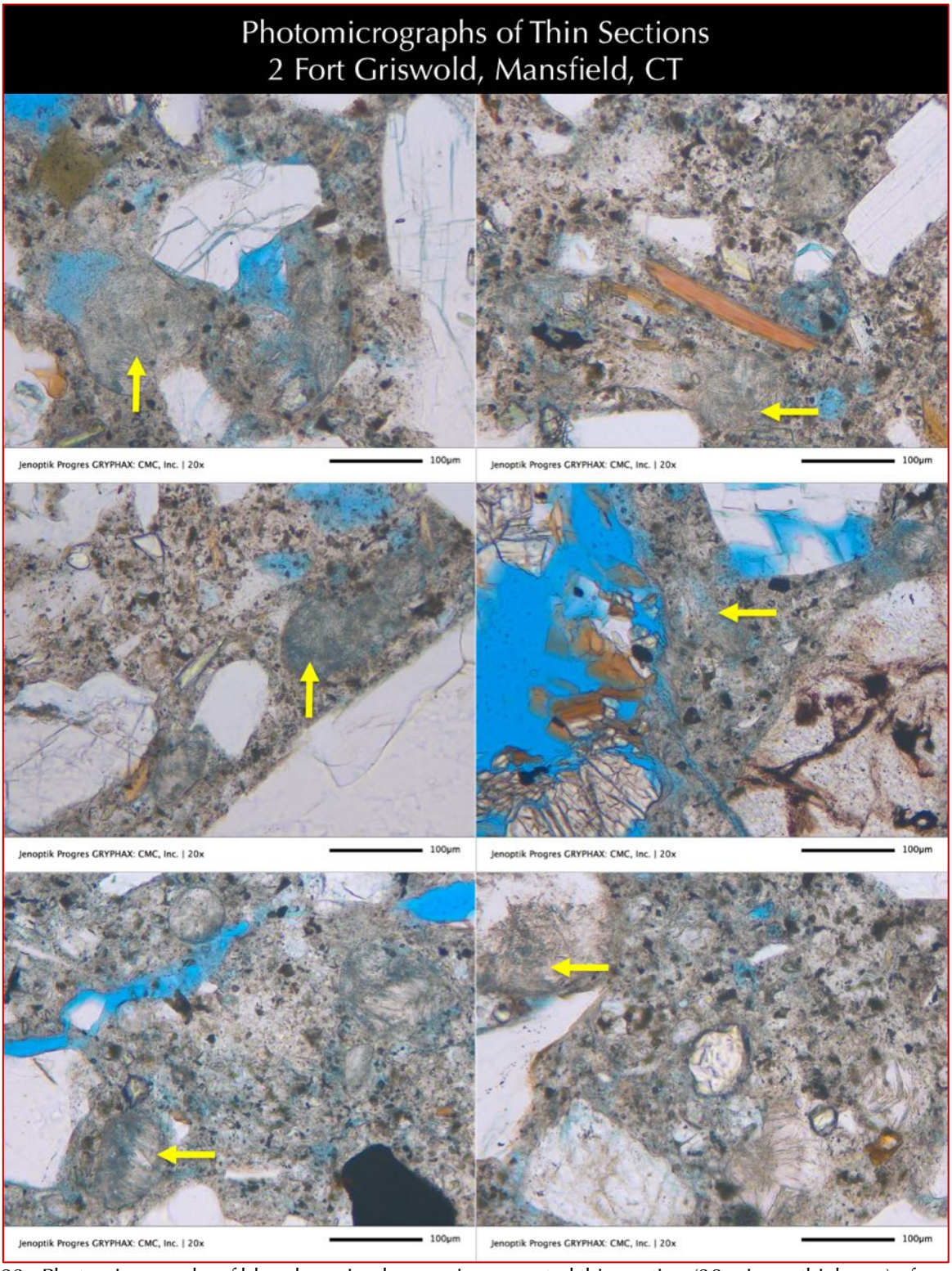


Figure 33: Photomicrographs of blue dye-mixed epoxy-impregnated thin section (30 micron thickness) of core from 2 Fort Griswold showing the mortar fraction of concrete away from crushed gneiss coarse aggregate particles. Notice many fine, fibrous and acicular secondary ettringite deposits lining the walls of coarse voids as well as filling the smaller voids, secondary ettringite in cracks, and also in confined areas in paste (many are marked with arrows).

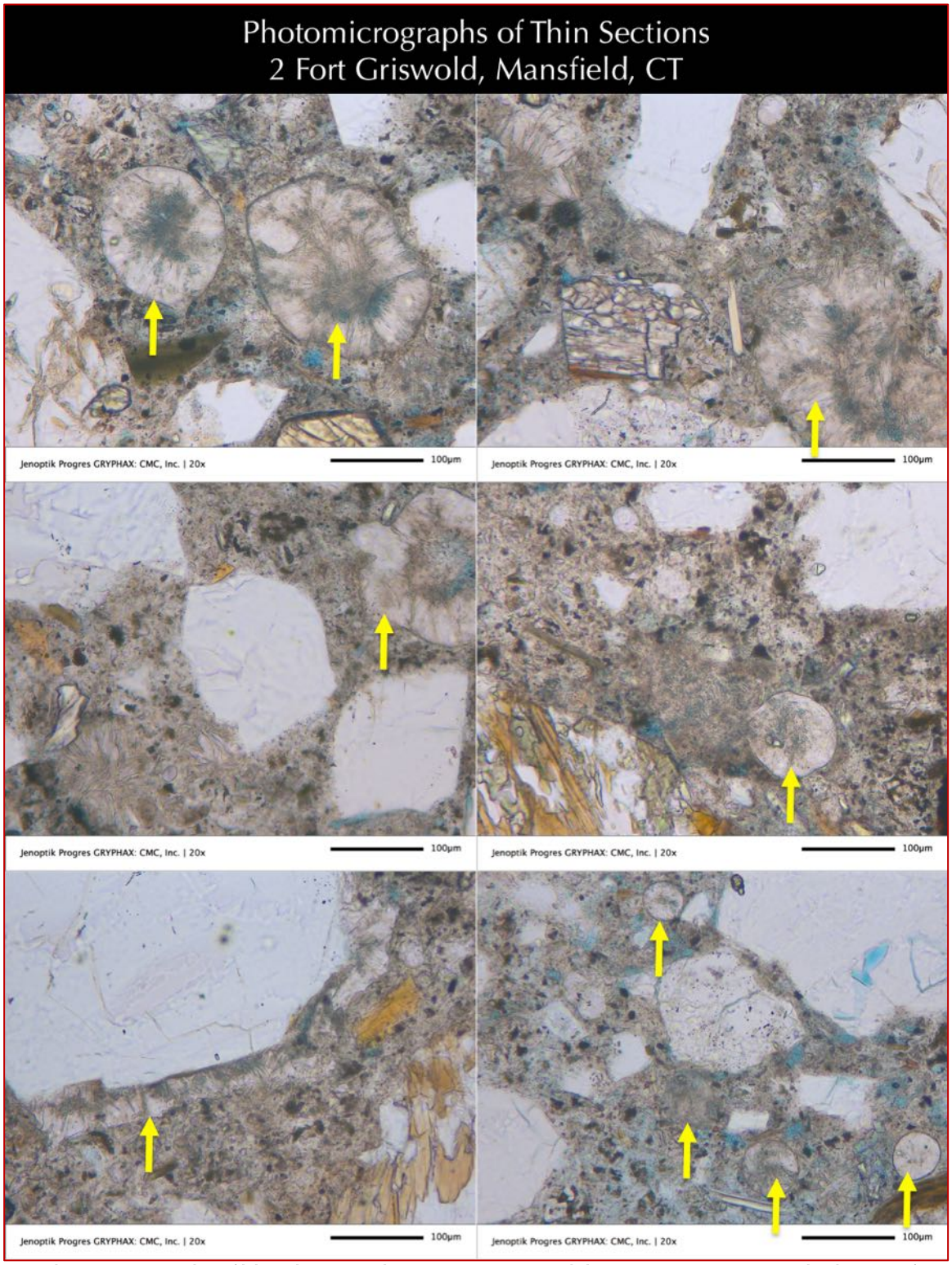


Figure 34: Photomicrographs of blue dye-mixed epoxy-impregnated thin section (30 micron thickness) of core from 2 Fort Griswold showing the mortar fraction of concrete away from crushed gneiss coarse aggregate particles. Notice many fine, fibrous and acicular secondary ettringite deposits lining the walls of coarse voids as well as filling the smaller voids, secondary ettringite in cracks, and also in confined areas in paste (many are marked with arrows).

## COARSE AGGREGATES

Coarse aggregates in cores from both foundations are compositionally similar crushed gneiss, which are a mixture of three different color tones of gravel and crushed gravel coarse aggregate particles –

(i) A dominant dark gray to black gneiss consisting of quartz, albite feldspar, biotite mica, and pyrope garnet porphyroblasts, anhedral to subhedral equigranular to gneissose arrangement of minerals;

(ii) A subordinate light to medium brown granite gneiss of quartz, albite feldspar, garnet, biotite mica and occasional pyroxene (augite) grains; and

(iii) A minor white granite gneiss with quartzo-feldspathic minerals and black specs of mica flakes in parallel alternate (gneissose) arrangements.

The brown and dark gray particles contained relatively more iron minerals than the dominant white granite gneiss particles. All coarse aggregate particles have nominal maximum sizes of $^{3}/_{4}$ in. (19 mm). Particles are angular, dense, hard, and medium to dark gray, gneissose-textured, equidimensional to elongated, variably altered, uncoated, and variably cracked. Coarse aggregate particles are well-graded and well-distributed. There is no evidence of alkali-aggregate reactions of coarse aggregate particles in the concrete in either core.

Coarse aggregate particles in concretes are similar to many unsound coarse aggregates found in other residential foundations in eastern Connecticut that have shown pyrrhotite-related distress. The similarity is in the dominance of dark gray and brown crushed quartzo-feldspathic and biotite gneiss particles as found in other foundations that have contained majority of pyrrhotite to cause oxidation-related distress. Therefore, coarse aggregates in both residences are judged to have come from a source similar to the other distressed foundations, which is reported to be from the hydrothermal vein of pyrrhotite crystallization in the Becker's quarry in Ellington, CT. The subject quarry has reportedly provided the unsound aggregates containing pyrrhotite to cause distress in numerous residential foundations across eastern Connecticut.

## FINE AGGREGATES

Fine aggregates in both cores are compositionally similar natural siliceous sands having nominal maximum sizes of $^{3}/_{8}$ in. (9.5 mm). Particles contain major amounts of quartz and quartzite, and subordinate amounts of feldspar, mica, ferruginous rock, and mafic minerals. Particles are variably colored, subangular to subrounded, dense, hard, equidimensional to elongated, unaltered, uncoated, and uncracked. Fine aggregate particles are well-graded and well-distributed. There is no evidence of alkali-aggregate reaction of fine aggregate. Fine aggregate particles in both cores are sound during their service in the concretes.

| Properties and Compositions of Aggregates | 1 Liberty Drive | 2 Fort Griswold |
|---|---|---|
| Coarse Aggregates | | |
| Types | Crushed Stone | Crushed Stone |
| Nominal maximum size (in.) | 3/4 in. (19 mm) | 3/4 in. (19 mm) |
| Rock Types | A dominant dark gray to black gneiss consisting of parallel alignment of quartz, albite feldspar, biotite mica, and occasional pyrope garnet porphyroblasts, anhedral to subhedral equigranular to gneissose arrangement of minerals;<br>A subordinate light to medium brown granite gneiss of quartz, albite feldspar, garnet, biotite mica and occasional pyroxene (augite) grains; and<br>A minor white granite gneiss with quartzo-feldspathic minerals and black specs of mica flakes in parallel alternate (gneissose) arrangements | |
| Angularity, Density, Hardness, Color, Texture, Sphericity | Angular, dense, hard, medium to dark gray, massive textured, equidimensional to elongated | |
| Cracking, Alteration, Coating | Variably altered, Uncoated, and variably cracked | Variably altered, Uncoated, and variably cracked |
| Grading & Distribution | Well-graded and Well-distributed | Well-graded and Well-distributed |
| Soundness | Sound | Sound |
| Alkali-Aggregate Reactivity | None | None |
| Fine Aggregates | | |
| Types | Natural siliceous sand | Natural siliceous sand |
| Nominal maximum size (in.) | 3/8 in. (9.5 mm) | 3/8 in. (9.5 mm) |
| Rock Types | Major amounts of quartz and quartzite, and subordinate amounts of feldspar, mica, ferruginous rock, and mafic minerals | |
| Cracking, Alteration, Coating | Variably colored, subangular to subrounded, dense, hard, equidimensional to elongated | |
| Grading & Distribution | Well-graded and Well-distributed | Well-graded and Well-distributed |
| Soundness | Sound | Sound |
| Alkali-Aggregate Reactivity | None | None |

Table 1: Properties of coarse and fine aggregates of concretes from 1 Liberty Drive and 2 Fort Griswold.

## PASTE

Properties and composition of hardened cement pastes are summarized in Table 2. Pastes at the near-surface carbonated zones along the interior foundation wall surfaces and along the major vertical cracks at the interior foundation walls in both residence are beige-toned due to atmospheric carbonation during service, but interior bodies of concretes within the walls are medium gray, non-carbonated, dense and hard. Freshly fractured surfaces of pastes have subvitreous lusters and subconchoidal textures. Residual and relict Portland cement particles are present and estimated to constitute 8 to 10 percent of the paste volumes. Hydration of Portland cement is normal

in both cores. The textural and compositional features of the pastes are indicative of cement contents similar in both concretes and estimated to be 6 to 6$^1/_2$ bags of Portland cement per cubic yard. Both concretes have water-cement ratios (*w/c)* more or less similar throughout the bodies and are estimated to be from 0.40 to 0.45. There is evidence of deleterious secondary ettringite deposits in both cores that are also found in the cores from other homes in Connecticut that have shown distress due to oxidation of pyrrhotite. Bonds between the coarse and fine aggregate particles and paste are moderately tight to weak along the cracks. There is evidence of microcracking due to deleterious reactions from pyrrhotite oxidations, which is found in other homes in eastern Connecticut that have shown pyrrhotite-oxidation-related distress. The overall qualities and conditions of the concretes in the foundation walls of both residence are found to be distressed at the time of this investigation with evidence of chemical deterioration due to oxidation of pyrrhotite that is common in other homes affected by pyrrhotite-oxidation-related cracking.

| Properties and Compositions of Paste | 1 Liberty Drive | 2 Fort Griswold |
|---|---|---|
| Color, Hardness, Porosity, Luster | Gray, dense and hard, Subtranslucent vitreous | |
| Residual Portland Cement Particles | Normal, 8 to 10 percent by paste volume | |
| Calcium hydroxide from cement hydration | Normal, 10 to 14 percent by paste volume | |
| Pozzolans, Slag, etc. | None | |
| Water-cement ratio (*w/c*), estimated | 0.40 to 0.45 | |
| Cementitious materials contents, estimated (equivalent to bags of cement per cubic yard) | 6 to 6$^1/_2$ | |
| Secondary Deposits | Evidence of poorly crystalline secondary ettringite in voids, cracks, and paste or relatively well crystalline secondary ettringite lining and filling many air-voids and sometimes in cracks as are found in other homes affected by pyrrhotite-oxidation-related distress | |
| Depth of Carbonation, mm | 20 to 25 mm from exposed interior surfaces of foundation walls and about 5 mm from the opposite exterior surfaces of walls in both residence | |
| Microcracking | Extensive microcracking in paste and unsound coarse aggregate particles | Moderate microcracking in paste and unsound coarse aggregate particles |
| Aggregate-paste Bond | Moderately tight to weak | Moderately tight |
| Bleeding, Tempering | None | None |
| Chemical deterioration | Evidence of profuse secondary ettringite from pyrrhotite oxidation related release of sulfates indicating presence of moisture and excess sulfates from pyrrhotite, as found in other homes from eastern Connecticut due to oxidation of pyrrhotite in crushed gneiss coarse aggregate during service | |

Table 2: Composition and properties of paste in two cores.

## AIR

In both cores air occurs as: (a) numerous fine, discrete, spherical and near-spherical voids having sizes of 1 mm; and (b) a few coarse near-spherical and irregularly shaped voids that are characteristic of entrapped air. Concrete in both cores are air-entrained having estimated air content of 6 to 8 percent.

## SEM-EDS STUDIES

Figures 35 to 45 provide SEM-EDS analyses of concrete from 1 Liberty Drive. Figures 46 to 51 provide SEM-EDS analyses of concrete from 2 Fort Griswold.

1. Figures 35, 39, and 46 show X-ray elemental maps to detect pyrrhotite grains in concrete that are highlighted in the iron (Fe) and sulfur (S) maps.
2. Figures 36, 37, 38, 46, 47, and 49 show X-ray elemental maps and compositional analyses of oxidized pyrrhotite grains where iron oxide veins are found within pyrrhotite mass. X-ray elemental maps show iron oxide veins highlighted in Fe and O maps with corresponding dark veins in the S-maps. This is a taletell microstructural feature of oxidation of pyrrhotite to cause expansions and associated distress.
3. Figures 40, 42, 45, 48, and 51 show compositional analyses of paste showing typical calcium silicate hydrate compositions of paste along with analyses of secondary ettringite and disseminated pyrrhotite grains. Important result from paste compositions in both cores is no contamination of sulfate ($SO_3$) from release of oxidation of pyrrhotite as found in other homes.
4. Figures 41 and 44 show X-ray elemental maps of paste showing secondary ettringite in voids highlighted in Ca, Al, and S maps, calcium silicate hydrate composition of paste highlighted in Ca and Si maps, and feldspar grains highlighted in Al, Si, and K maps.

SEM-EDS studies showed:

1. Evidence of secondary ettringite crystallization along aggregate-paste interfaces, as found in other homes;
2. Evidence of secondary ettringite crystallization in air-voids, as found in other homes of distressed foundations;
3. No evidence of sulfate contamination of paste from released sulfates from oxidation of pyrrhotite in coarse aggregates as found in other homes;
4. No evidence of gaps around aggregate due to expansion of sulfate-contaminated paste, as found in other homes;
5. Evidence of iron sulfide mineral in aggregate, identified as having lower S/Fe atomic ratio than pyrite to indicate pyrrhotite as found in other homes;
6. Evidence of oxidation of pyrrhotite and formation of iron oxide veins within pyrrhotite as found in other homes;
7. Evidence of unsoundness of pyrrhotite-bearing aggregate from expansion and cracking as found in other homes;
8. No evidence of internal sulfate attack in paste from high sulfur (as $SO_3$) level of paste compared to normal Portland cement paste, due to secondary ettringite infestation in confined areas in paste – as found in other homes;
9. No evidence of internal sulfate attack in paste from gaps around aggregates due to expansion of paste and secondary ettringite crystallization along aggregate-paste interfaces – as found in other homes.

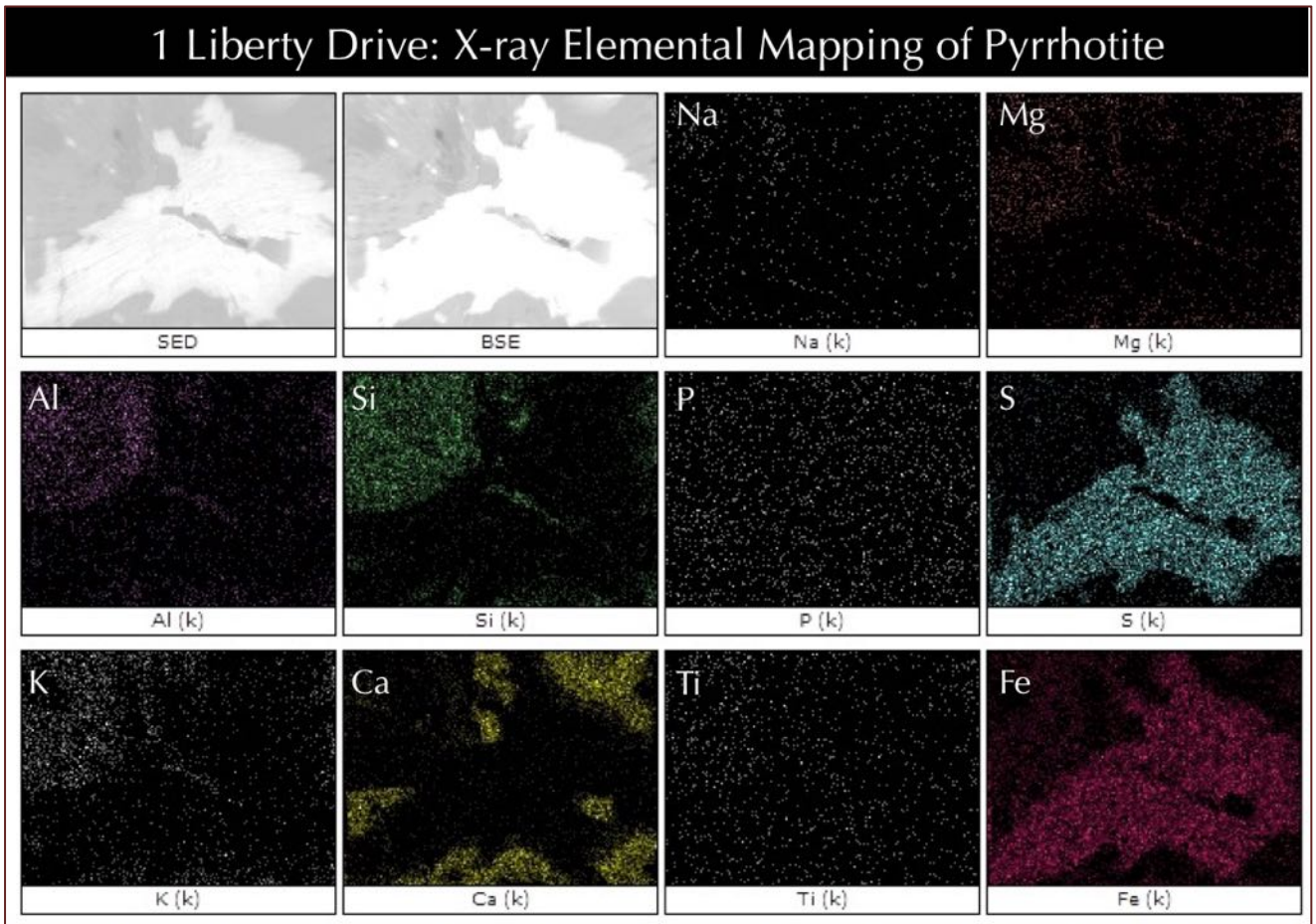


| Probe | CaO | $SiO_2$ | $Al_2O_3$ | $Na_2O$ | MgO | $SO_3$ | $K_2O$ | $TiO_2$ | FeO | Total | Phase |
|---|---|---|---|---|---|---|---|---|---|---|---|
| 1 | 0.04 | 2.85 | 0.07 | 0.13 | 0.09 | 26.75 | 0.04 | 0.05 | 69.99 | 100.01 | Pyrrhotite |
| 2 | 0.45 | 0.74 | 0.04 | 0.07 | 0.05 | 19.55 | 0.39 | 0.03 | 78.68 | 100.00 | Pyrrhotite |
| 3 | 0.76 | 0.06 | 0.08 | 0.15 | 0.11 | 21.06 | 0.36 | 0.13 | 77.30 | 100.01 | Pyrrhotite |

Figure 35: Secondary electron image (top left), corresponding backscatter electron image (2nd from top left) and corresponding X-ray elemental maps (rest) of Core from 1 Liberty Drive showing pyrrhotite grains highlighted in iron (Fe) and sulfur (S) maps, calcium silicate hydrate paste highlighted in calcium (Ca) and silicon (Si) maps, and feldspar grains in aggregate highlighted in aluminum (Al), silicon (Si), and potassium (K) maps. The bottom Table shows compositional analysis of pyrrhotite grains showing 70 to 78% FeO and 20 to 26% $SO_3$.

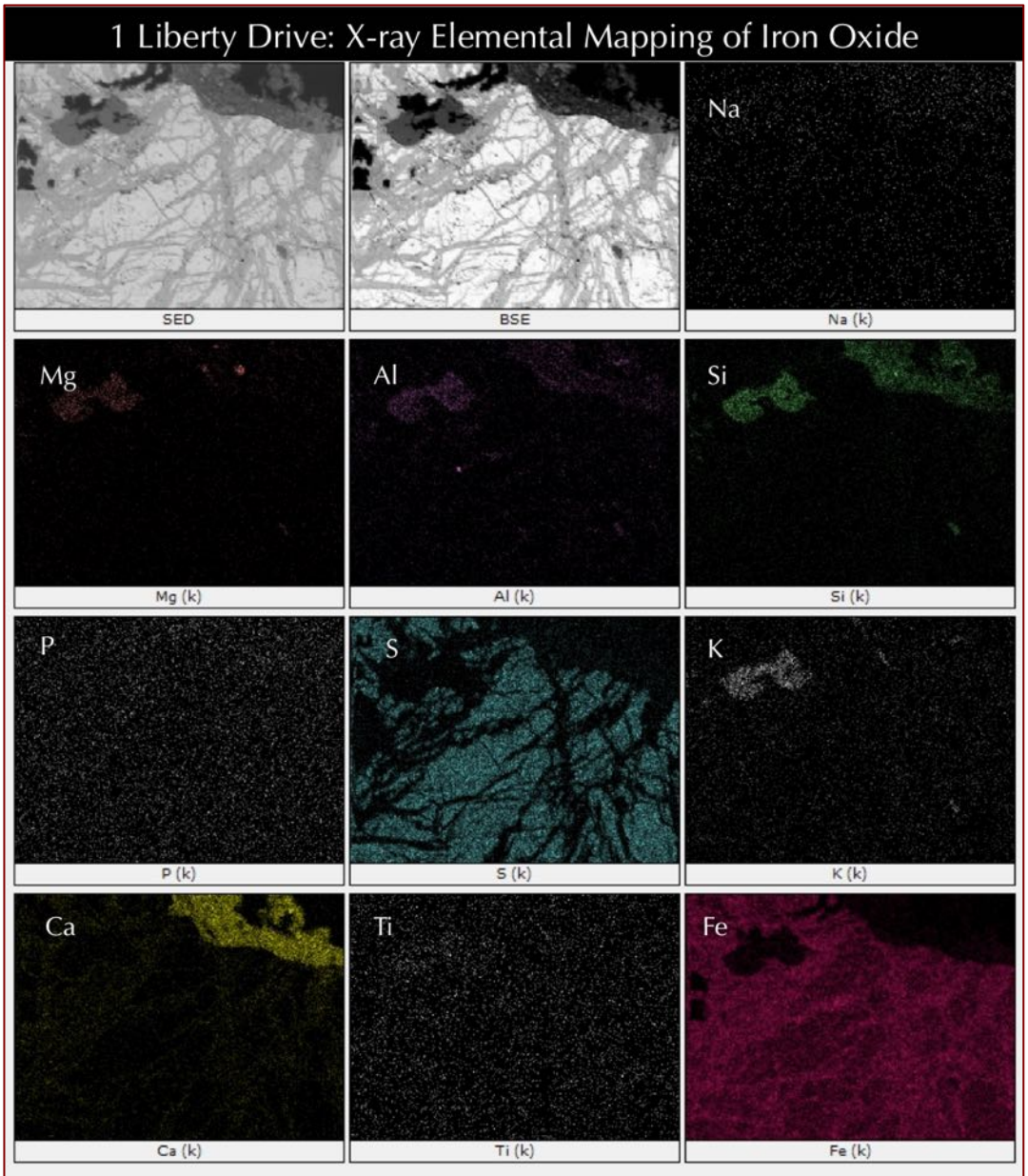


Analysis of Dark Oxidized Veins in Pyrrhotite

| Probe | CaO | $SiO_2$ | $Al_2O_3$ | $Na_2O$ | MgO | $SO_3$ | $K_2O$ | $TiO_2$ | FeO | Total | Phase |
|---|---|---|---|---|---|---|---|---|---|---|---|
| 1 | 4.48 | 0.01 | 0.02 | 0.04 | 0.03 | 0.01 | 0.01 | 0.75 | 94.65 | 100.00 | Iron Oxide |
| 2 | 3.79 | 0.01 | 0.14 | 0.04 | 0.03 | 0.01 | 0.22 | 0.01 | 95.75 | 100.00 | Iron Oxide |
| 3 | 3.24 | 0.01 | 0.02 | 0.04 | 0.03 | 0.01 | 0.01 | 0.01 | 96.63 | 100.00 | Iron Oxide |

Figure 36: Secondary electron image (top left), corresponding backscatter electron image (2nd from top left) and corresponding X-ray elemental maps (rest) of Core from 1 Liberty Drive showing pyrrhotite grains highlighted in iron (Fe) and sulfur (S) maps, oxidized iron within pyrrhotite that appear as dark veins in S map, calcium silicate hydrate paste highlighted in calcium (Ca) and silicon (Si) maps, and feldspar grains in aggregate highlighted in aluminum (Al), silicon (Si), and potassium (K) maps. Some biotite grains are highlighted in Mg map. The bottom Table shows compositional analysis of oxidized iron veins in pyrrhotite showing 95 to 96% FeO.

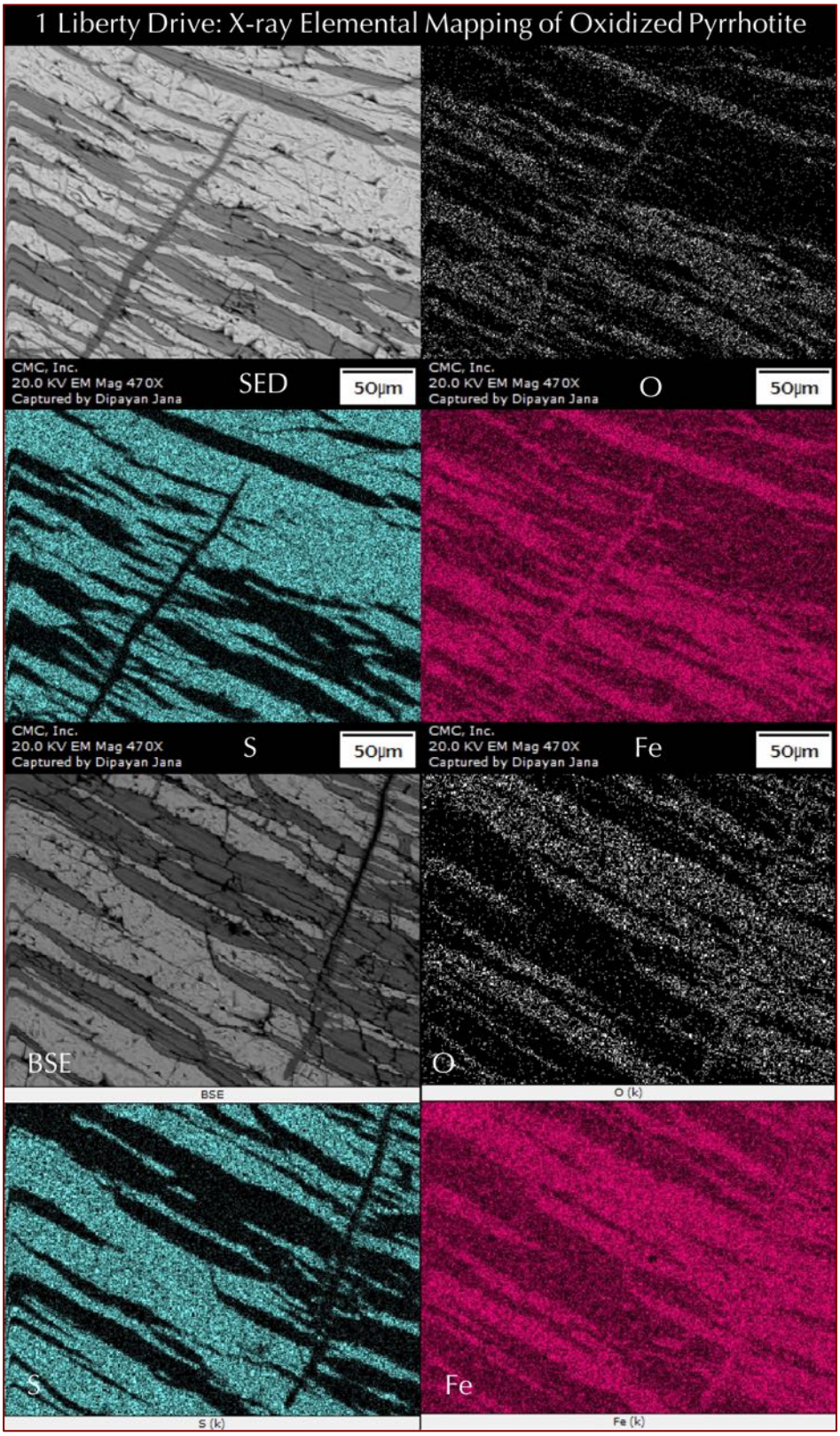


Figure 37: Secondary electron image (top left) and corresponding X-ray elemental maps of an oxidized pyrrhotite grain showing veins of oxidized iron within the pyrrhotite as highlighted by iron (Fe) and oxygen (O) maps for oxidized iron veins, which appear as dark veins in S-map within the pyrrhotite as highlighted in Fe and S maps. Similar compositional features are seen in another oxidized pyrrhotite grain in the bottom two rows.

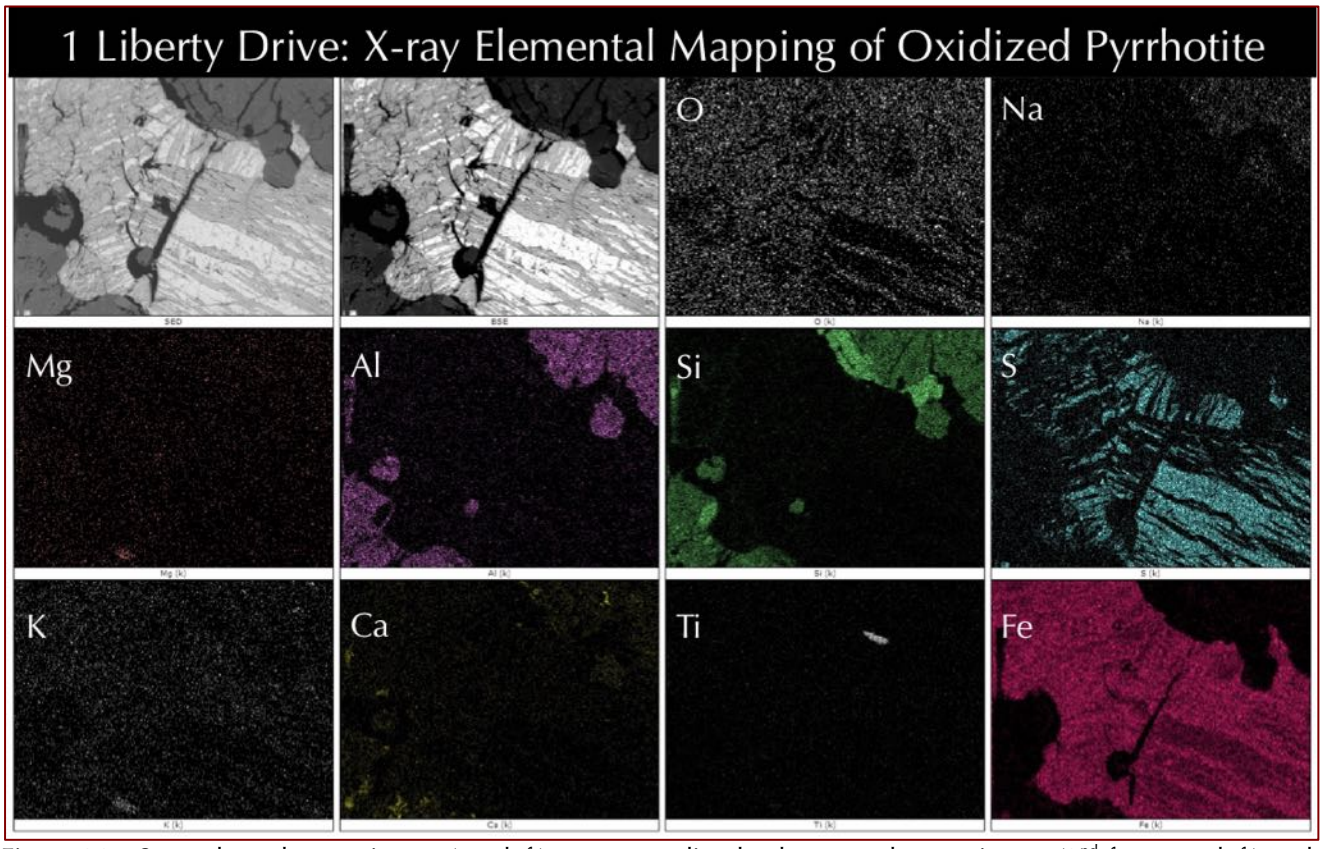


Figure 38: Secondary electron image (top left), corresponding backscatter electron image (2nd from top left) and corresponding X-ray elemental maps (rest) of Core from 1 Liberty Drive showing a veined oxidized pyrrhotite grain highlighted in iron (Fe) and sulfur (S) maps, that has veins of oxidized iron as highlighted in Fe and O maps (which appear as dark veins in S map).

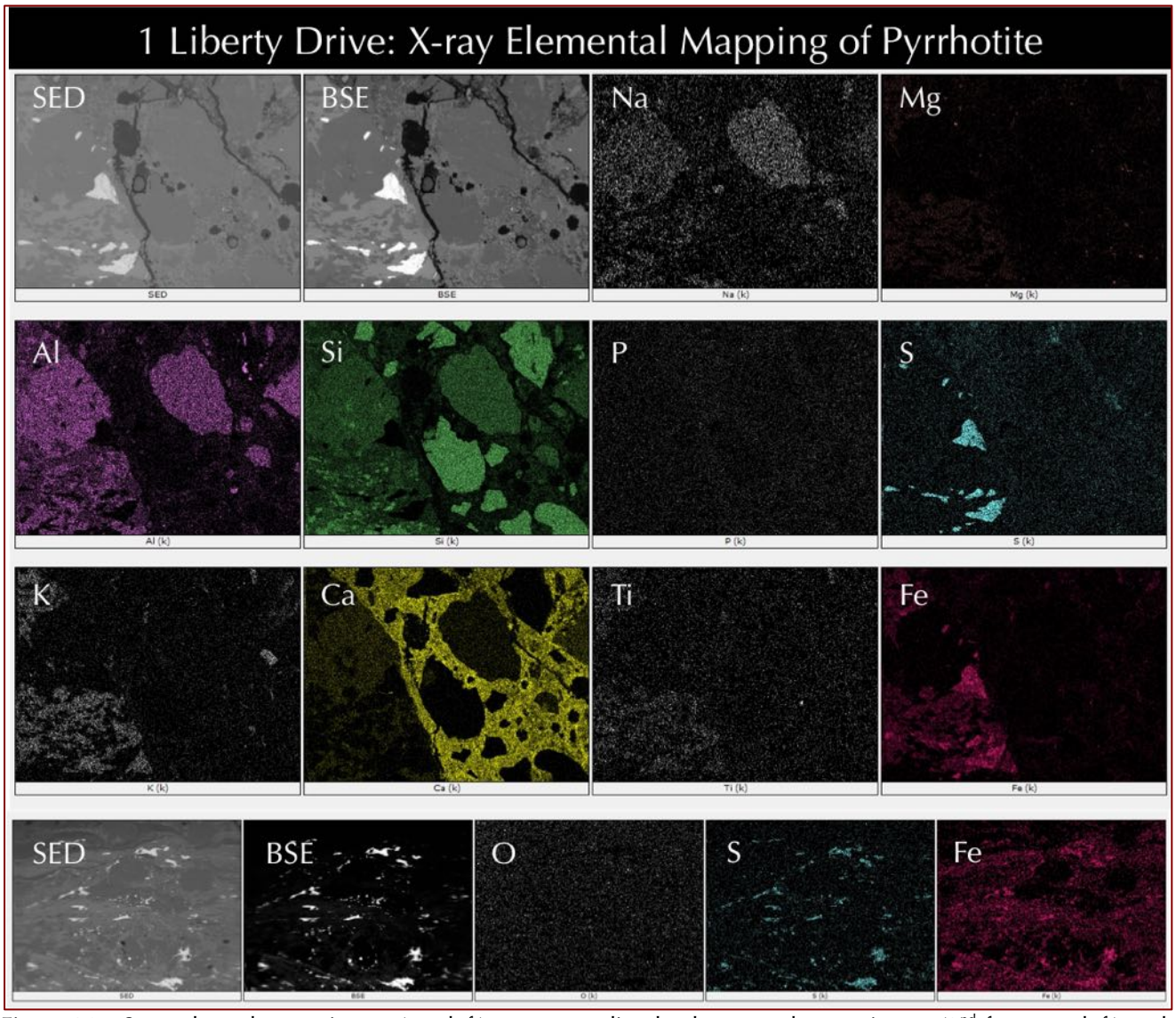


Figure 39: Secondary electron image (top left), corresponding backscatter electron image (2nd from top left) and corresponding X-ray elemental maps (rest) of Core from 1 Liberty Drive showing disseminated pyrrhotite grains highlighted in iron (Fe) and sulfur (S) maps, calcium silicate hydrate paste highlighted in calcium (Ca) and silicon (Si) maps, and feldspar grains in aggregate highlighted in aluminum (Al), silicon (Si), and potassium (K) maps. The bottom row shows another area of paste where fine disseminated pyrrhotite grains are seen in Fe and S maps.

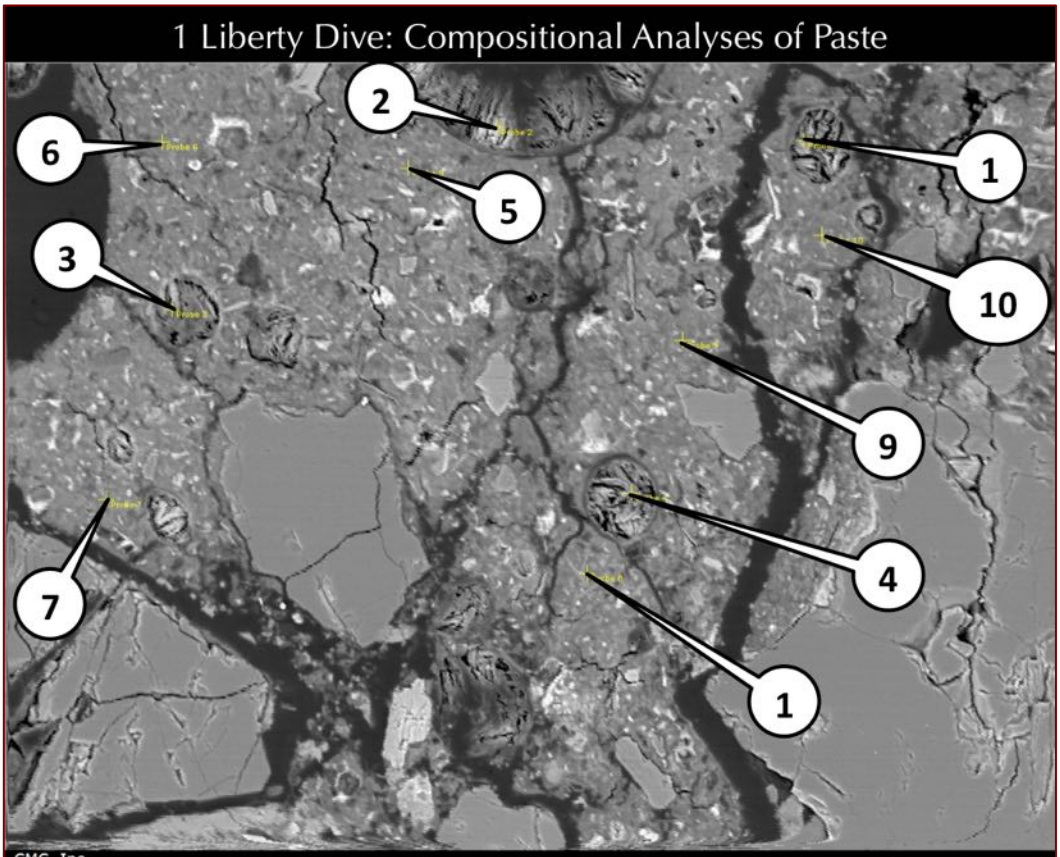


| Probe | CaO | $SiO_2$ | $Al_2O_3$ | $Na_2O$ | MgO | $SO_3$ | $K_2O$ | $TiO_2$ | FeO | Total | Phase |
|---|---|---|---|---|---|---|---|---|---|---|---|
| 1 | 68.98 | 9.24 | 9.52 | 0.01 | 0.00 | 11.80 | 0.45 | 0.01 | 0.01 | 100.02 | Ettringite |
| 2 | 61.01 | 11.42 | 13.10 | 0.01 | 0.00 | 11.56 | 0.30 | 0.11 | 2.49 | 100.00 | Ettringite |
| 3 | 60.32 | 7.84 | 15.94 | 0.01 | 0.01 | 12.43 | 0.00 | 2.14 | 1.31 | 100.00 | Ettringite |
| 4 | 63.27 | 6.07 | 11.52 | 0.01 | 0.04 | 16.40 | 0.66 | 0.01 | 2.02 | 100.00 | Paste |
| 5 | 61.12 | 32.02 | 0.84 | 0.01 | 0.01 | 0.01 | 0.01 | 0.46 | 5.52 | 100.00 | Paste |
| 6 | 56.44 | 33.12 | 2.88 | 0.02 | 0.01 | 0.01 | 0.01 | 0.72 | 6.80 | 100.01 | Paste |
| 7 | 57.05 | 34.08 | 1.57 | 0.02 | 0.01 | 0.01 | 0.18 | 2.46 | 4.63 | 100.01 | Paste |
| 8 | 53.16 | 33.02 | 4.15 | 0.01 | 0.01 | 0.00 | 0.00 | 0.01 | 9.63 | 99.99 | Paste |
| 9 | 56.83 | 27.85 | 5.04 | 0.02 | 0.24 | 0.53 | 0.25 | 0.01 | 9.23 | 100.00 | Paste |
| 10 | 48.00 | 38.51 | 6.39 | 0.01 | 0.48 | 0.01 | 1.99 | 0.13 | 4.49 | 100.01 | Paste |

Figure 40: Backscatter electron image (top) and X-ray compositional analyses of concrete in the Core from 1 Liberty Drive showing compositions of secondary ettringite deposits in voids and various areas of paste at the tips of callouts that are provided in the Table below the image. Secondary ettringite shows high Ca, Al, and S whereas paste shows typical calcium silicate hydrate composition with negligible or no evidence of contamination by sulfates released from pyrrhotite oxidation, which is typically found in many other pyrrhotite-related distress in the area.

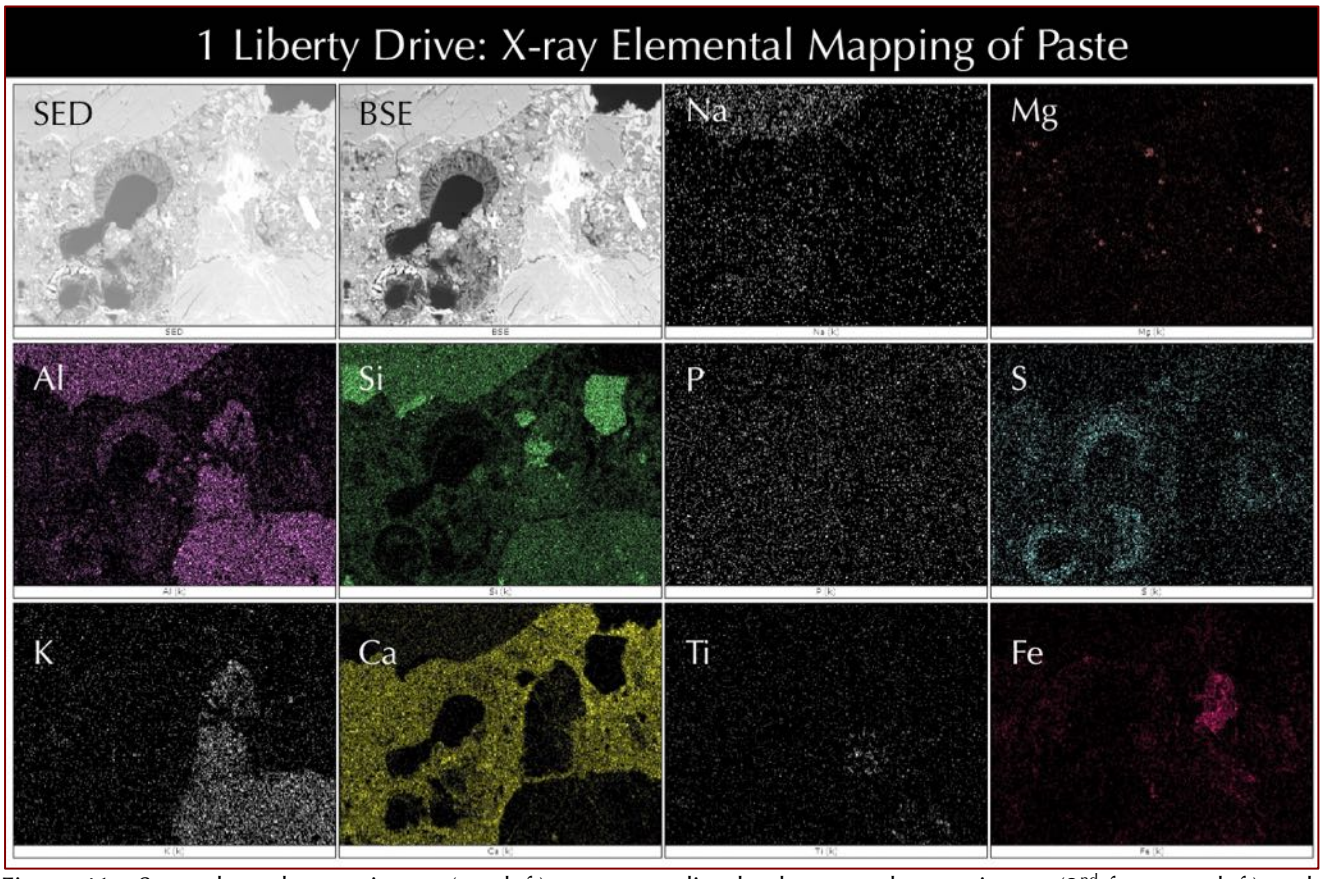


Figure 41: Secondary electron image (top left), corresponding backscatter electron image (2nd from top left) and corresponding X-ray elemental maps (rest) of Core from 1 Liberty Drive showing calcium silicate hydrate paste highlighted in calcium (Ca) and silicon (Si) maps, feldspar grains in aggregate highlighted in aluminum (Al), silicon (Si), and sodium and potassium (Na and K) maps, and secondary ettringite deposits in air voids highlighted in Ca, Al, and S maps.

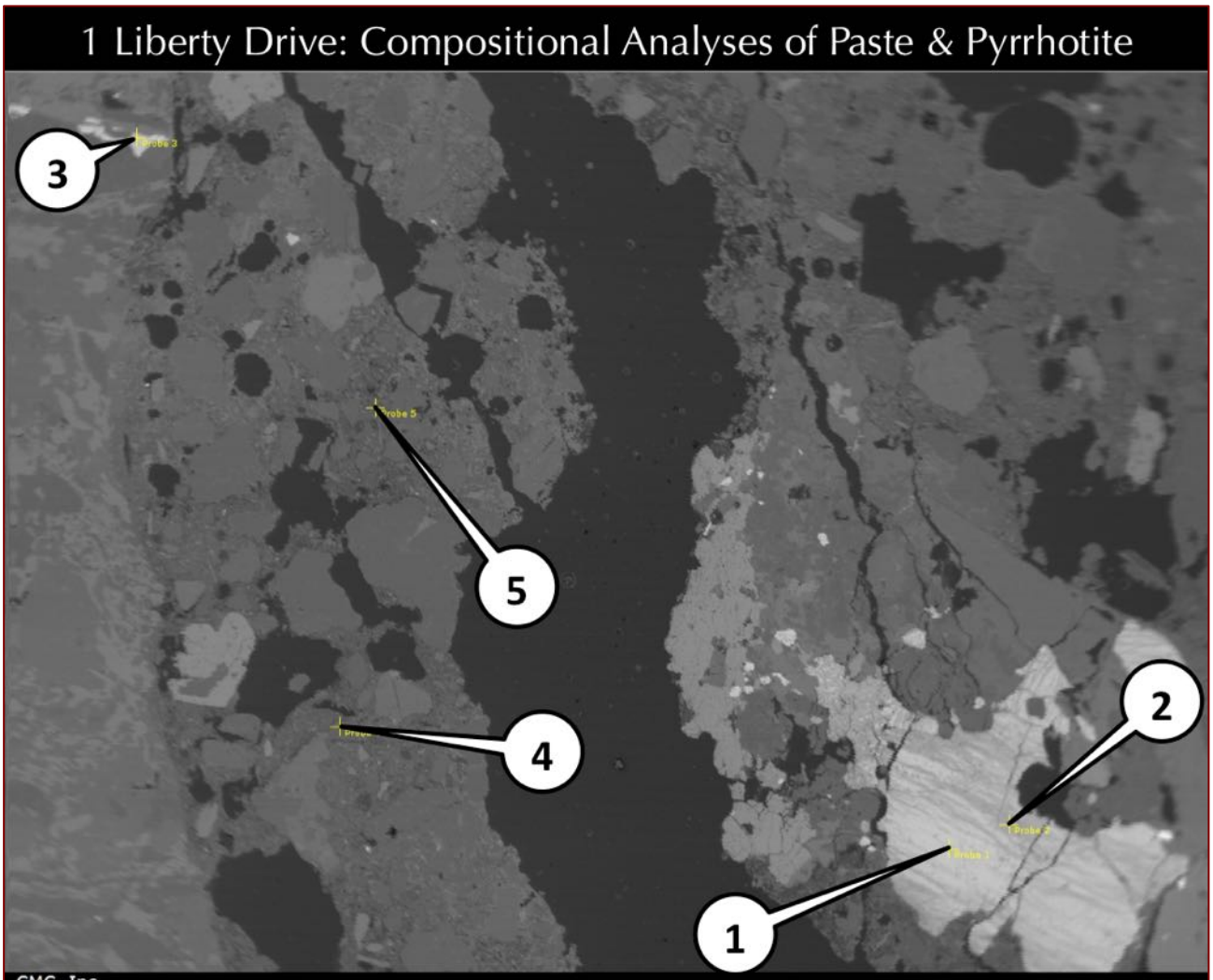


| Probe | CaO | $SiO_2$ | $Al_2O_3$ | $Na_2O$ | MgO | $SO_3$ | $K_2O$ | $TiO_2$ | FeO | Total | Phase |
|---|---|---|---|---|---|---|---|---|---|---|---|
| 1 | 0.03 | 0.19 | 0.29 | 0.10 | 0.25 | 27.52 | 0.03 | 0.69 | 70.90 | 100.00 | Pyrrhotite |
| 2 | 0.24 | 0.64 | 0.01 | 0.02 | 0.02 | 2.17 | 0.32 | 0.01 | 96.58 | 100.01 | Iron Oxide |
| 3 | 0.03 | 0.19 | 0.29 | 0.10 | 0.25 | 22.52 | 0.03 | 0.69 | 75.90 | 100.00 | Pyrrhotite |
| 4 | 52.91 | 28.05 | 4.60 | 0.01 | 0.69 | 0.00 | 1.10 | 1.52 | 11.12 | 100.00 | Paste |
| 5 | 52.50 | 23.71 | 5.55 | 0.01 | 1.02 | 0.00 | 0.18 | 0.01 | 17.02 | 100.00 | Paste |

Figure 42: Backscatter electron image (top) and X-ray compositional analyses of concrete in the Core from 1 Liberty Drive showing compositions of pyrrhotite, oxidized iron, and various areas of paste at the tips of callouts that are provided in the Table below the image. Two pyrrhotite grains show typical high FeO and $SO_3$, oxidized iron veins within pyrrhotite show mostly FeO, whereas paste shows typical calcium silicate hydrate composition with no evidence of contamination by sulfates released from pyrrhotite oxidation, which is typically found in many other pyrrhotite-related distress in the area.

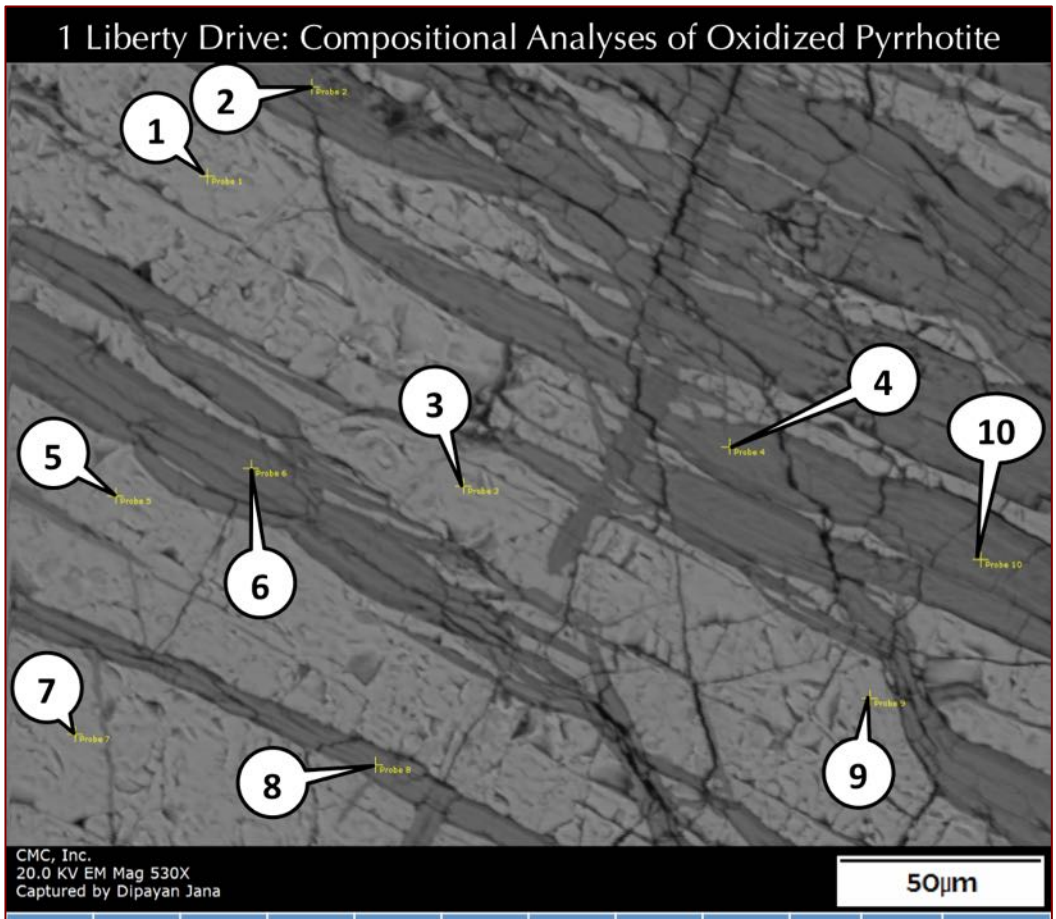


| Probe | CaO | $SiO_2$ | $Al_2O_3$ | $Na_2O$ | MgO | $SO_3$ | $K_2O$ | $TiO_2$ | FeO | Total | Phase |
|---|---|---|---|---|---|---|---|---|---|---|---|
| 1 | 0.24 | 0.28 | 0.10 | 0.17 | 0.12 | 32.72 | 0.15 | 0.15 | 66.07 | 100.00 | Pyrrhotite |
| 2 | 1.51 | 1.19 | 0.01 | 0.02 | 0.01 | 0.63 | 0.15 | 0.94 | 95.54 | 100.00 | Iron Oxide |
| 3 | 0.24 | 0.28 | 0.10 | 0.17 | 0.12 | 32.72 | 0.15 | 0.15 | 66.07 | 100.00 | Pyrrhotite |
| 4 | 0.65 | 1.47 | 0.01 | 0.02 | 0.01 | 0.00 | 1.40 | 0.01 | 96.44 | 100.01 | Iron Oxide |
| 5 | 0.24 | 0.28 | 0.10 | 0.17 | 0.12 | 32.72 | 0.15 | 0.15 | 66.07 | 100.00 | Pyrrhotite |
| 6 | 0.00 | 1.05 | 0.01 | 0.02 | 0.01 | 0.13 | 1.47 | 0.12 | 97.19 | 100.00 | Iron Oxide |
| 7 | 0.06 | 0.08 | 0.10 | 0.20 | 0.15 | 28.98 | 0.06 | 1.13 | 69.25 | 100.01 | Pyrrhotite |
| 8 | 0.13 | 0.36 | 0.11 | 0.01 | 0.01 | 0.11 | 1.30 | 0.00 | 97.96 | 99.99 | Iron Oxide |
| 9 | 0.05 | 0.06 | 0.09 | 0.17 | 0.12 | 34.87 | 0.03 | 0.06 | 64.55 | 100.00 | Pyrrhotite |
| 10 | 1.26 | 1.37 | 0.01 | 0.01 | 0.01 | 0.00 | 0.91 | 0.01 | 96.42 | 100.00 | Iron Oxide |

Figure 43: Backscatter electron image (top) and X-ray compositional analyses of concrete in the Core from 1 Liberty Drive showing compositions of oxidized iron veins within a pyrrhotite measured at the tips of callouts that are provided in the Table below the image. Pyrrhotite shows typical high FeO and $SO_3$ whereas oxidized iron veins within pyrrhotite show mostly FeO.

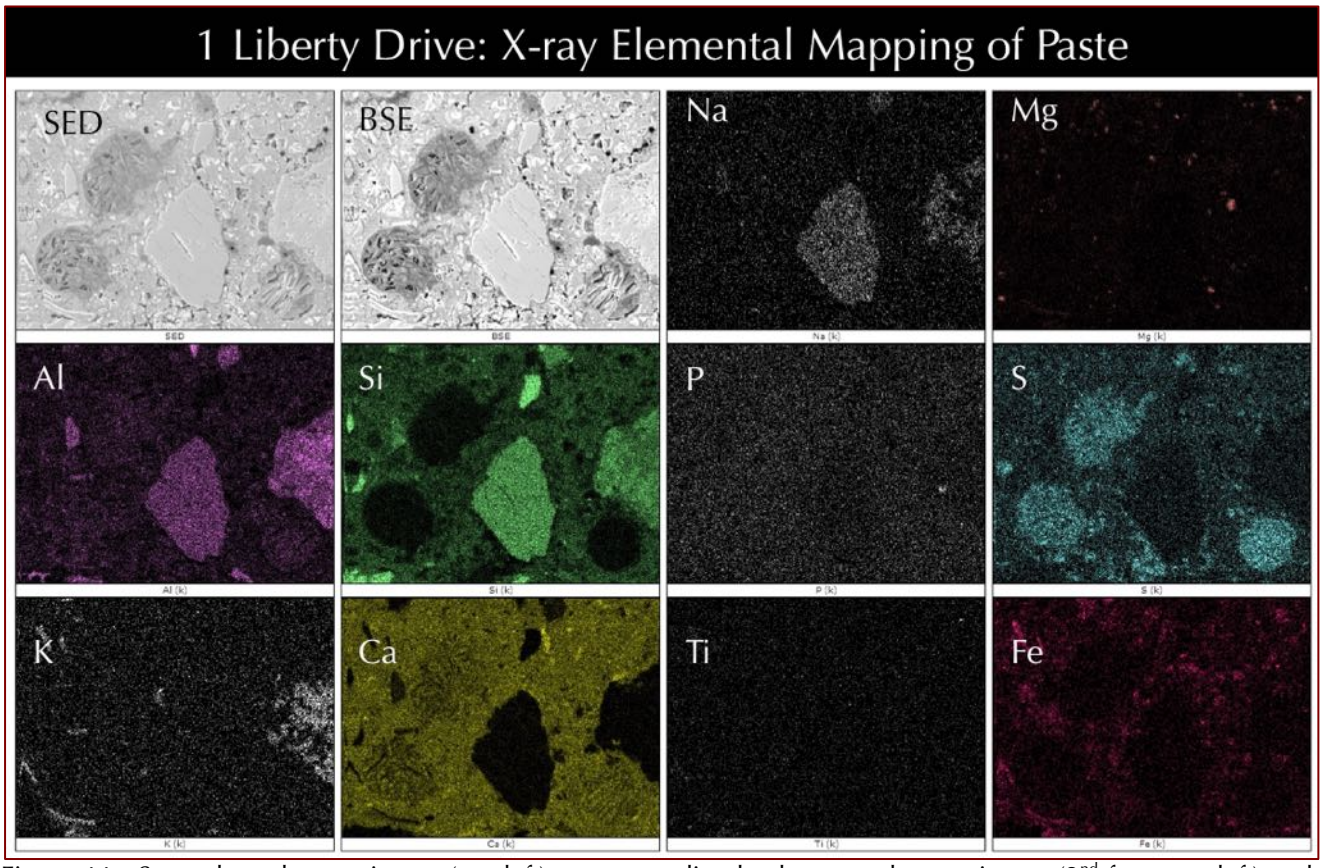


Figure 44: Secondary electron image (top left), corresponding backscatter electron image (2nd from top left) and corresponding X-ray elemental maps (rest) of Core from 1 Liberty Drive showing calcium silicate hydrate paste highlighted in calcium (Ca) and silicon (Si) maps, feldspar grains in aggregate highlighted in aluminum (Al), silicon (Si), and sodium and potassium (Na and K) maps, and secondary ettringite deposits in air voids highlighted in Ca, Al, and S maps.

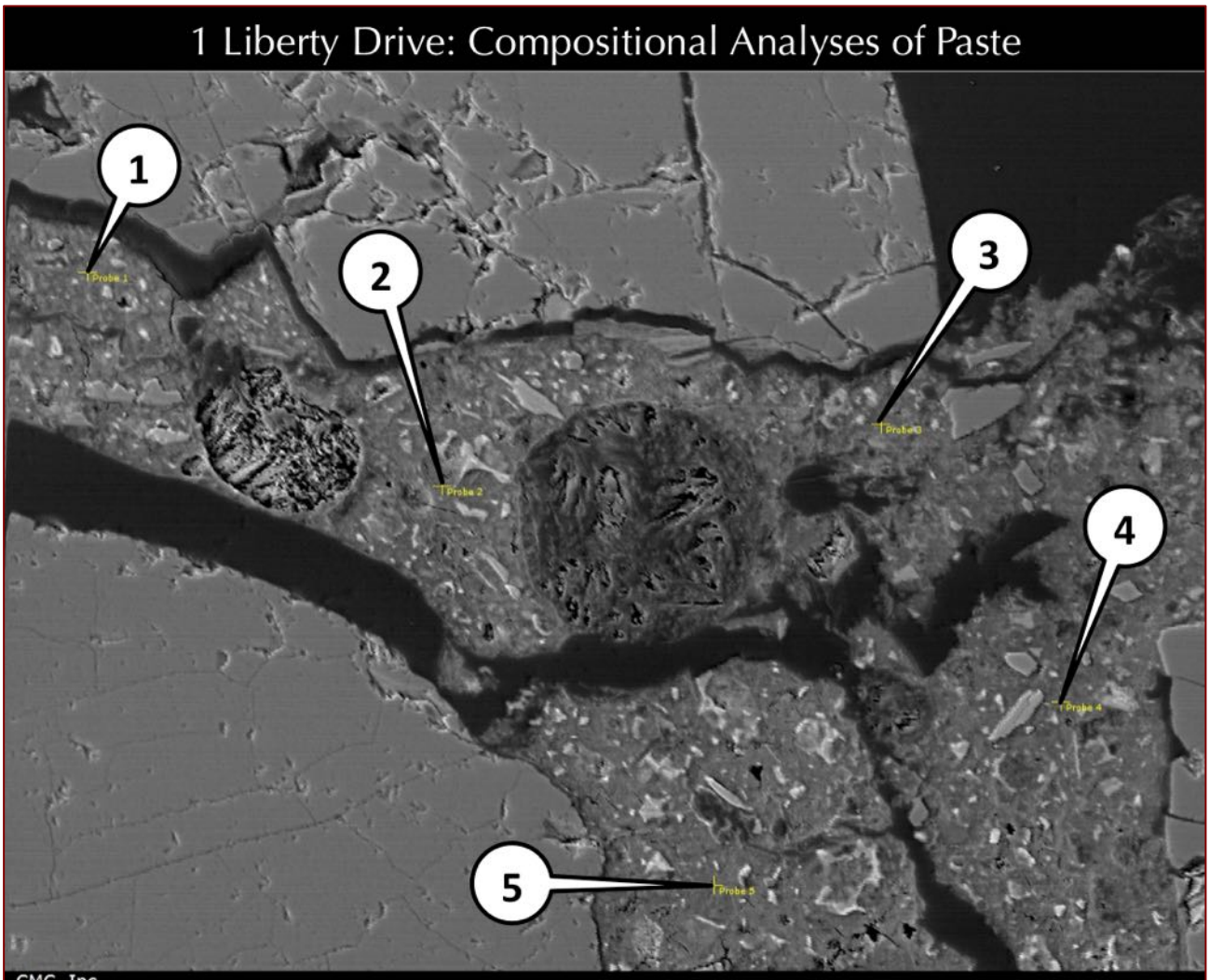


| Probe | CaO | $SiO_2$ | $Al_2O_3$ | $Na_2O$ | MgO | $SO_3$ | $K_2O$ | $TiO_2$ | FeO | Total | Phase |
|---|---|---|---|---|---|---|---|---|---|---|---|
| 1 | 59.13 | 24.35 | 7.79 | 0.01 | 0.18 | 0.01 | 0.64 | 1.10 | 6.80 | 100.01 | Paste |
| 2 | 51.30 | 39.49 | 6.25 | 0.02 | 0.89 | 0.01 | 0.01 | 0.35 | 1.70 | 100.02 | Paste |
| 3 | 59.28 | 31.93 | 3.73 | 0.01 | 0.01 | 0.00 | 0.00 | 0.75 | 4.28 | 99.99 | Paste |
| 4 | 58.29 | 27.08 | 5.07 | 0.01 | 0.00 | 0.00 | 0.41 | 0.01 | 9.12 | 99.99 | Paste |
| 5 | 54.63 | 17.14 | 24.47 | 0.01 | 0.01 | 0.01 | 0.66 | 0.01 | 3.07 | 100.01 | Paste |

Figure 45: Backscatter electron image (top) and X-ray compositional analyses of concrete in the Core from 1 Liberty Drive showing compositions of various areas of paste at the tips of callouts that are provided in the Table below the image. Paste shows typical calcium silicate hydrate composition with negligible or no evidence of contamination by sulfates released from pyrrhotite oxidation, which is typically found in many other pyrrhotite-related distress in the area.

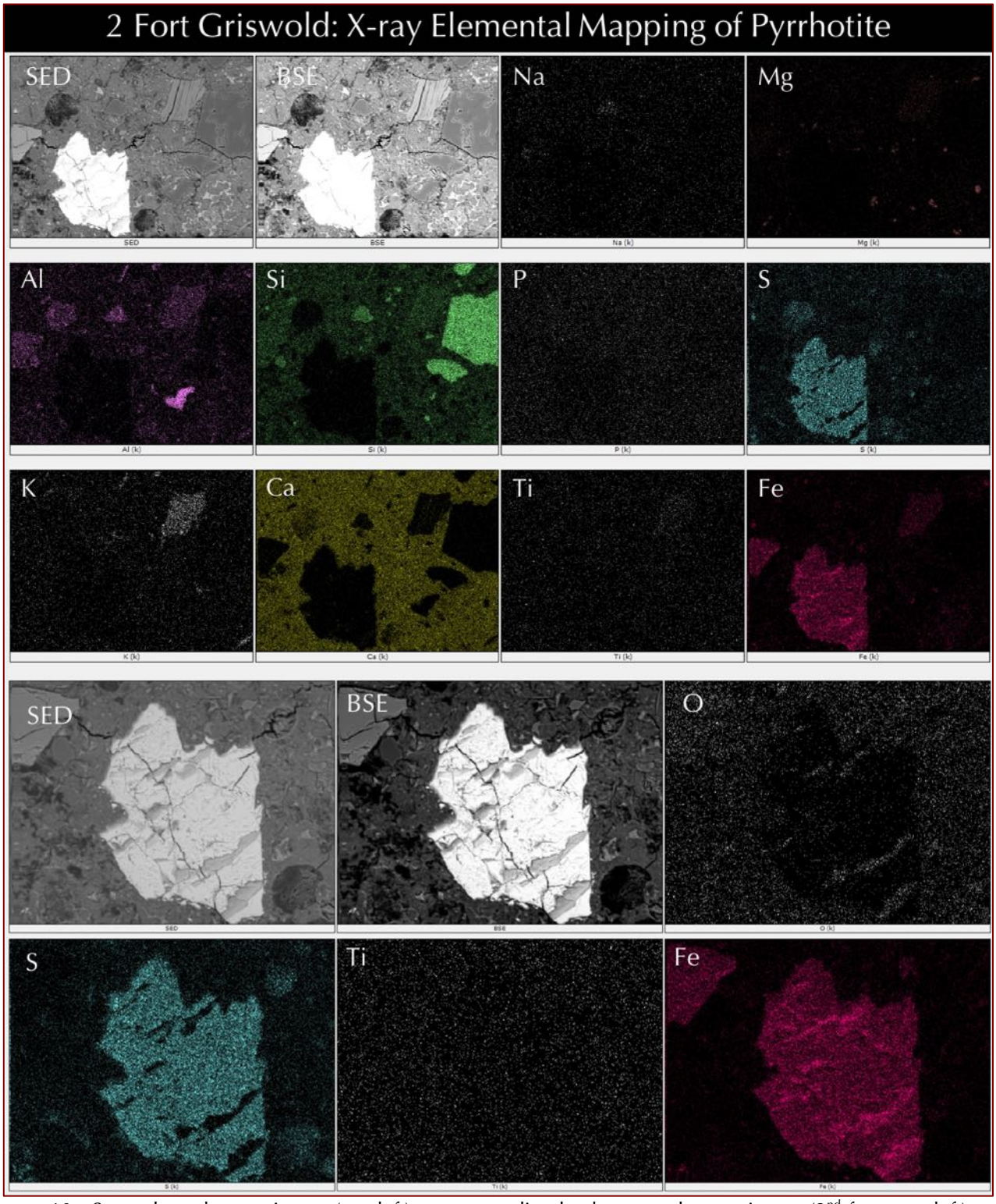


Figure 46: Secondary electron image (top left), corresponding backscatter electron image (2nd from top left) and corresponding X-ray elemental maps (rest) of Core from 2 Fort Griswold showing pyrrhotite grains highlighted in iron (Fe) and sulfur (S) maps, calcium silicate hydrate paste highlighted in calcium (Ca) and silicon (Si) maps, and feldspar grains in aggregate highlighted in aluminum (Al), silicon (Si), and potassium (K) maps. The bottom set shows another pyrrhotite grain highlighted in Fe and S maps that has veins of oxidized iron as highlighted in Fe and O maps and appeared as dark veins in S map.

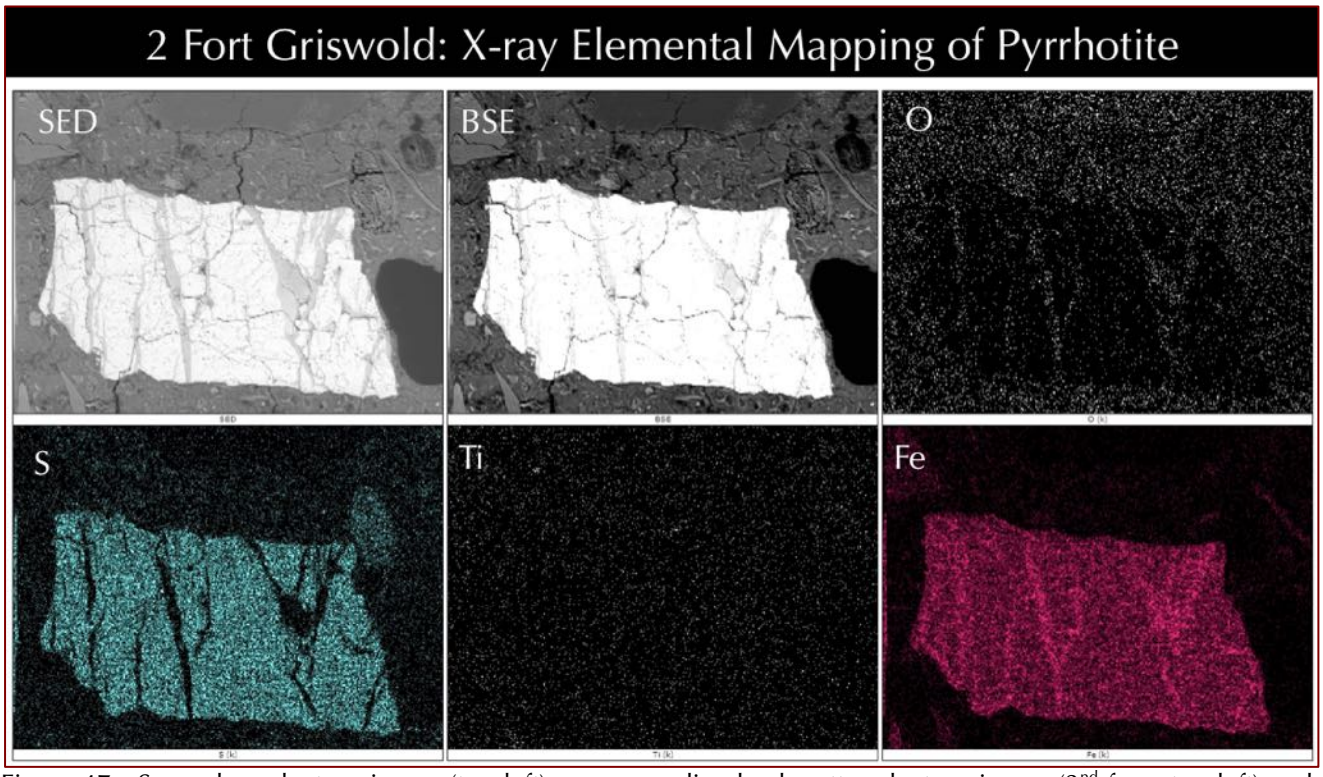


Figure 47: Secondary electron image (top left), corresponding backscatter electron image (2nd from top left) and corresponding X-ray elemental maps (rest) of Core from 2 Fort Griswold showing an oxidized pyrrhotite grain highlighted in Fe and S maps that has veins of oxidized iron as highlighted in Fe and O maps and appeared as dark veins in S map. Notice O map shows veins in pyrrhotite as well as the paste around pyrrhotite whereas it appears dark within the pyrrhotite grain.

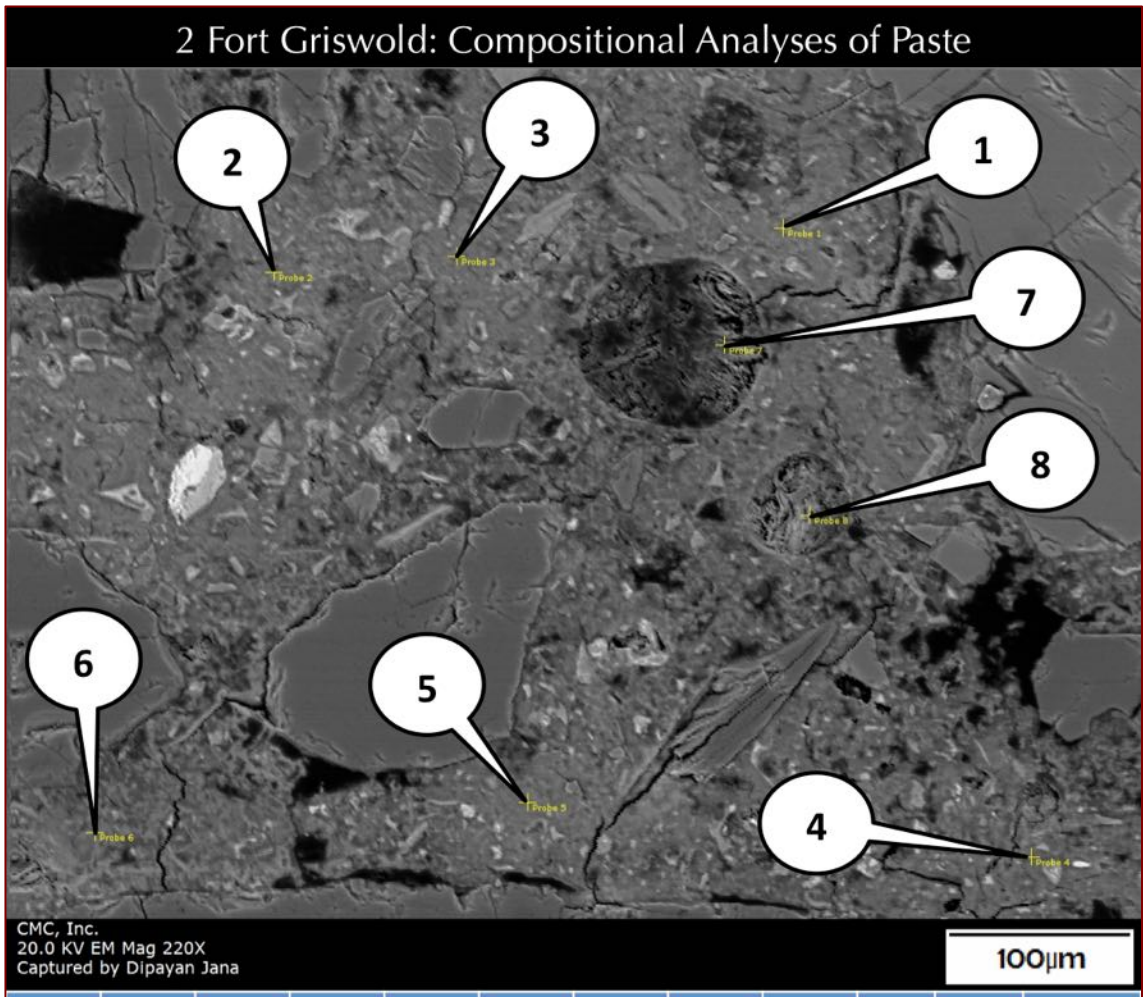


| Probe | CaO | $SiO_2$ | $Al_2O_3$ | $Na_2O$ | MgO | $SO_3$ | $K_2O$ | $TiO_2$ | FeO | Total | Phase |
|---|---|---|---|---|---|---|---|---|---|---|---|
| 1 | 66.87 | 21.78 | 4.43 | 0.01 | 0.73 | 0.00 | 0.84 | 1.65 | 3.67 | 99.98 | Paste |
| 2 | 49.48 | 29.99 | 6.21 | 0.25 | 2.69 | 0.00 | 3.13 | 0.28 | 7.97 | 100.00 | Paste |
| 3 | 63.83 | 29.39 | 2.06 | 0.01 | 0.01 | 0.00 | 0.21 | 0.54 | 3.95 | 100.00 | Paste |
| 4 | 60.59 | 29.50 | 4.58 | 0.04 | 1.63 | 0.00 | 0.07 | 0.31 | 3.28 | 100.00 | Paste |
| 5 | 58.66 | 28.92 | 4.38 | 0.01 | 0.24 | 0.00 | 0.17 | 1.69 | 5.92 | 99.99 | Paste |
| 6 | 66.89 | 26.02 | 3.46 | 0.01 | 0.00 | 0.61 | 1.05 | 0.01 | 1.95 | 100.00 | Paste |
| 7 | 58.21 | 6.78 | 21.25 | 0.01 | 0.00 | 13.70 | 0.00 | 0.04 | 0.01 | 100.00 | Ettringite |
| 8 | 56.69 | 5.49 | 21.50 | 0.01 | 0.01 | 15.42 | 0.67 | 0.01 | 0.20 | 100.00 | Ettringite |

Figure 48: Backscatter electron image (top) and X-ray compositional analyses of concrete in the Core from 2 Fort Griswold showing compositions of secondary ettringite deposits in voids and various areas of paste at the tips of callouts that are provided in the Table below the image. Secondary ettringite shows high Ca, Al, and S whereas paste shows typical calcium silicate hydrate composition with negligible or no evidence of contamination by sulfates released from pyrrhotite oxidation, which is typically found in many other pyrrhotite-related distress in the area.

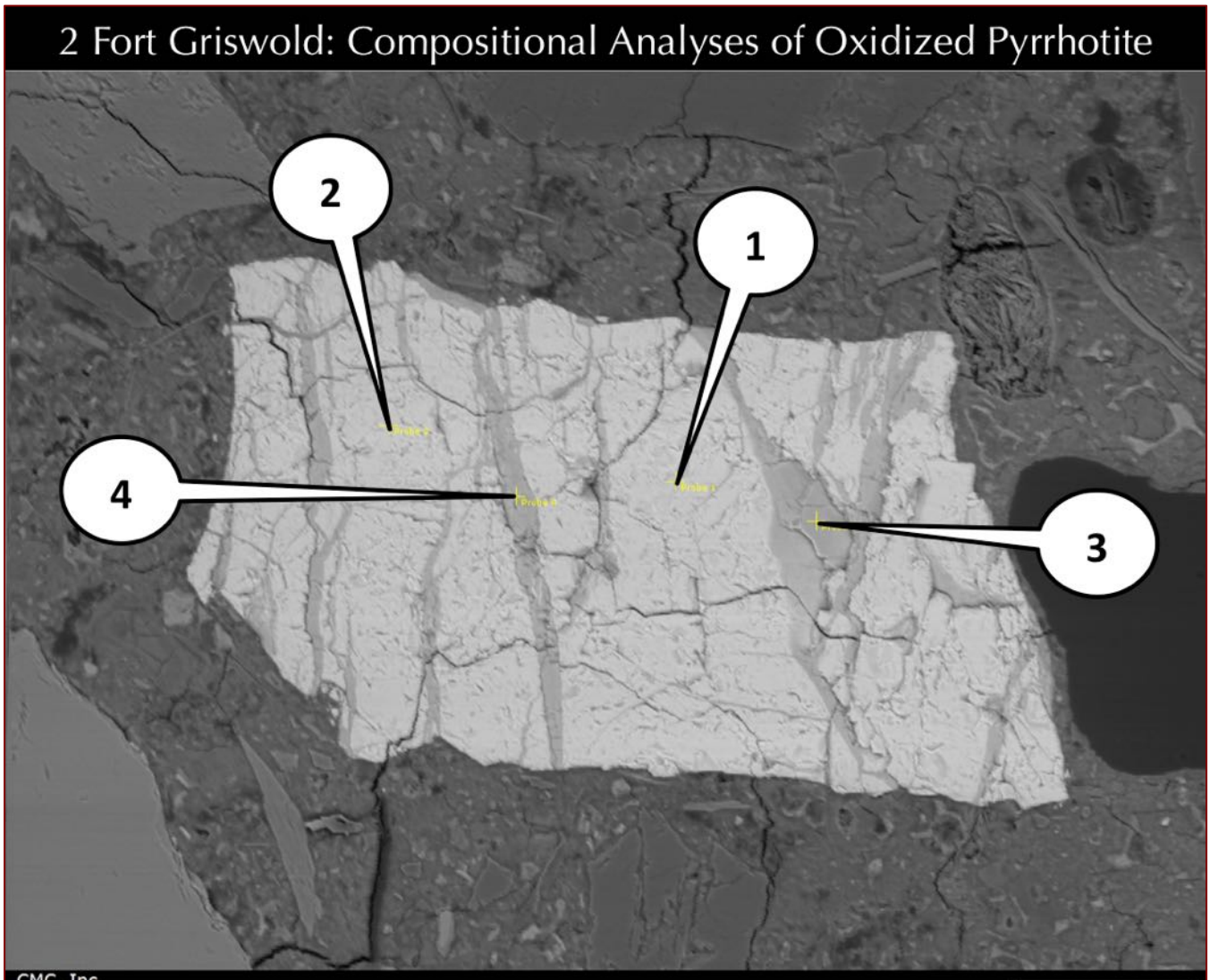


| Probe | CaO | $SiO_2$ | $Al_2O_3$ | $Na_2O$ | MgO | $SO_3$ | $K_2O$ | $TiO_2$ | FeO | Total | Phase |
|---|---|---|---|---|---|---|---|---|---|---|---|
| 1 | 0.06 | 0.09 | 0.01 | 0.02 | 0.02 | 32.61 | 0.01 | 0.01 | 67.18 | 100.01 | Pyrrhotite |
| 2 | 0.11 | 0.38 | 0.23 | 0.01 | 0.01 | 30.33 | 0.00 | 0.50 | 68.41 | 99.98 | Pyrrhotite |
| 3 | 3.30 | 1.66 | 1.87 | 0.00 | 0.00 | 0.00 | 0.31 | 0.00 | 92.86 | 100.00 | Iron Oxide |
| 4 | 0.99 | 1.62 | 0.11 | 0.00 | 0.00 | 0.00 | 0.80 | 0.13 | 96.35 | 100.00 | Iron Oxide |

Figure 49: Backscatter electron image (top) and X-ray compositional analyses of concrete in the Core from 2 Fort Griswold showing compositions of oxidized iron veins within a pyrrhotite measured at the tips of callouts that are provided in the Table below the image. Pyrrhotite shows typical high FeO and $SO_3$ whereas oxidized iron veins within pyrrhotite show mostly FeO. Figure 47 shows elemental maps of this oxidized pyrrhotite grain.

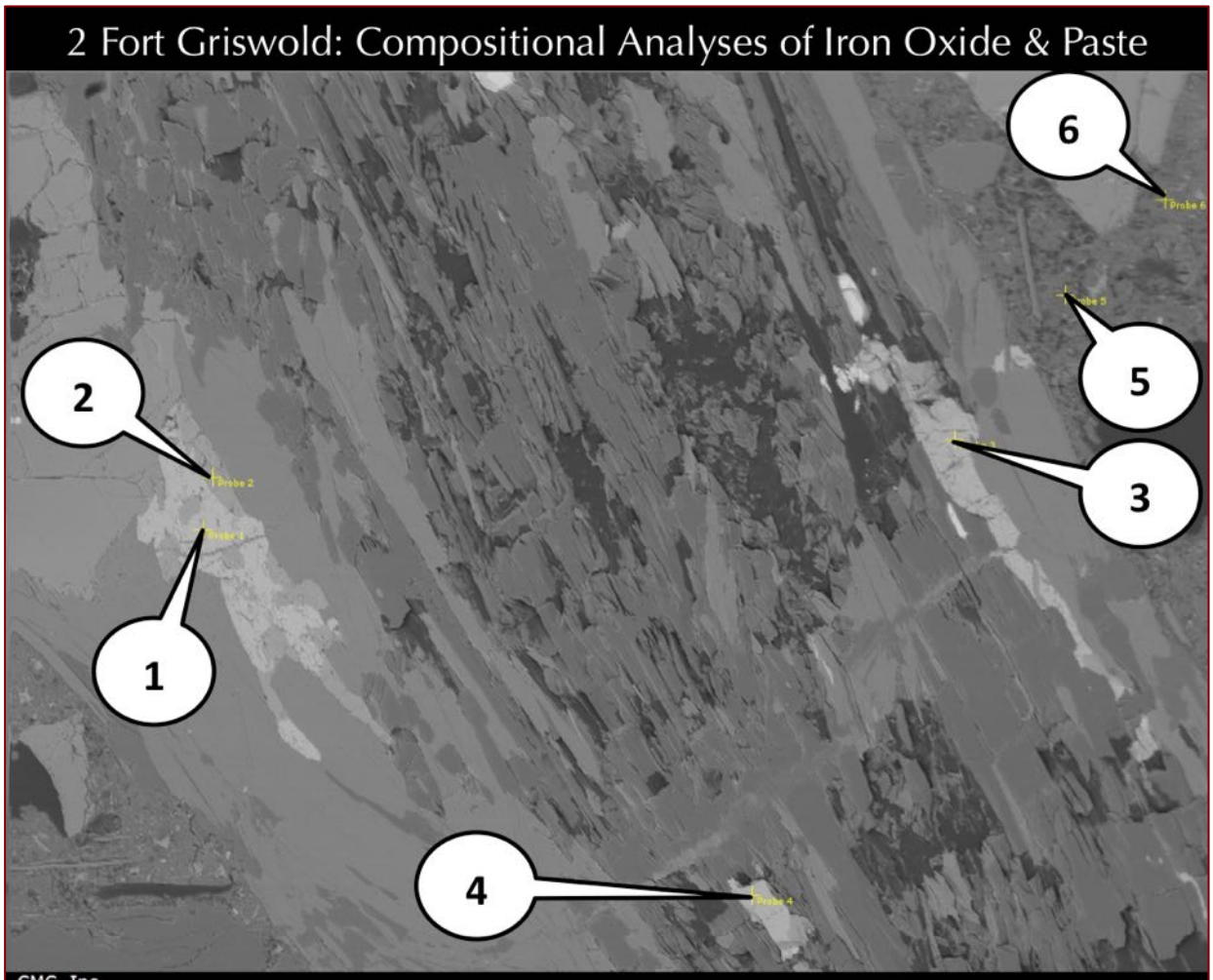


| Probe | CaO | $SiO_2$ | $Al_2O_3$ | $Na_2O$ | MgO | $SO_3$ | $K_2O$ | $TiO_2$ | FeO | Total | Phase |
|---|---|---|---|---|---|---|---|---|---|---|---|
| 1 | 0.00 | 0.57 | 0.00 | 0.01 | 0.01 | 0.00 | 0.19 | 46.72 | 52.50 | 100.00 | Fe-Ti-Oxide |
| 2 | 0.00 | 0.84 | 0.00 | 0.01 | 0.00 | 0.00 | 0.00 | 98.63 | 0.51 | 99.99 | Rutile |
| 3 | 0.00 | 0.75 | 0.16 | 0.01 | 0.00 | 0.00 | 0.00 | 43.59 | 55.48 | 99.99 | Fe-Ti-Oxide |
| 4 | 0.39 | 44.73 | 50.07 | 0.03 | 0.04 | 0.00 | 0.00 | 0.29 | 4.43 | 99.98 | Si-Al |
| 5 | 66.41 | 21.04 | 4.94 | 0.00 | 1.14 | 0.00 | 0.58 | 0.39 | 5.51 | 100.01 | Paste |
| 6 | 61.03 | 27.36 | 4.19 | 0.01 | 0.74 | 0.02 | 1.32 | 0.00 | 5.33 | 100.00 | Paste |

Figure 50: Backscatter electron image (top) and X-ray compositional analyses of concrete in the Core from 2 Fort Griswold showing compositions of paste, oxidized iron veins within a pyrrhotite, iron-titanium oxide, and titanium oxide (rutile) measured at the tips of callouts that are provided in the Table below the image.

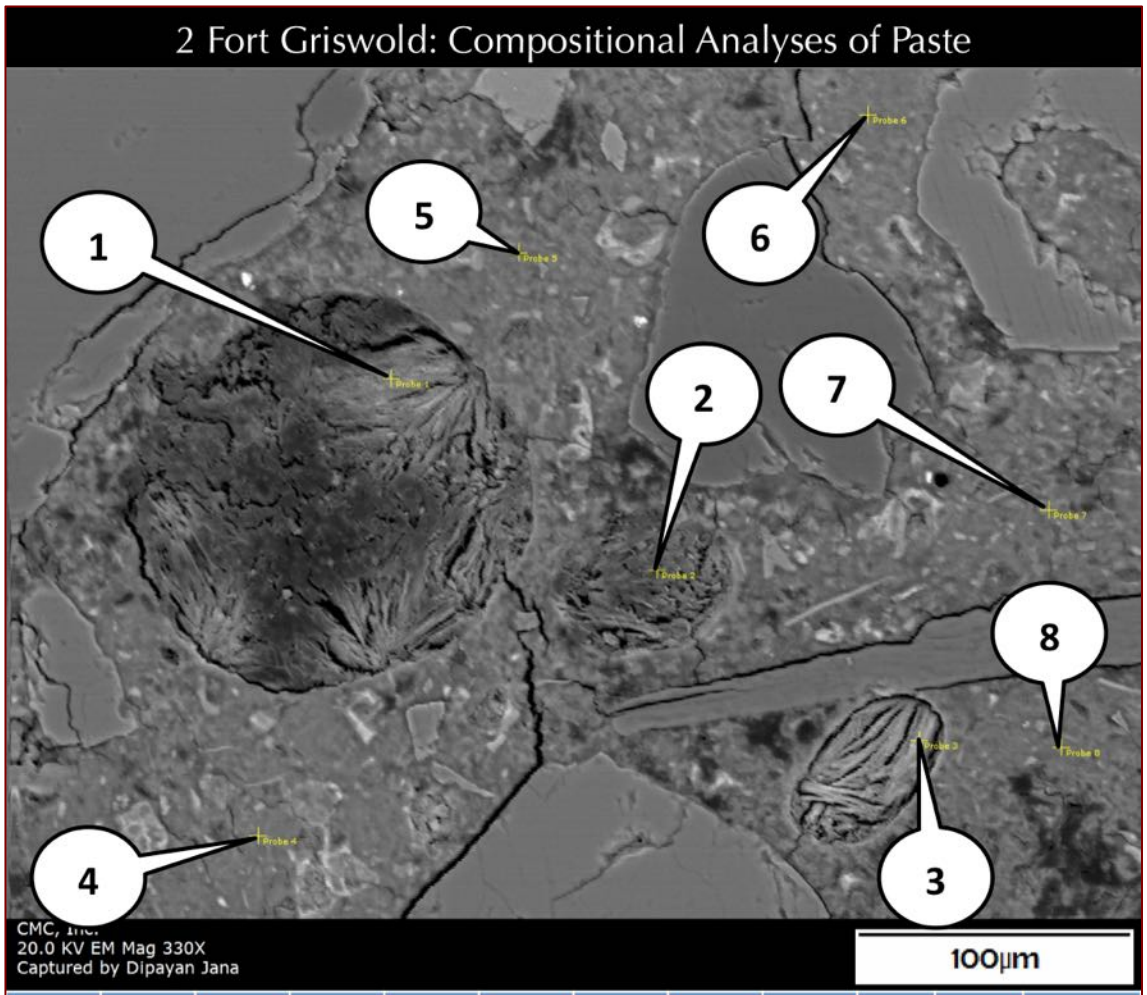


| Probe | CaO | $SiO_2$ | $Al_2O_3$ | $Na_2O$ | MgO | $SO_3$ | $K_2O$ | $TiO_2$ | FeO | Total | Phase |
|---|---|---|---|---|---|---|---|---|---|---|---|
| 1 | 60.38 | 6.27 | 14.49 | 0.03 | 0.12 | 16.35 | 0.40 | 0.00 | 1.97 | 100.01 | Ettringite |
| 2 | 54.83 | 10.49 | 17.06 | 0.84 | 0.49 | 14.12 | 0.30 | 1.18 | 0.69 | 100.00 | Ettringite |
| 3 | 59.78 | 3.32 | 15.96 | 0.00 | 0.00 | 20.25 | 0.23 | 0.05 | 0.40 | 99.99 | Ettringite |
| 4 | 57.24 | 28.43 | 4.51 | 0.00 | 0.58 | 0.00 | 0.30 | 3.25 | 5.68 | 99.99 | Paste |
| 5 | 62.13 | 28.31 | 5.18 | 0.00 | 0.22 | 0.00 | 0.59 | 0.31 | 3.25 | 99.99 | Paste |
| 6 | 60.57 | 26.03 | 5.17 | 0.00 | 1.35 | 0.00 | 0.18 | 0.48 | 6.22 | 100.00 | Paste |
| 7 | 65.81 | 20.62 | 7.11 | 0.00 | 0.43 | 1.66 | 0.82 | 0.00 | 3.55 | 100.00 | Paste |
| 8 | 58.57 | 28.34 | 6.06 | 0.00 | 0.90 | 0.00 | 1.64 | 0.00 | 4.48 | 99.99 | Paste |

Figure 51: Backscatter electron image (top) and X-ray compositional analyses of concrete in the Core from 2 Fort Griswold showing compositions of secondary ettringite deposits in voids and various areas of paste at the tips of callouts that are provided in the Table below the image. Secondary ettringite shows high Ca, Al, and S whereas paste shows typical calcium silicate hydrate composition with negligible or no evidence of contamination by sulfates released from pyrrhotite oxidation, which is typically found in many other pyrrhotite-related distress in the area.

## XRD & XRF STUDIES OF CONCRETES AND COARSE AGGREGATES FOR SULFIDE MINERALOGY, OXIDATION PRODUCTS, AND SULFUR ($SO_3$) CONTENTS

**1 Liberty Drive**

*Coarse Aggregate - 1*

XRD Analysis of Coarse Aggregate:

Quartz – 35.2%
Albite – 42.7%
Augite – 6.7%
Biotite – 2.4%
Ferrihydrite – 1.4%
Pyrope – 1.1%
Ettringite – 1.0%

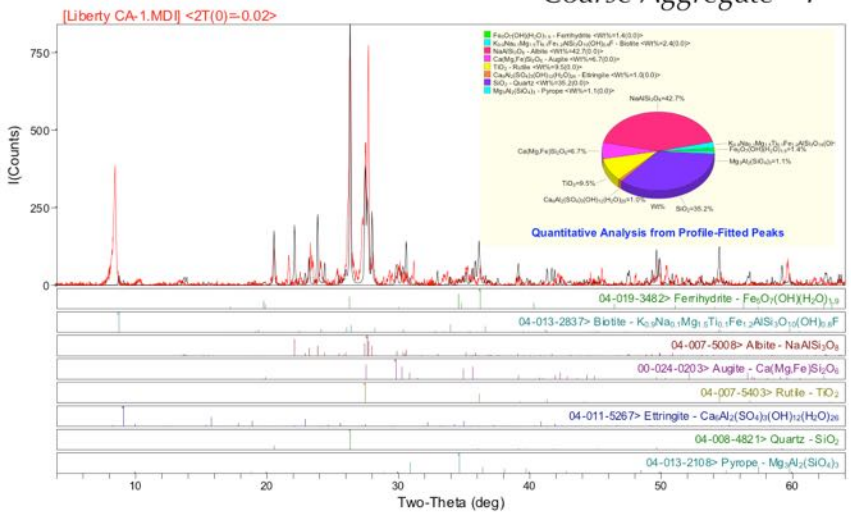


XRF Analysis of Coarse Aggregate:

$SiO_2$ – 54.9%
$Al_2O_3$ – 14.5%
CaO – 5.32%
MgO – 3.16%
$Na_2O$ – 2.27%
$K_2O$ – 2.48%
$Fe_2O_3$ – 7.07%
$TiO_2$ – 0.918%
$P_2O_5$ – 0.113%
$SO_3$ – 0.79%

*Coarse Aggregate - 2*

XRD Analysis of Coarse Aggregate:

Quartz – 46.0%
Albite – 32.4%
Augite – 7.2%
Biotite – 3.3%
Rutile – 7.8%
Pyrope – 2.2%

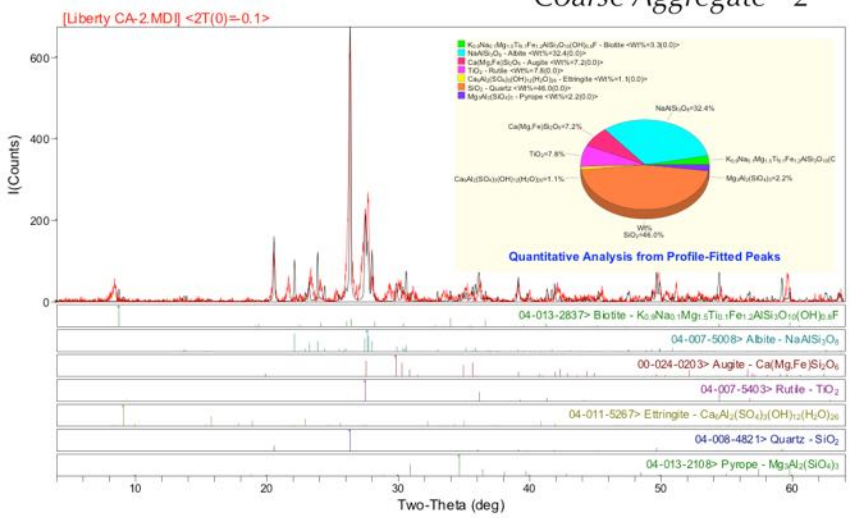


XRF Analysis of Coarse Aggregate:

$SiO_2$ – 60.8%
$Al_2O_3$ – 14.5%
CaO – 5.38%
MgO – 1.64%
$Na_2O$ – 2.63%
$K_2O$ – 1.87%
$Fe_2O_3$ – 4.91%
$TiO_2$ – 0.626%
$P_2O_5$ – 0.0414%
$SO_3$ – 0.81%

Figure 52: X-ray diffraction patterns (middle), quantitative proportions of minerals (middle pie-graph and tabulated in the left column), and corresponding X-ray fluorescence analyses of oxide compositions (in the right column) of two coarse aggregate particles extracted from the core at 1 Liberty Drive showing typical mineralogical and chemical compositions of coarse aggregate, detection of oxidized pyrrhotite as ferrihydrite, quartz, albite feldspar, augite, biotite, and pyrope garnet mineralogy of crushed gneiss, and secondary ettringite in aggregate, as well as the absence of pyrrhotite except its oxidation product ferrihydrite. Notice 0.8 percent sulfate ($SO_3$) in aggregates.

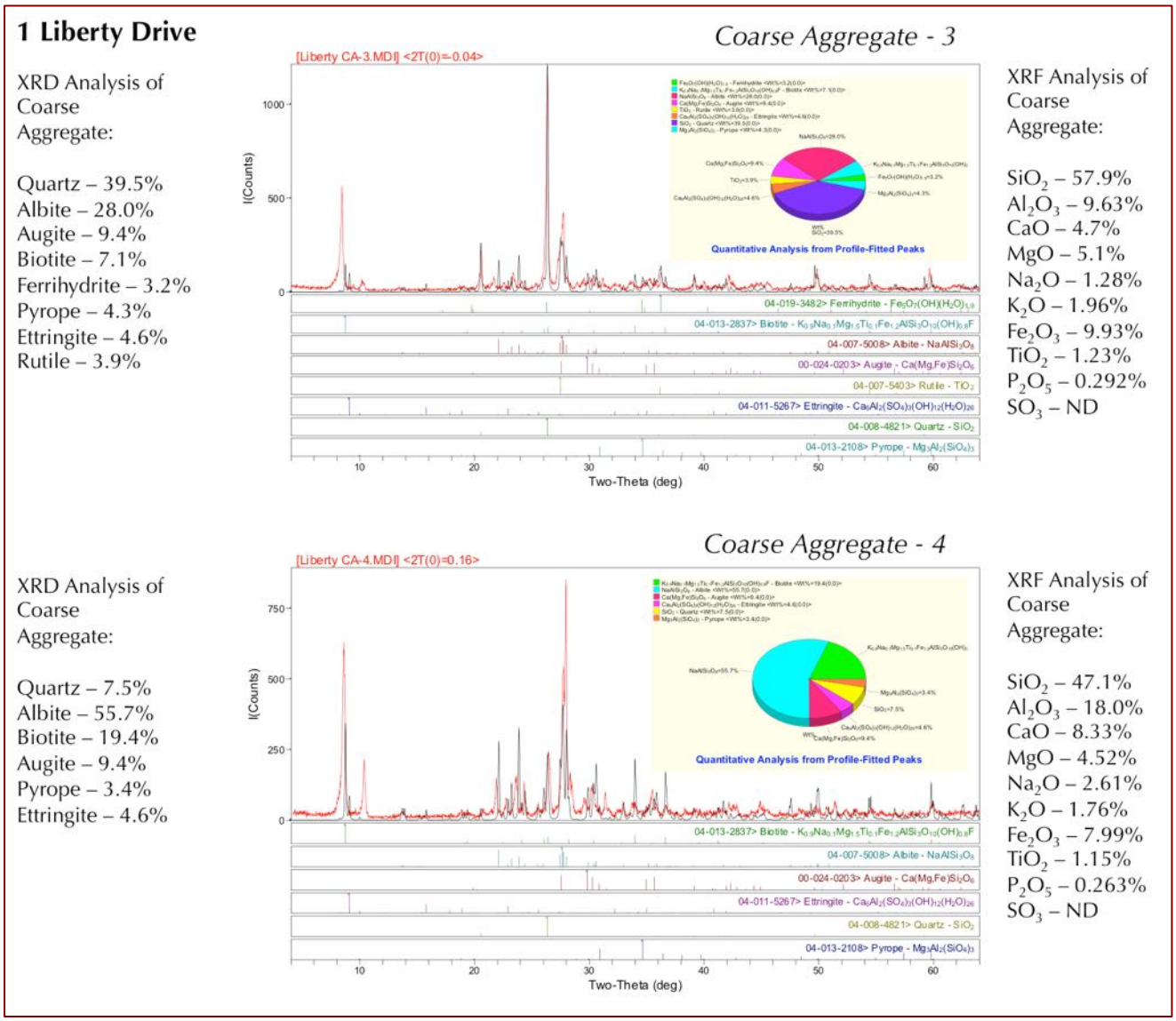


Figure 53: X-ray diffraction patterns (middle), quantitative proportions of minerals (middle pie-graph and tabulated in the left column), and corresponding X-ray fluorescence analyses of oxide compositions (in the right column) of two coarse aggregate particles extracted from the core at 1 Liberty Drive showing typical mineralogical and chemical compositions of coarse aggregate, detection of oxidized pyrrhotite as ferrihydrite, quartz, albite feldspar, augite, biotite, and pyrope garnet mineralogy of crushed gneiss, and secondary ettringite in aggregate, as well as the absence of pyrrhotite except its oxidation product ferrihydrite. Notice absence of sulfate ($SO_3$) in the aggregates in XRF analyses.

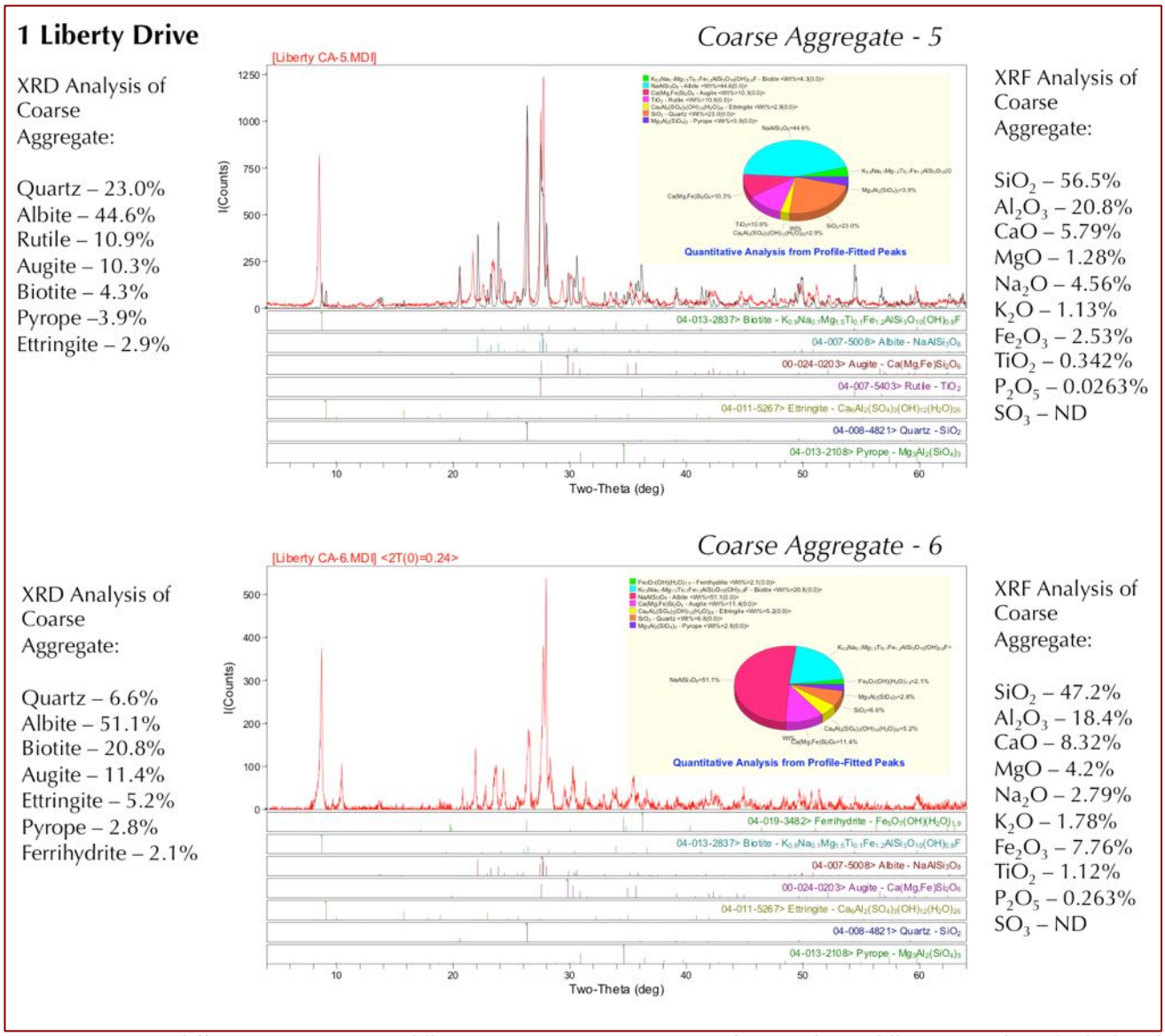


Figure 54: X-ray diffraction patterns (middle), quantitative proportions of minerals (middle pie-graph and tabulated in the left column), and corresponding X-ray fluorescence analyses of oxide compositions (in the right column) of two coarse aggregate particles extracted from the core at 1 Liberty Drive showing typical mineralogical and chemical compositions of coarse aggregate, detection of oxidized pyrrhotite as ferrihydrite, quartz, albite feldspar, augite, biotite, and pyrope garnet mineralogy of crushed gneiss, and secondary ettringite in aggregate, as well as the absence of pyrrhotite except its oxidation product ferrihydrite. Notice absence of sulfate ($SO_3$) in the aggregates in XRF analyses.

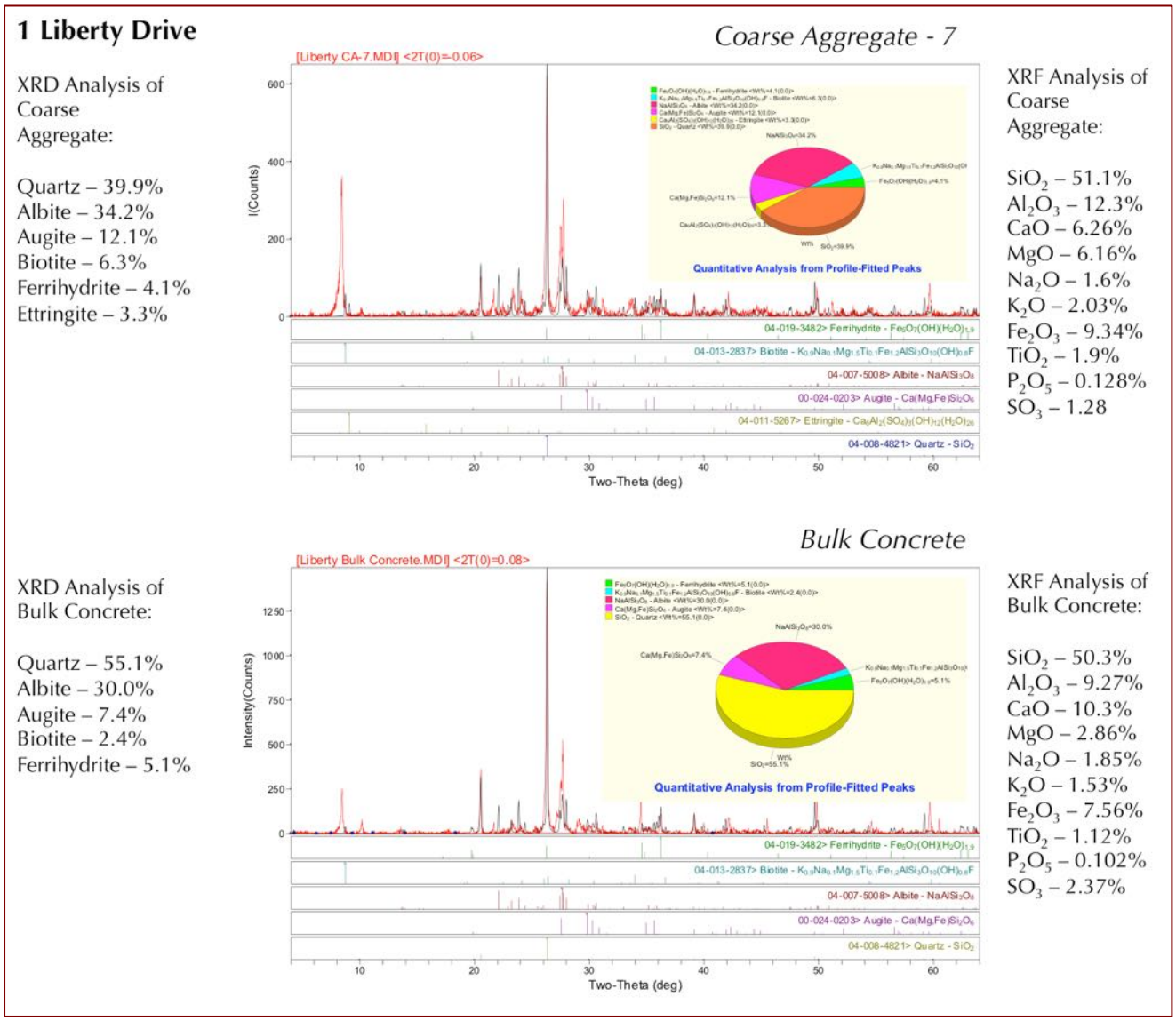


Figure 55: X-ray diffraction patterns (middle), quantitative proportions of minerals (middle pie-graph and tabulated in the left column), and corresponding X-ray fluorescence analyses of oxide compositions (in the right column) of a coarse aggregate particle extracted from the core at 1 Liberty Drive and the bulk concrete showing typical mineralogical and chemical compositions of coarse aggregate and concrete, detection of oxidized pyrrhotite as ferrihydrite, quartz, albite feldspar, augite, biotite, and pyrope garnet mineralogy of crushed gneiss, and secondary ettringite in aggregate, as well as the absence of pyrrhotite except its oxidation product ferrihydrite in aggregate and concrete. Notice high sulfate content of bulk concrete (2.37% $SO_3$), which is noticeably higher than the sulfate typically found in a typical Portland cement concrete (0.45% $SO_3$) assuming 3 percent sulfate ($SO_3$) in cement and 15 percent cement by mass in concrete.

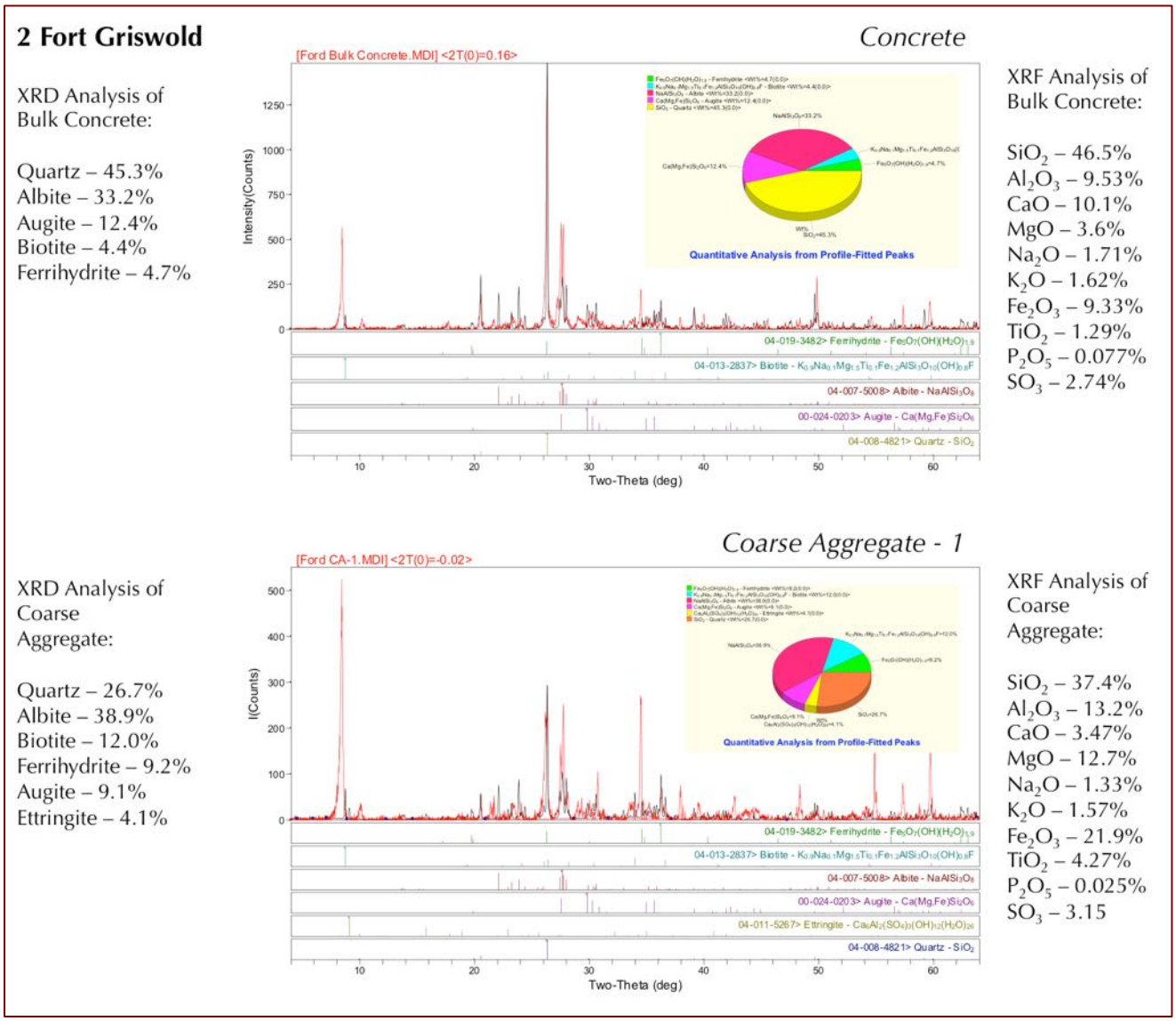


Figure 56: X-ray diffraction patterns (middle), quantitative proportions of minerals (middle pie-graph and tabulated in the left column), and corresponding X-ray fluorescence analyses of oxide compositions (in the right column) of a coarse aggregate particle extracted from the core at 2 Fort Griswold and the bulk concrete showing typical mineralogical and chemical compositions of coarse aggregate and concrete, detection of oxidized pyrrhotite as ferrihydrite, quartz, albite feldspar, augite, biotite, and pyrope garnet mineralogy of crushed gneiss, and secondary ettringite in aggregate, as well as the absence of pyrrhotite except its oxidation product ferrihydrite in aggregate and concrete. Notice high sulfate content of bulk concrete (2.74% $SO_3$), which is noticeably higher than the sulfate typically found in a typical Portland cement concrete (0.45% $SO_3$) assuming 3 percent sulfate ($SO_3$) in cement and 15 percent cement by mass in concrete. Notice high (3.15% $SO_3$) sulfate content in the aggregate compared to the 0.8% $SO_3$ found in some coarse aggregates in the core from 1 Liberty Drive.

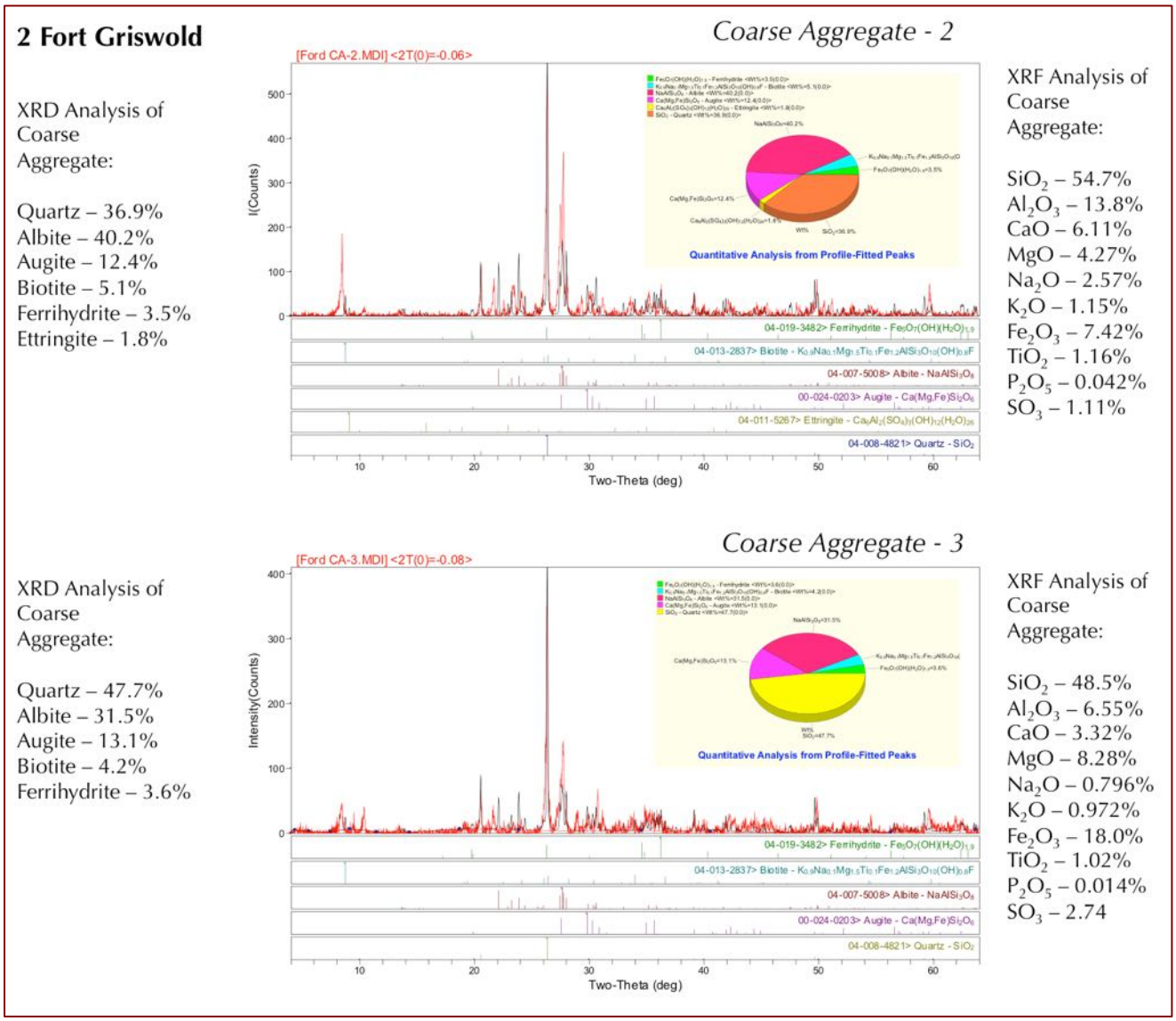


Figure 57: X-ray diffraction patterns (middle), quantitative proportions of minerals (middle pie-graph and tabulated in the left column), and corresponding X-ray fluorescence analyses of oxide compositions (in the right column) of two coarse aggregate particles extracted from the core at 2 Fort Griswold showing typical mineralogical and chemical compositions of coarse aggregate, detection of oxidized pyrrhotite as ferrihydrite, quartz, albite feldspar, augite, biotite, and pyrope garnet mineralogy of crushed gneiss, and secondary ettringite in aggregate, as well as the absence of pyrrhotite except its oxidation product ferrihydrite. Notice high (1.1 to 2.7% $SO_3$) sulfate contents in the aggregates compared to the 0.8% $SO_3$ found in some coarse aggregates in the core from 1 Liberty Drive.

## COMPARISON OF CHEMISTRY & MINERALOGY OF CONCRETES AND COARSE AGGREGATES WITH OTHER STUDIES

| Oxide wt.% from XRF | Coarse Aggregates From 1 Liberty Drive | | | | | | | Coarse Aggregates From 2 Fort Griswold | | | Bulk Concrete from 1 Liberty Drive | Bulk Concrete from 2 Fort Griswold |
|---|---|---|---|---|---|---|---|---|---|---|---|---|
| | L1 | L2 | L3 | L4 | L5 | L6 | L7 | F1 | F2 | F3 | | |
| $SiO_2$ | 54.9 | 60.8 | 57.9 | 47.1 | 56.5 | 47.2 | 51.1 | 37.4 | 54.7 | 48.5 | 50.3 | 46.5 |
| $Al_2O_3$ | 14.5 | 14.5 | 9.63 | 18 | 20.8 | 18.4 | 12.3 | 13.2 | 13.8 | 6.55 | 9.27 | 9.53 |
| $Fe_2O_3$ | 7.07 | 4.91 | 9.93 | 7.99 | 2.53 | 7.76 | 9.34 | 21.9 | 7.42 | 18 | 7.56 | 9.33 |
| CaO | 5.32 | 5.38 | 4.7 | 8.33 | 5.79 | 8.32 | 6.26 | 3.47 | 6.11 | 3.32 | 10.3 | 10.1 |
| MgO | 3.16 | 1.64 | 5.1 | 4.52 | 1.28 | 4.2 | 6.16 | 12.7 | 4.27 | 8.28 | 2.86 | 3.6 |
| $Na_2O$ | 2.27 | 2.63 | 1.28 | 2.61 | 4.56 | 2.79 | 1.6 | 1.33 | 2.57 | 0.796 | 1.85 | 1.71 |
| $K_2O$ | 2.48 | 1.87 | 1.96 | 1.76 | 1.13 | 1.78 | 2.03 | 1.57 | 1.15 | 0.972 | 1.53 | 1.62 |
| $TiO_2$ | 0.918 | 0.626 | 1.23 | 1.15 | 0.342 | 1.12 | 1.9 | 4.27 | 1.16 | 1.02 | 1.12 | 1.29 |
| $P_2O_5$ | 0.11 | 0.041 | 0.292 | 0.263 | 0.026 | 0.263 | 0.128 | 0.025 | 0.042 | 0.014 | 0.102 | 0.078 |
| $SO_3$ | 0.79 | 0.81 | ND | ND | ND | ND | 1.28 | 3.15 | 1.11 | 2.74 | 2.37 | 2.74 |
| Balance | 8.51 | 6.74 | 7.99 | 8.43 | 7.45 | 8.42 | 7.89 | 0.97 | 7.68 | 9.81 | 12.7 | 13.6 |
| Total | 100 | 100 | 100 | 100 | 100 | 100 | 100 | 100 | 100 | 100 | 100 | 100 |

Table 3: Results of XRF analyses of coarse aggregate particles extracted from the cores from 1 Liberty Drive (L1 to L7) and 2 Fort Griswold (F1 to F3), and of bulk concretes (last two columns).

| Oxide (wt.%) From XRF | Other Study Mansfield, CT | | Other Study Ellington, CT | | | Other Study Mansfield Centre, CT | | | Other Study Tolland, CT | | |
|---|---|---|---|---|---|---|---|---|---|---|---|
| | 1 | 2 | 3 | 4 | 5 | 6 | 7 | 8 | 9 | 10 | 11 |
| $SiO_2$ | 65.1 | 59.9 | 33.0 | 56.0 | 54.5 | 63.10 | 46.80 | 57.00 | 40.4 | 37.1 | 28.4 |
| $Al_2O_3$ | 13.9 | 9.85 | 8.60 | 10.30 | 10.60 | 10.70 | 18.40 | 10.00 | 8.54 | 9.08 | 10.7 |
| $Fe_2O_3$ | 4.93 | 4.0 | 22.50 | 6.17 | 7.29 | 5.22 | 11.00 | 4.10 | 5.93 | 8.02 | 25.6 |
| CaO | 4.12 | 8.34 | 8.54 | 10.30 | 8.92 | 4.55 | 4.33 | 10.30 | 11.1 | 10.7 | 6.45 |
| MgO | 1.16 | 2.01 | 3.51 | 1.60 | 3.12 | 3.34 | 4.02 | 1.67 | 2.62 | 3.43 | 9.07 |
| $Na_2O$ | 3.94 | 2.07 | | | | 1.61 | 3.28 | 2.34 | | | |
| $K_2O$ | 1.81 | 2.05 | 0.82 | 1.13 | 1.75 | 1.67 | 2.42 | 1.91 | 1.56 | 1.15 | 1.21 |
| $TiO_2$ | 0.36 | 0.38 | 2.53 | 0.56 | 1.00 | 0.68 | 1.43 | 0.44 | 0.612 | 1.21 | 4.35 |
| $P_2O_5$ | 0.12 | 0.08 | - | 0.05 | 0.09 | 0.15 | 0.05 | 0.11 | 0.08 | 0.09 | 0.02 |
| $SO_3$ | ND | 0.10 | 10.8 | 2.05 | 1.45 | 0.01 | 0.91 | 0.68 | 0.51 | 1.58 | 2.43 |
| Balance | 5.14 | 11.2 | 7.66 | 9.57 | 9.89 | 8.96 | 7.29 | 11.50 | 23.9 | 26 | 9.43 |
| Total | 100 | 100 | 100 | 100 | 100 | 100 | 100 | 100 | 100 | 100 | 100 |

Table 4: Comparison of XRF data of other studies from eastern Connecticut that have shown pyrrhotite presence in concrete. NOTE: Column# 2, 5, 8, 9, and 10 – Bulk Concrete; Column# 1, 3, and 7 – Dark gray biotite-garnet-gneiss coarse aggregate; Column# 4, 6, and 11 Light to dark brown gneiss coarse aggregate.

| Phases From XRD | Coarse Aggregates From 1 Liberty Drive | | | | | | | Coarse Aggregates From 2 Fort Griswold | | | Bulk Concrete from 1 Liberty Drive | Bulk Concrete from 2 Fort Griswold |
|---|---|---|---|---|---|---|---|---|---|---|---|---|
| | L1 | L2 | L3 | L4 | L5 | L6 | L7 | F1 | F2 | F3 | | |
| Quartz | 35.2 | 46.0 | 39.5 | 7.5 | 23.0 | 6.6 | 39.9 | 26.2 | 36.9 | 47.7 | 55.1 | 45.3 |
| Albite | 42.7 | 32.4 | 28.0 | 55.7 | 44.6 | 51.1 | 34.2 | 38.9 | 40.2 | 31.5 | 30.0 | 33.2 |
| Pyrope Garnet | 1.1 | 2.2 | 4.3 | 3.4 | 3.9 | 2.8 | - | - | - | - | - | - |
| Biotite | 2.4 | 3.3 | 7.1 | 19.4 | 4.3 | 20.8 | 6.3 | 12.6 | 5.1 | 4.2 | 2.4 | 4.4 |
| Pyrrhotite | - | - | - | - | - | - | - | - | - | - | - | - |
| Ferrihydrite | 1.4 | - | 3.2 | - | - | 2.1 | 4.1 | 9.2 | 3.5 | 3.6 | 5.1 | 4.7 |
| Augite | 6.7 | 7.2 | 9.4 | 9.4 | 10.3 | 11.4 | 12.1 | 9.1 | 12.4 | 13.1 | 7.4 | 12.4 |
| Ettringite | 1.0 | - | 4.6 | 4.6 | 2.9 | 5.2 | 3.3 | 4.1 | 1.8 | - | - | - |
| Rutile | - | 7.8 | 3.9 | - | 10.9 | - | - | - | - | - | - | - |

Table 5: Results of XRD analyses of coarse aggregate particles extracted from the cores from 1 Liberty Drive (L1 to L7) and 2 Fort Griswold (F1 to F3), and of bulk concretes (last two columns). For both cores, pyrrhotite in coarse aggregate particles is detected only in optical microscopy and SEM studies but is present at levels below the detection limit of XRD.

| Phases From XRD | Other Study Mansfield, CT | | Other Study Ellington, CT | | | Other Study Mansfield Centre, CT | | | Other Study Tolland, CT | | |
|---|---|---|---|---|---|---|---|---|---|---|---|
| | 1 | 2 | 3 | 4 | 5 | 6 | 7 | 8 | 9 | 10 | 11 |
| Quartz | 44.4 | 64.3 | 40.7 | 50.1 | 54.3 | - | 53.0 | 45.9 | 41.2 | 28.7 | 4.0 |
| Albite | 42.6 | 28.1 | 31.0 | 34.8 | 33.2 | - | 26.4 | 37.4 | 24.0 | 29.8 | 32.1 |
| Pyrope Garnet | - | - | 7.7 | 4.8 | 0.0 | - | - | 8.8 | 1.8 | 1.5 | 23.0 |
| Biotite | 7.4 | 4.8 | 4.0 | 2.9 | 5.1 | - | 13.8 | 6.1 | 8.4 | 8.2 | 24.2 |
| Pyrrhotite | - | - | 7.9 | 0.0 | 0.9 | - | - | 1.8 | 1.5 | 2.5 | 1.9 |
| Ferrihydrite | 5.6 | 2.9 | 6.5 | 2.3 | 5.1 | - | 6.8 | - | 6.4 | 7.4 | 2.7 |
| Calcite | - | - | 0.0 | 0.0 | 1.5 | | | | 2.8 | 3.6 | 2.6 |

Table 6: Comparison of XRD data of some other studies from eastern Connecticut that have shown pyrrhotite presence in concrete. NOTE: Column# 2, 5, 8, 9, and 10 – Bulk Concrete; Column# 1, 3, and 7 – Dark gray biotite-garnet-gneiss coarse aggregate; Column# 4, 6, and 11 Light to dark brown gneiss coarse aggregate.

## ION CHROMATOGRAPHY FOR POTENTIAL SULFATE RELEASE OF AGGREGATES IN ACCELERATED OXIDATION TEST

Pulverized concretes, and, multiple pulverized crushed gneiss coarse aggregate particles carefully extracted (and cleared of adhered pastes) from the cores of both foundations were analyzed for potential release of sulfates in an oxidizing environment by an accelerated oxidation test.

Pulverized samples were immersed in 10 mL strong oxidant (35% hydrogen peroxide) solution (diluted to first 50 mL for digestion and subsequently to final 100 mL) for oxidation of iron sulfide minerals to be leached out to the solution, and then finally filtered under vacuum to determine amount of leached sulfates in the filtrates. For each coarse aggregate particle extracted from the cores, particles were first crushed in a pulverizer down to finer than 0.45 mm size, and then approximately one gram of pulverized aggregate was selected for determining amount of sulfate released after 10 days of continuous immersion in the oxidizing solution with intermitted stirring with magnetic stirrers.

After digestion, samples were filtered first through two 2.5-micron filter papers under vacuum suction, and subsequently through 0.2 micron , the filtrate was then re-filtered through two 0.2-micron filter papers of the filtrates to remove all solid particulates. After two filtrations, filtrates were diluted to 100 mL with deionized water and analyzed in Metrohm IC.

All coarse aggregate particles showed release of variable amounts but noticeable release of sulfates in an oxidizing environment after digestion for 10 days. Amounts of sulfates released from coarse aggregate particles in the core from 2 Fort Griswold are overall higher than that from 1 Liberty Drive. This could be due to the presence of higher proportion of iron sulfide grains in those aggregates in the core from 2 Fort Griswold compared to the aggregates extracted from the core from 1 Liberty Drive.

Overall sulfate released from bulk concrete is also higher for the core from 2 Fort Griswold (1.573% $SO_4^{2-}$) than the core from 1 Liberty Drive (1.432% $SO_4^{2-}$), which is consistent with higher bulk sulfate (as $SO_3$) content in the core from 2 Fort Griswold (2.74% $SO_3$) than the core from 1 Liberty Drive (2.37% $SO_3$) as determined in XRF studies.

Therefore, accelerated oxidation tests showed potential for continued release of sulfates from coarse aggregate particles in the presence of moisture as the main oxidant in the foundation walls.

Figure 58 shows results of accelerated oxidation tests of seven coarse aggregate particles extracted from the core from 1 Liberty Drive, three coarse aggregate particles extracted from the core from 2 Fort Griswold, and bulk concretes of two cores from both foundations. All samples show measurable amounts of sulfates released in oxidizing solutions after 10 days of digestion.

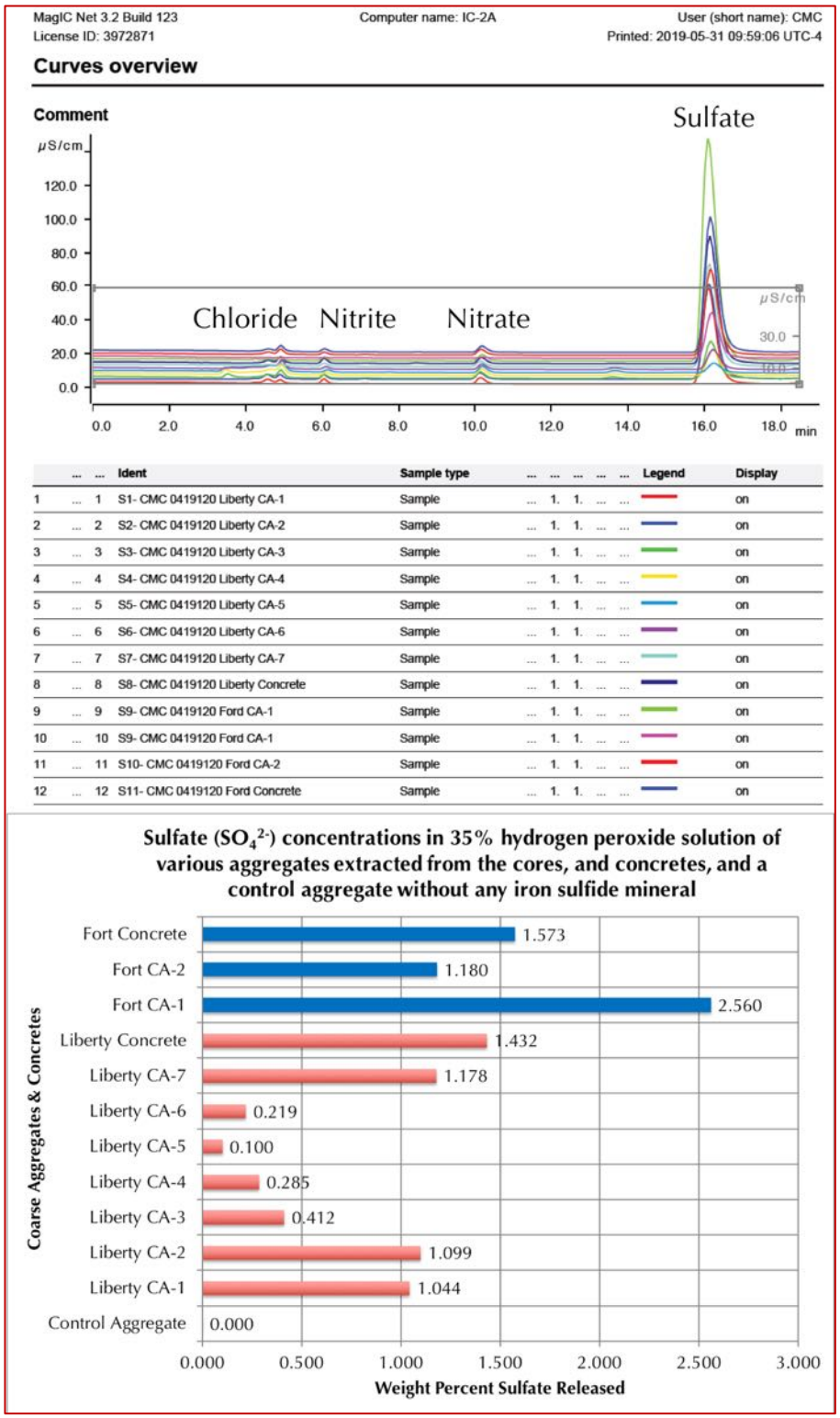


Figure 58: Accelerated oxidation tests of crushed gneiss coarse aggregate particles extracted from the cores from 1 Liberty Drive and 2 Fort Griswold, along with pulverized concretes of cores after digestion in hydrogen peroxide solutions for 10 days to determine various levels of sulfates released from oxidation. Coarse aggregates and concrete from 2 Fort Griswold show an overall greater release of sulfates than the aggregates and concrete in the core from 1 Liberty Drive. Top graph shows superposed chromatograms of all samples.

## DISCUSSION

### IRON SULFIDE MINERALS IN CONCRETE AGGREGATES[1]

Iron sulfide minerals (e.g., pyrite $FeS_2$, or pyrrhotite $Fe_{1-x}S$, x varies from 0 to 0.125) occurring mostly as 'accessory' minerals in many concrete aggregates are known to cause various deteriorations in concrete in service. **Oxidation of iron sulfide minerals in concrete** can cause various deteriorations from **unsightly staining** on the exposed surface to **popouts** of near-surface unsound aggregates (Jana 2008) and associated local fracturing to in extreme cases severe **cracking, microcracking, and loss of strength** of concrete from **internal sulfate attacks** by reactions between released sulfate and hydrogen ion (sulfuric acid) from oxidation reactions with cement hydration products – all resulting in expansive reactions leading to structural instability. The mineral pyrrhotite has been found to be the most reactive and detrimental to the durability of concrete (Jana 2019). If a suspicion arises regarding a possible pyrrhotite-related distress in a concrete structure then identification of the type of iron sulfide mineral responsible for the distress, and quantification of the total sulfur content in the pyrrhotite-bearing aggregate would be prudent to determine whether the mineral may have an effect on the durability of concrete.

#### Background

Iron sulfide minerals occur commonly as minor, but significant accessory minerals in a variety of rocks. Pyrite is the most common of all sulfide minerals. It is a common accessory mineral in igneous, metamorphic, and sedimentary rocks, and is a major phase in many sulfide ore bodies. In hand sample, this mineral has a metallic luster and pale yellow color. Microscopically, pyrite is a cubic isotropic mineral with a yellowish-white color in reflected light (Deer et al., 1992). Pyrite, with the chemical formula $FeS_2$, is composed of 46.6% Fe and 53.5% S.

Pyrrhotite is the second most common iron sulfide in nature, found as a primary accessory mineral in ultra-mafic and mafic rocks, metamorphosed igneous and sedimentary rocks, and as a secondary mineral in hydrothermal deposits (Jana 2019). It is mostly found with other iron sulfides, particularly pentlandite ($(Fe,Ni)_9S_8$), but also commonly found associated with pyrite, marcasite (orthorhombic $FeS_2$), magnetite ($Fe_3O_4$) and chalcopyrite ($CuFeS_2$) (Deer et al, 1992; Belzile et al, 2004). These different minerals can all coexist within a grain of pyrrhotite or in contact with the grain (Uytenbogaardt, Burke, 1971). In hand sample, this mineral has a metallic luster and bronze brown, yellow, or reddish color. Microscopically, pyrrhotite is a monoclinic or pseudohexagonal anisotropic mineral with a pink cream or skin color in reflected light (Deer et al, 1992). Pyrrhotite has an unbalanced chemical formula $Fe_{1-x}S$, with × ranging from 0 (FeS) to 0.125 ($Fe_7S_8$).

---

[1] Excerpts from American Concrete Institute's technical notes on pyrrhotite-related distress in concrete, plus author's own addition.

## Mechanism of Distress by: (1) Oxidation of Iron Sulfides (Primary Expansion Causing Surface Staining, Popout, Cracking), (2) Release of Sulfates and Internal Sulfate Attack (Secondary Expansion Causing Further Cracking)

It is well known from the literature that sulfide minerals are unstable in oxidizing conditions. According to Divet and Davy (1996), high pH conditions, such as those found in concrete, enhance iron sulfide oxidation. Upon exposure to water and oxygen, sulfide minerals (pyrite, pyrrhotite) oxidize to form acidic, iron oxides/hydroxides, and sulfate-rich by-products with an increase in solid volumes from the sulfide minerals to their oxidized products (Belzile et al. 2004, Rodrigues et al. 2012). The oxidation of ferrous iron ($Fe^{2+}$) produces ferric ions ($Fe^{3+}$) that can precipitate out of solution to form ferric hydroxide, if pH is not too low. $Fe^{2+}$ is oxidized and precipitated as ferric oxyhydroxides, principally **ferrihydrite** [$Fe(OH)_3$] and **goethite** [FeO(OH)]. The sulfuric acid (sulfate and hydrogen ion, $H_2SO_4$) generated through oxidation reactions reacts with cement hydration products, e.g., with the portlandite [$Ca(OH)_2$], to form **gypsum** [$CaSO_4 \bullet 2H_2O$] (Grattan-Bellew and Eden 1975, Shayan 1998, Rodrigues et al. 2012), with calcium aluminate or monosulfoaluminate hydrates to form **ettringite [**$Ca_6Al_2(SO_4)_3(OH)_{12}{\cdot}26H_2O$**]**, or, **thaumasite** [$Ca_6[Si(OH)_6]_2(CO_3)_2(SO)_4)_2(H_2O)_{22}$] latter one if carbonate minerals are present. Both the processes of *oxidation of iron sulfides*, and *reactions between released sulfates and cement hydration products* are expansive in natures resulting in concrete deteriorations.

Figure 59 from various authors (e.g., Rodrigues et al. 2012, Oliveira et al., 2014, Willi and Zhoing 2016) summarizes mechanism of two-stage expansions resulting in concrete deterioration from: (a) *primary expansion due to oxidation of iron sulfide minerals to ferric oxyhydroxides, principally goethite and ferrihydrite and associated solid volumes' increases*, and (b) *secondary expansion due to internal sulfate attacks of released sulfate and hydrogen ions (sulfuric acid) from oxidation to cement hydration products*, e.g., calcium hydroxide and calcium sulfoaluminate hydrate to form gypsum (with a solid volume increase of 42) or more commonly due to formation of ettringite (with a solid volume increase of 172).

The above expansive mineral formation results in **rust staining and pop-outs at the aggregate site in milder cases most commonly associated with pyrite**, to **severe cracking and decreased strength due to internal sulfate attack in paste from released sulfates in the most severe cases associated with pyrrhotite**.

In the case of pyrrhotite, the degree of cracking damage correlates with the deterioration of the mineral and the quantity of resultant expansive sulfates in the paste. **Not all concretes with pyrrhotite in aggregates, however, result in deterioration**. As shown in the case studies in Table 7, the rate and extent of damage can be variable. The rate and severity of damage are dependent on a number of factors including: (a) the interaction between the particle and the surrounding host rock that forms the aggregate (Oliveira et al. 2014) and the concrete paste, (b) the concrete quality, (c) the environmental conditions to which the concrete element is exposed to (exposure to oxygen, moisture, and temperature), (d) crystal structure, (e) the mineral associations (more than one sulfide minerals present), (f)

concrete pH, (g) trace metal content, and (h) bacterial activity (Belzile et al. 2004). The extents of controlling factors are not yet fully understood in light of the limitations of reproducing the deterioration in the laboratory.

### Pyrrhotite Limit

**Standardization of the amount of iron sulfide minerals that are considered acceptable in concrete aggregates is not well established**. American, Canadian, British, and French standards for concrete aggregates mention iron sulfides and their related problems with use in concrete, but have not established acceptable limits of iron sulfide contents in aggregates. Limits have been established for total sulfur ($S_T$) by mass in French at 0.4%, European at 1%, or 0.1% if pyrrhotite is present. The limits as to the amount of pyrrhotite that would lead to damage has not been identified to date; this may be quite difficult because the reactivity of pyrrhotite may vary according to its crystallographic characteristics, while many factors are involved in this deleterious mechanism. No precise guidelines or methods have been proposed to evaluate the potential reactivity of sulfide containing aggregates.

Recently, an extensive investigation was carried out over a four-year period by researchers from four Canadian organizations aimed at developing an evaluation protocol for iron sulfide bearing aggregate (Rodrigues et al., 2016). The resulting recommended protocol involved a three-phase testing program including (a) measurement of total sulfur, (b) oxygen consumption determination, and (c) accelerated mortar bar expansion test. Limits are proposed for each phase of the protocol, but are in need of additional validation. These tests can be used as a general screening, but would need to be supplemented by further testing to identify the sulfate sulfur and the sulfate mineral type. Significant research is still needed to identify appropriate limits.

## CASE STUDIES OF CONCRETE DETERIORATION DUE TO OXIDATION OF IRON SULFIDE MINERALS IN AGGREGATES

Examples of deterioration of concrete structures due to oxidation corrosion of iron sulfate minerals, with pyrrhotite date back to 1955, and span a range of aggregate types. Structural damage to buildings due to pyrite or pyrrhotite breakdown has been observed in many places around the world since the mid-1950s, including Ireland, Wales, Spain, Canada, Namibia, and Japan. In the United States, pyrite-induced swelling has been observed in Ohio, West Virginia, Pennsylvania, Missouri, Kansas, and Kentucky, and more recently thousands of homes in Connecticut have been affected by pyrrhotite in concrete foundations.

Following are summaries of cases studies on concrete deterioration around the world that are described due to unsoundness of aggregates containing iron sulfide minerals, all of which have concluded that expansions associated with oxidation of iron sulfide minerals followed by additional expansions associated with internal sulfate attacks between the released sulfates and cement hydration products have caused the deterioration in form of map cracking, heaving, displacement of affected elements, and in severe cases crumbling of concrete elements. The last row is for oxidation of pyritic shale in the substrate causing heaving of structural elements, or, blistering of floor tiles when

pyritie is present in the concrete aggregates at the surface of floor slab, but all other case studies are from pyrrhotite-oxidation related damages.

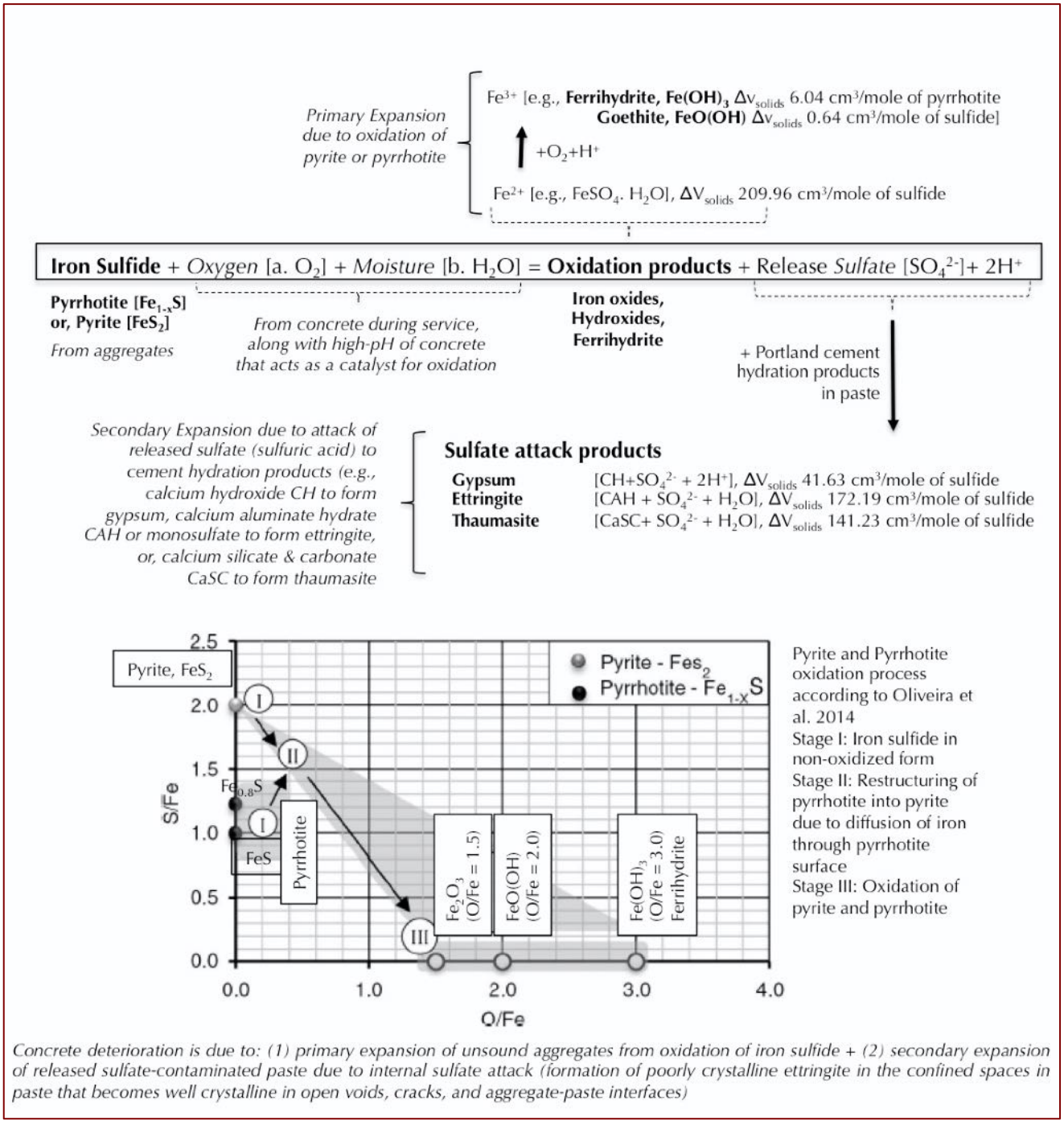


Figure 59: Mechanisms of oxidation of iron sulfide minerals in concrete according to various authors (Jana 2019), and primary expansion due to oxidation of iron sulfide to various forms of iron oxides, hydroxides, ferrihydrite, followed by secondary expansions due to reactions between the released sulfates and hydrogen ions from oxidation reactions (sulfuric acid) and cement hydration products (calcium hydroxide, calcium aluminate, and monosulfoaluminate hydrate) to form ettringite (or thaumasite if carbonate ions are present).

| • Locality (References) | • Pyrrhotite containing rocks<br>• Associated sulfide minerals | • Average sulfur content in aggregate<br>• Pyrrhotite content | • Structure affected<br>• Type of Damage<br>• Time taken to manifest the damage | Proposed Mechanisms of Distress |
|---|---|---|---|---|
| • *Oslo, Norway* (Moum and Rosenqvist 1959) | • Sedimentary rocks (alum shales some with slight metamorphism)<br>• Pyrite occurred with pyrrhotite | • 6% (highly variable), all shales that weathered 'explosively' due to oxidation contained more than 0.2% sulfur as monoclinic pyrrhotite.<br>• Pyrrhotite content is related to rate of alteration of pyrite and rate of weathering of shale | • Foundation<br>• Upheaval of foundation, cracking, crumbling, yellowish deposit of jarosite [$KFe_3(OH)_6(SO_4)_2$] and brown-iron oxide ($Fe_2O_3$. $nH_2O$) on weathered shales.<br>• Within 9 months | Swelling of shale due to oxidation of pyrrhotite and internal sulfate attack from released sulfate; reactivity of alum shale and resultant damage increased with increasing pyrrhotite content, with no occurrence of damage when alum shale was free of pyrrhotite; acidic and sulfate-rich water percolated through alum shale has caused acid attack and internal sulfate attack in concrete |
| • *Trois-Rivières area, Quebec, Canada* (Tagnit-Hamou, et.al. 2005; Rodrigues, et.al. 2012; Duchesne and Benoit 2013) | • Quarried intrusive igneous rock anorthositic gabbro (norite) with different degrees of metamorphism<br>• Pyrite and chalcopyrite. Only pyrrhotite showed signs of oxidation but pyrite and chalcopyrite were largely unaffected. A thin coating of iron carbonate (siderite) on sulfides provided carbonates to promoted thaumasite form of attack in addition to internal sulfate attack from pyrrhotite oxidation | • As low as 0.30% to 2.92% total sulfur by mass of aggregate in pyrrhotite-bearing coarse aggregates that have caused damage, all damaged concrete exceeded the European limit of 0.1% sulfur in aggregate when pyrrhotite is present by 3 times to as high as 30 times.<br>• Less than 5 to 10 percent total sulfide minerals by volume, average 75% of sulfide minerals was pyrrhotite and lesser pyrite and chalcopyrite from a study of 223 house basements containing varying amounts of iron sulfide in gabbro coarse aggregate | • Residential foundations and commercial buildings.<br>• Map cracking (cracks up to 40 mm in width) and yellowish or brownish staining), popouts of oxidized pyrrhotite with white rim of secondary reaction products, and open cracks more pronounced at the corners of the foundation blocks<br>• More than 1000 to as high as estimated 4000 residential and commercial buildings were affected within 3 to 5 years after construction | Oxidation of sulfide minerals (mainly pyrrhotite) in anorthositic gabbro coarse aggregate in concrete has: (a) formed various "rust" minerals (e.g., ferric oxyhydroxides such as goethite FeO(OH), limonite, and ferrihydrite) and (b) released sulfuric acid/sulfates, which then reacted with cement hydration products resulting in further expansive formation of gypsum, ettringite, and thaumasite in concrete. Oxidation of pyrrhotite followed by internal sulfate attack of cement paste is the main mechanism of concrete deterioration. |
| • *Northeastern Connecticut, USA* (Wille and Zhong 2016) | • Foliated schist and gneissic metamorphic rocks, granofels, foliated quartz diorite in a hydrothermally altered vein from a particular quarry in Willington, CT (Becker's quarry).<br>• Pyrrhotite as the predominant iron sulfide mineral present in metamorphic rocks containing quartz, plagioclase feldspar, micas, and garnet | • Average 2.54% sulfur in pyrrhotite-bearing quarry aggregate<br>• Pyrrhotite was not detected in XRD analysis of quarry aggregate by Wille and Zhong due to possible presence below the 5% detection limit of XRD | • Residential foundations.<br>• Map cracking, crumbling, deformation of wall, reddish-brown discoloration, whitish formation of secondary ettringite and thaumasite in the vicinity of surface cracks. Cores from foundation walls of houses showed noticeably lower compressive strengths (some no strength due to complete crumbling) compared to the cores from slabs, indicating possible effect of more oxidation in wall than slab and hence more damage in wall than slab<br>• 10 to 20 years after construction, estimated 34,000 homes are at risk | Primary expansion due to oxidation of pyrrhotite followed by secondary expansion due to internal sulfate attack by released sulfates |
| • *Catalan Pyrenees, Spain* | • Schist containing quartz, muscovite mica, chlorite and | • 2% sulfur (as $SO_3$ from XRF) in schist. | • Tórán Dam<br>• Map cracking and non-recoverable movements, more | Oxidation of pyrite and pyrrhotite forming surface stains of greyish brown iron hydroxides (goethite) |

| • Locality (References) | • Pyrrhotite containing rocks<br>• Associated sulfide minerals | • Average sulfur content in aggregate<br>• Pyrrhotite content | • Structure affected<br>• Type of Damage<br>• Time taken to manifest the damage | Proposed Mechanisms of Distress |
|---|---|---|---|---|
| (Araujo et al. 2008) | non-expansive illitic clay.<br>• Pyrite and Pyrrhotite | • Predominantly pyrrhotite (S/Fe ratio 0.62 as opposed to 1.15 of pyrite) but XRD also detected some pyrite | dramatic expansion in the downstream face of the dam for upstream displacement of the crest | and lighter-green potassium iron sulfates (jarosite), gypsum efflorescence from sulfate attack; and causing expansions, e.g., 6.04 $cm^3$/mol from primary expansion from oxidation of iron sulfides followed by 172.19 $cm^3$/mol from internal sulfate attack by reaction between released sulfates and cement phases |
| • *Central Pyrenees, Spain* (Ayora et al. 1998; Oliveira et al. 2014) | • Schist containing bands of pyrrhotite that created planes of weakness and present cracks that serve as preferential paths for entrance of oxygen thus aggregates having pyrrhotite bands with cracks showed more pronounced oxidation than ones without cracks.<br>• Pyrite | • Median sulfur ($SO_3$) content of 1.42% for rocks from a quarry that have known to cause severe damage when used as aggregate in dam | • Graus and Tavascan Dams<br>• Map cracking, damage in downstream face and galleries of the Graus Dam due to severe cracking and movement | Alteration from acidic solution produced by weathering and oxidation of pyrrhotite in aggregates followed by expansion due to internal sulfate attack and formation of ettringite and gypsum. Characteristic ratios of 2.44 for the Fe/O ratio and of 2.63 for the S/O ratio in pyrrhotite marked critical limits that produced the activation and acceleration of pyrrhotite oxidation leading to an increase of expansive reactions and risk of structural damage. |
| • *Ottawa, Quebec City, Matane, and Montreal, Canada* (Quigley and Vogan 1970; Berard 1970; Berube et al. 1986; Penner et al. 1972)<br>• *Ireland*<br>• *Wales* (Hawkins and Pinches 1987)<br>• *Marcellus Shale, USA* (Hoover and Lehmann 2009)<br>• *Chattanooga Shale, Kentucky, USA* (Anderson 2008)<br>• SW England in Cornwall and Devon | • Black shale containing pyrite (not pyrrhotite). Pyrite is most common in metamorphic and sedimentary rocks as either a primary mineral or a fine, widespread impregnation of subsequent origin.<br>• Pyrite is frequently found in association with coal and shale deposits<br>• Mundic (means mine waste) concrete blocks used in the foundations of thousands of 20th century homes in SW England, blocks were prepared using mine waste rocks as aggregates containing pyrite that has caused serious damage (Mundic decay) in foundations | The minimum amount of pyrite that will cause heaving problems is not known with certainty. Some reports describe difficulties with contents as low as 0.1 per cent by weight. In the Ottawa area heaving problems have been encountered only in rock formations with much higher pyrite contents, although a systematic sampling program has not been carried out. Pyrite weathering is a chemical-micro-biological oxidation process; some of the oxidation reactions are solely chemical, others are attributed to autotrophic bacteria of the ferrobacillus-thiobacillus group, and still others are both chemical and micro- biological. | • Foundation, basement floor above weathered pyritic substrate. Pyrite weathering was identified as early as 1950 as a major foundation problem in the U.S.A. in buildings dating back to 1920.<br>• Pyrite oxidation in the Chattanooga Shale has caused serious foundation problems in numerous buildings and structures in Estill County, KY.<br>• Heaving of pyritic substrate causes cracking, lifting of concrete floor slabs; differences in levels across floor slabs; cracking, buckling lifting of elements resting on the concrete floor slabs, doors, stairs, fixtures; cracking, bulging, movement of internal or external walls.<br>• Blistering and de-bonding of vinyl tile from concrete floor is reported due to oxidation of pyritic aggregates at the surface of concrete floor (Shayan 1988) | Oxidation of pyrite in shale or coal causes formation of *gypsum* from reactions between (a) sulfates or sulfuric acid released from pyrite oxidation and calcium hydroxide component of cement hydration (if pyritic rock is used as aggregate in concrete), and/or (b) between sulfuric acid from oxidation and associated calcite in pyritic rocks cause heaving and associated volume changes. When calcite converts to gypsum, the volume increases by a factor of 2, but of greater importance is the force associated with the growth of gypsum crystals, which can be very high. When gypsum grows in rock under buildings it tends to form needle-like crystals that force the layers apart, resulting in much greater heave than would occur with simple volume expansion during formation. Another oxidation product found in all weathered pyritic materials is jarosite, $KFe_3(SO_4)_2(OH)_6$, recognized by its bright yellow-brown color. The calculated volume increase from pyrite to jarosite is 115 percent, which is another main contributor to volume increase and heaving. |

Table 7: Case studies on concrete deterioratios due to oxidation of iron sulfide minerals in aggregates (Jana 2019).

## PYRRHOTITE EPIDEMIC IN EASTERN CONNECTICUT

Figure 60 shows regional spread of the latest reported incident of widespread outbreak of deterioration of concrete due to pyrrhotite oxidation in the aggregate along northeastern Connecticut with many hundreds of homes being affected. Figures 61 through 64 show various manifestations of distress in the affected homes from various sources. Typical visual deterioration was in the form of map cracking, some causing deformation of the wall, extensive longitudinal to random cracking of the wall, reddish-brown discoloration, and whitish formation in the vicinity of surface cracking most of which are shown in Figures 61 to 64. Currently, much of the information available on this problem is limited to newspaper articles but the cause of deterioration has initially been confirmed by an investigation conducted at the University of Connecticut (Wille and Zhong, 2016) and subsequently by Jana 2019 as oxidation of pyrrhotite present in the aggregate. In contrast to the problems encountered in Quebec, manifestation of the damage in Connecticut has taken as much as 10 to 20 years.

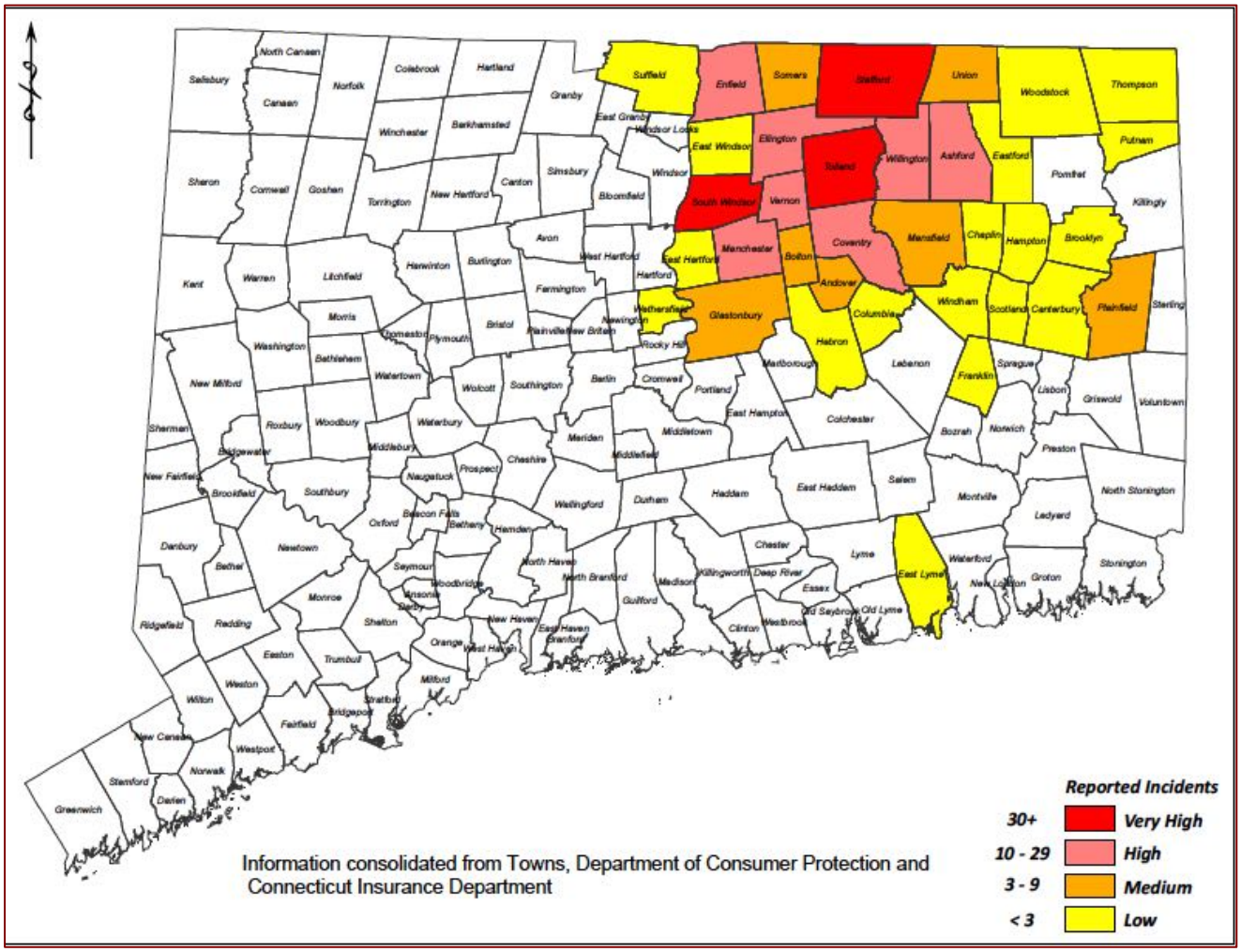


Figure 60: Reported incidences of pyrrhotite-related concrete deterioration in northeastern Connecticut. Note the present residential house in Mansfield Center falls under Medium-risk zone for concrete containing aggregates reportedly supplied from the Becker's quarry (Jana 2019).

Most of the damage to date has been linked to one quarry operating in Willington, CT. The geology in the vicinity of the quarry is made up of metamorphic rocks predominately from two to three formations. The formations are comprised predominantly of foliated schists and gneissic rock, granofels, and a foliated quartz diorite. Quartz, plagioclase or oligoclase are primary minerals with micas, and noted are garnet and graphite as common accessory minerals. Iron sulfides are found predominately as pyrrhotite.

Wille and Zhong (2016) did extensive mechanical, mineralogical, microstructural and chemical tests on the core samples taken from 7 houses and did visual inspection of 14 additional houses, from which the primary findings they found are:

a) Ubiquitous in all cases of concrete deterioration are the presence of pyrrhotite in aggregates and their oxidation products, such as goethite [FeO(OH)], and ferrihydrite [$Fe(OH)_3$];
b) Sodium sulfate and hydrated forms of sodium sulfate (thenardite and mirabilite) based white efflorescence deposits at the vicinity of surface cracks;
c) Porous paste and aggregate-paste interfaces, abundance of secondary ettringite crystallization in aggregate-paste interfaces and other open spaces; cracking is often associated with these open spaces and either within the voids or extends into cement paste
d) Oxidation of pyrrhotite in the presence of water and oxygen is reported to have caused the distress by expansive formation of ferrihydrite, and subsequent release of sulfate to paste, sulfate-aluminate reactions with aluminate phases in paste, and expansive formation of secondary ettringite crystals.
e) In the presence of carbonate ions secondary thaumasite crystallization is also noted.

*The present study showed many evidences for pyrrhotite-related distress in concrete foundation found in the study of Wille and Zhong (2016), numerous other studies conducted by our laboratories, and in Jana 2019*. However, contrary to other pyrrhotite-related distress, present study could not detect sulfate infestation in the paste from sulfates released from oxidation of pyrrhotite, but found evidence of formation of poorly crystalline secondary ettringite in the voids, cracks, and porous as well as confined areas in paste that has potential to cause the expansion and cracking in many other foundations. Present study detected relatively well-formed secondary ettringite in voids and cracks that are the result of exposure to moisture causing oxidation of pyrrhotite. Profuse development of secondary ettringite confirm the presence of excess sulfate beyond the amount contributed from cement, i.e. from sulfate released from oxidation of pyrrhotite that was precipitated as secondary ettringite in the presence of moisture.


Figure 61: Cracking of concrete foundations in Connecticut due to oxidation of pyrrhotite bearing aggregates in concrete. Notice wide cracks in the top row as well as a network of numerous fine cracks in the wall in the bottom right row all from pyrrhotite oxidation and associated expansion of concrete.


Figure 62: Cracking of concrete foundations in Connecticut due to oxidation of pyrrhotite bearing aggregates in concrete. Notice dark reddish-brown rust staining on the wall and associated cracking in the top row from pyrrhotite oxidation and formation of ferric oxy-hydroxide oxidation products (goethite, limonite, ferrihydrite rust minerals). Notice wide cracks in the 2nd through 4th rows from pyrrhotite oxidation and associated expansion of concrete.


Figure 63: Cracking of concrete foundation in Connecticut due to oxidation of pyrrhotite bearing aggregates in concrete. Notice wide cracks in the foundation walls, extensive cracking of walls in the top left photo all reportedly from pyrrhotite oxidation and associated expansion of concrete.


Figure 64: Cracking of concrete foundation in Connecticut due to oxidation of pyrrhotite bearing aggregates in concrete. Notice extensive cracking of foundation in all photos reportedly from pyrrhotite oxidation and associated expansion of concrete.

## CONCLUSIONS

Oxidation of pyrrhotite in concrete aggregates has caused severe damage to concrete foundations in several thousands of residential and commercial buildings in Quebec, Canada, in three concrete dams in Central Pyrenees, Spain, and anticipated to have deteriorated several thousands of residential foundations in eastern Connecticut that have reportedly received concrete containing pyrrhotite-bearing aggregates from the Becker's quarry in Ellington, CT. The amount of pyrrhotite required to cause damage has been found to be as low as 0.3% (total sulfur by mass of aggregate). Recommendations in Europe limit the sulfur content of sulfide-containing aggregates to 1% sulfur by mass unless the presence of pyrrhotite is confirmed in which case the limit is just 0.1% sulfur by mass. Limits on the sulfur contents in aggregates have not yet been imposed in North America at the time of this investigation.

In light of this known problem of pyrrhotite in concrete aggregate from around the world, and particularly from the Becker's quarry in CT, and the resulting distress in many residential foundations in northeastern Connecticut, two concrete cores were collected from cracked foundation walls at 1 Liberty Drive and 2 Fort Griswold in Mansfield, Connecticut i.e. within the known area of 'pyrrhotite epidemic.' The cores were provided with the concern of: (a) whether or not the distressed concrete foundations contain pyrrhotite in their aggregate, and, if detected, (b) if pyrrhotite has played the role for cracking of concrete foundation, as in the case of other residential foundations from eastern Connecticut that have shown widespread cracking from pyrrhotite oxidation and resultant sulfate attacks in concretes.

Field photographs of the subject foundation walls showed extensive cracking either as a network of closed polygonal-shaped cracks at 1 Liberty Drive or parallel cracks often with intersecting ones at 2 Fort Griswold. Concrete cores were drilled over visible cracks on the foundation walls through the entire wall thickness. Laboratory investigations were conducted to determine the possible presence of pyrrhotite in concrete, and, its potentially deleterious role in concrete deterioration, if any. Pyrrhotite's possible presence along with overall condition of concretes and aggregates were examined by detailed petrographic examinations (optical microscopy) *a la* ASTM C 856, whereas possible roles of pyrrhotite, its potential oxidation products and sulfate levels, and microstructures of deteriorated concrete around pyrrhotite-bearing aggregates are examined by scanning electron microscopy and energy-dispersive X-ray microanalysis (SEM-EDS) of multiple thin sections of concretes (*a la* ASTM C 1723), X-ray diffraction (XRD) and X-ray fluorescence (XRF) of multiple pyrrhotite-bearing coarse aggregate particles extracted from the concretes, and ion chromatography (IC *a la* ASTM D 4327) of extracted aggregate particles digested in a strong oxidant of 35% hydrogen peroxide solution in an accelerated oxidation test, then diluted in distilled water to determine levels of sulfates released by these aggregates in relation to a control aggregate without any iron sulfide mineral. Detection of pyrrhotite by optical microscopy, SEM-EDS, and XRD, along with detection of its oxidation products by SEM-EDS and XRD, reaction microstructures and evidence of distress by SEM-EDS, sulfate contamination of paste by SEM-EDS, and measurement of release of sulfate levels by IC provide a good assessment of potential role of pyrrhotite in causing oxidation-related cracking in the foundation walls.

Petrographic examinations have determined the concretes in both foundations to be compositionally similar having similar crushed gneiss coarse aggregates, which is a testament of their possible derivation from the same mix/supplier. Furthermore, the observed concrete compositions are similar to the other distressed concretes from in eastern CT that were reportedly provided by JJ Mottes. The unsound pyrrhotite-bearing aggregates in the other distressed foundations were known to have quarried from a hydrothermal vein in Becker's quarry situated in Willington, CT that has extensive pyrrhotite crystallization. Concretes in both cores are made using: (a) crushed gneiss coarse aggregates having nominal maximum sizes of $^{3}/_{4}$ in. (19 mm), (b) natural siliceous sand fine aggregates having nominal maximum sizes of $^{3}/_{8}$ in. (9.5 mm) and containing major amounts of quartz and quartzite, and subordinate amounts of feldspar, mica, ferruginous rock, and mafic minerals; (c) hardened pastes of Portland cement as the sole cementitious components having cement contents similar in both cores and estimated to be 6 to $6^{1}/_{2}$ bags per cubic yard, water-cement ratios (*w/c*) similar within the bodies in both cores, estimated to be 0.45 to 0.50, and (d) air contents estimated to be 6 to 8 percent; concretes in both cores are air-entrained. Overall compositions of concretes, including the crushed gneiss coarse aggregate particles present in the examined concretes are similar to concretes (containing similar crushed gneiss coarse aggregates) from other distressed foundations from eastern Connecticut that were examined by this laboratory and confirmed pyrrhotite-oxidation-related cracking.

Similar to other pyrrhotite-related cracking of residential foundations, along with numerous visible cracks, petrographic examinations of both cores have detected numerous microcracks in the foundation walls similar to the microcracks found in other distressed walls from the neighborhood that are diagnosed to be due to deleterious chemical reactions from pyrrhotite-oxidation. Extensive cracking of cores, especially the one from 1 Liberty Drive, are not only evident when received, but also during subsequent examinations of lapped and saw-cut cross sections, especially after impregnating the cross sections with a fluorescent dye-mixed epoxy and viewed in ultraviolet light where many microcracks are readily revealed due to penetration of fluorescent epoxy into the cracks and then become highlighted in UV light. Many unsound crushed gneiss coarse aggregate particles in both cores showed internal cracking, many of which are due to oxidation of pyrrhotite in crushed gneiss coarse aggregates causing internal fracturing, parallel fine microcracking and disintegration of oxidized pyrrhotite grains, along with development of veins of oxidized iron within pyrrhotite matrix that are highlighted in Fe-O maps and corresponding depletions in S-maps of oxidized veins in SEM studies.

Petrographic examinations detected mixtures of three different color tones of gravel and crushed gravel coarse aggregate particles in the cores: (a) dominant dark gray to black gneiss consisting of parallel alignment of quartz, albite feldspar, biotite mica, and occasional pyrope garnet porphyroblasts, anhedral to subhedral equigranular to gneissose arrangement of minerals; (b) subordinate light to medium brown granite gneiss of quartz, albite feldspar, garnet, biotite mica and occasional pyroxene (augite) grains; and (c) minor white granite gneiss with quartzo-feldspathic minerals and black specs of mica flakes in parallel alternate (gneissose) arrangements. Brown and dark gray gneiss contain more iron sulfide and iron oxide minerals than the minor white granite gneiss. All particles are angular, dense, hard, and medium to dark gray to brown, gneissose-textured, equidimensional to elongated, variably

altered, uncoated, and variably cracked. Coarse aggregate particles are well-graded and well-distributed. There is no evidence of alkali-aggregate reactions of coarse aggregates in concretes.

Similar to the predominant dark gray to brown pyrrhotite-bearing gneiss that have caused pyrrhotite oxidation and subsequent distress in other case studies, present study from both foundations also showed more dark gray to brown unsound pyrrhotite-bearing garnetiferous quartzo-feldspathic gneiss compared to lighter colored (white with black specs of mica) granite gneiss to contain disseminated unsound pyrrhotite to cause distress. Unlike other studies, however, pastes in the present concrete cores are free of any sulfate contamination released from pyrrhotite oxidation. However, both cores showed profuse development of secondary ettringite in cracks, microcracks, voids, and pore spaces in paste due to the presence of moisture and sulfate from pyrrhotite oxidation during service.

XRD analyses of ten different dark gray and brown coarse aggregate particles extracted from the cores as well as XRD analysis of the bulk concretes of both cores showed mineralogical similarities to cores from many other distressed foundations, including the absence of any detectable pyrrhotite in XRD (despite its detection in optical microscopy and SEM-EDS) but the presence of ferrihydrite type iron hydroxide phase. Pyrrhotite grains were oxidized to ferrihydrite to be detected in XRD, however the amount of pyrrhotite and its oxidation product ferrihydrite may not have been enough to cause sufficient release of sulfates to cause sulfate contamination of paste except forming profuse secondary ettringite in voids, cracks, and porous areas of paste. XRF studies of dark gray and brown crushed gneiss coarse aggregates showed sulfate contents, probably due to variable pyrrhotite contents in these particles but the bulk concrete showed noticeable sulfate (as $SO_3$) in both cores, which is discussed later. Despite the absence of sulfate contamination in the paste to be noted in SEM-EDS studies and absence of detectable pyrrhotite in the concretes or extracted aggregates from XRD studies, the overall sulfate (as $SO_3$) contents of concretes in both foundations are very high, e.g., 2.37 percent in the core from 1 Liberty Drive and 2.74 percent in the core from 2 Fort Griswold. These concrete sulfate (as $SO_3$) contents are notably higher than sulfate contents typically found in a normal Portland cement concrete, e.g., 0.45 percent sulfate (as $SO_3$) with 3 percent sulfate (as $SO_3$) in Portland cement and 15 percent Portland cement by mass in concrete.

Microcracking within many pyrrhotite-bearing crushed gneiss coarse aggregates occurs due to pyrrhotite oxidation, which is often associated with reddish-brown oxidation products of pyrrhotite, and microcracks often extend from unsound aggregates to paste – this is the first microstructural evidence of distress due to primary expansion of unsound aggregate *per se* that are distinct in numerous photomicrographs of thin sections of concretes from other residential foundations of eastern Connecticut studied as well as in the present study. Detailed examinations of crushed gneiss coarse aggregate particles in the present cores, both from stereomicroscopical examination of lapped cross sections and petrographic microscopical examination of thin sections have detected widespread occurrences of similar microcracking and associated reddish-brown oxidation product of pyrrhotite from oxidation and related distress to cause visible microcracking in concretes.

Petrographic examinations of distressed residential foundations in the present study as well as from other distressed homes of eastern Connecticut have also detected abundant secondary ettringite crystallization lining or filling many air voids and occasionally lining some microcracks that are indicative of prolonged presence of moisture in concretes during service, which is an essential pre-requisite for pyrrhotite oxidation. Presence of moisture also indicates availability of sulfates to be released from pyrrhotite-oxidation and for subsequent ettringite crystallization, which, however, may or may not have necessarily derived from pyrrhotite oxidation since ettringite-filled air-voids are a very common microstructural feature in a concrete exposed to moisture without even any iron sulfide contaminant. Any Portland cement concrete exposed to moisture during service forms secondary ettringite deposits lining and filling air voids. To establish the source of secondary ettringite i.e. from Portland cement's sulfate and/or from oxidation of pyrrhotite-bearing aggregates require determination of sulfate levels in concrete i.e. if the level is higher than that expected from a typical Portland cement concrete where sulfate (as $SO_3$) content in cement is around 3 weight percent i.e. giving about 0.45 percent sulfate in concrete for a usual cement content of 15 percent by mass of a normal weight concrete. Excess sulfate in concrete above 0.45 percent from cement's contribution would then correspond to the pyrrhotite-aggregate source if no other sulfate source were present. To determine the sulfate ($SO_3$) level of bulk concrete, thin slices of concretes were sectioned through the entire lengths of the cores traversing the full thickness of the foundation wall and pulverized for XRF analysis, which, as mentioned, showed 2.37 percent in the core from 1 Liberty Drive and 2.74 percent in the core from 2 Fort Griswold, which are significantly higher than the sulfates normally contributed from Portland cement. Clearly, the observed sulfate contents of present concrete indicate a sulfate source other than Portland cement, which is determined to be numerous disseminated pyrrhotite inclusions in coarse aggregates. Consistent with above observation, petrographic examinations of paste in the present cores detected potentially deleterious secondary ettringite, as found in other distressed foundations, indicating, again that moisture, the essential ingredient for release of sulfate from pyrrhotite to the paste, was present for the present concretes during service in the respective foundations.

Therefore, similar to other pyrrhotite-oxidation-related cracking in residential foundations from eastern Connecticut, examined cores have shown microstructural evidence of (a) primary expansion of concrete due to oxidation of pyrrhotite in crushed gneiss coarse aggregate to cause cracking within the unsound aggregate particles or their extension into paste, and (b) secondary expansion of paste due to formation of poorly crystalline (perhaps also colloidal formed) secondary ettringite in relatively confined areas in paste along with voids, cracks and porous areas causing further expansion and associated cracking in other distressed foundations.

In accelerated pyrrhotite oxidation test, multiple crushed gneiss coarse aggregate particles were extracted from the cores, cleaned of adhered paste remains, crushed, then immersed in a 35% hydrogen peroxide (strong oxidant) solution for 10 days. Sulfates released from aggregates to the filtrates were measured (as $SO_4^{-2}$) in an anion exchange chromatograph. All particles showed noticeable release of sulfates from aggregates and concretes as opposed to no sulfate release from a control gneiss aggregate containing no pyrrhotite indicating the potential for continued sulfate release in the field during service in prolonged presence of moisture.

Case studies on pyrrhotite-oxidation-related distress of concrete foundations from eastern Connecticut by the present laboratory have confirmed and provided clear mechanisms of the common consensus that the observed cracking and reported crumbling of many concrete foundation walls in eastern Connecticut are due to: (a) oxidation of pyrrhotite in crushed garnetiferous quartzo-feldspathic gneiss coarse aggregate particles *in the presence of oxygen and moisture during service in concrete* with the formation of ferrihydrite causing expansion of the unsound aggregates and formation of cracks from unsound aggregates to paste, which was then followed by (b) additional expansion in the paste from reactions between sulfates released from pyrrhotite oxidation and cement hydration products (internal sulfate attack) and formation of poorly crystalline or perhaps colloidal ettringite within the confined spaces in paste. The present examined concrete cores, provided similar evidence of pyrrhotite-oxidation-related distress and its manifestation as cracking indicating moisture, the essential ingredient for pyrrhotite-oxidation and subsequent internal sulfate attack of concrete, was present in foundation walls during service.

Visible and invisible cracking in the present foundations and evidence of pyrrhotite-oxidation-related distress confirms: (a) source of coarse aggregates of present concretes possibly from the Becker's quarry, which has produced unsound aggregates for other distressed foundations, and (b) presence of moisture in these foundations during service. Perhaps slow uptake of moisture through the wall from the ground could have initiated pyrrhotite oxidation and resultant cracking, which is similar in other residential foundations of eastern Connecticut that have shown distress after 10 to 20 years of construction, the time period within which the present foundations reportedly fall.

In summary: concretes from two foundations at 1 Liberty Drive and 2 Fort Griswold have not only confirmed the presence of disseminated pyrrhotite inclusions in crushed gneiss coarse aggregates but also evidence of pyrrhotite-oxidation-related cracking. Crushed gneiss coarse aggregates are similar to the ones from other distressed foundations in having a greater proportion of dark gray and brown granite gneiss than the white gneiss where the former two gneiss types contained noticeable disseminated pyrrhotite inclusions as in other pyrrhotite-bearing dark gray and brown gneiss quarried from the hydrothermal vein of pyrrhotite crystallization in the Becker's quarry in Willington, CT that has provided the unsound aggregate for other distressed foundations. Extensive macro and micro cracking in foundations are testament of deleterious pyrrhotite oxidation. Very high sulfate (as $SO_3$) contents of concretes (as high as 2.7% $SO_3$) compared to 0.45% $SO_3$ in normal Portland cement concretes indicates additional sulfate sources beside Portland cement, which is confirmed to be from pyrrhotite in aggregates. XRD studies did not detect pyrrhotite in concretes or extracted coarse aggregates but the oxidation product ferrihydrite is detected, which is in conformance to optical microscopy, SEM-EDs and other studies. SEM-EDS studies have failed to detect any sulfate contamination in the paste, which occurs from sulfates released from pyrrhotite oxidation. However, optical microscopy and SEM-EDS studies both detected many deleterious secondary ettringite formation in paste, voids, and cracks, which (along with high total sulfate in concretes) are testament of additional sulfate sources beyond cement, from pyrrhotite with expansion and cracking from pyrrhotite oxidation. Ion chromatography of crushed gneiss coarse aggregates extracted from concretes showed potential release of sulfate in a highly oxidizing solution of hydrogen peroxide, indicating a similar potential release of sulfate in the field in prolonged oxidizing condition

from the presence of moisture. This indicates role of prolonged presence of moisture and moisture penetration through existing cracks in foundations to sustain pyrrhotite oxidation and continued distress.

Since there is no industry specification on the threshold pyrrhotite limit above which potential for oxidation-related distress can occur, and, in fact as low as 0.3% pyrrhotite by mass of aggregate in the host rock has reportedly shown severe distress in concrete (e.g., in Quebec Canada), the best solution is to avoid aggregates containing pyrrhotite for its known damaging affects without further laboratory verification of its potential unsoundness in concrete (e.g., from expansion of mortar bar or concrete prism tests similar to those used for ASR-expansion).

## REFERENCES

ACI Committee Report 201.2R, Guide to Durable Concrete, ACI Manual of Concrete Practice, Vol. 1, American Concrete Institute, 2008.

Anderson, W.H., Foundation Problems and Pyrite Oxidation in the Chattanooga Shale, Estill County, Kentucky, Kentucky Geological Survey Report of Investigation, 2008.

Araujo, G.S., Chinchon, S., and Aguado, A., Evaluation of the behavior of concrete gravity dams suffering from internal sulfate attack, *Revista ibracon de estruturas e materials* (Ibracon Structures and Materials Journal), Vol. 1, No. 1, pp 84-112, 2008.

ASTM C 856 "Standard Practice for Petrographic Examination of Hardened Concrete," Vol. 4.02, ASTM International, West Conshohocken, PA, 2014.

Ayora, C., Chinchon, S., Aguado, A. and Guirado, F. (1998). Weathering of iron sulfides and concrete alteration: thermodynamic model and observation in dams from Central Pyrenees, Spain. *Cement and Concrete Research*, Vol. 28, Issue 4, pp. 1223–1235.

Belzile, N., Y.W. Chen, M.F.Cai, and Y. Li. (2004). A review on pyrrhotite oxidation. J., *Geochem. Explor.*, Vol. 84, pp. 65–76.

Bérard, J., Black shale heaving at Ottawa, Canada: Discussion. Canadian Geotechnical Journal 1970. 7(2): 113-114.

Bérubé, M.A., Locat, J., Gélinas, P., Chagon, J.Y., and Lefrancois, P., Heaving of black shale in Québec City. Canadian Journal of Earth Sciences 1986. 23: 1774-1781.

Capitol Region Council of Governments (CRCOG) Meeting on July 2016

Casanova, I; Agulló, L.; Aguado, A. Aggregate Expansivity Due To Sulfide Oxidation - I. Reaction System And Rate Model, Cement And Concrete Research, Vol. 26, No. 7, 1996, P. 993-998.

Casanova, I.; Aguado, A.; Agulló, L. Aggregate Expansivity due to Sulfide Oxidation - II Physico-Chemical Modeling of Sulfate Attack, Cement and Concrete Research, vol. 27, no. 11, 1997, p. 1627-1632

Chinchón-Payá, S.; Aguado, A.; Chinchón, S., A comparative investigation of the degradation of pyrite and pyrrhotite under simulated laboratory conditions. Engineering Geology, v. 127, p. 75-80, 2012

Chinchón, J. S., Ayora, C., Aguado, A. and Guirado, F. (1995). Influence of weathering of iron sulfides contained in aggregates on concrete durability, *Cement and Concrete Research*, Vol. 25, No. 6, pp. 1264–1272.

Connecticut Geological and Natural History Survey, DEP, in cooperation with the U.S. Geological Survey, 2000, Bedrock Geology of Connecticut, data format: shape file, file name: bedrock, downloaded from: http://magic.lib.uconn.edu/cgi-bin/MAGIC_DBsearch2.pl? Geography=37800&Loc=0000 on 9/18/2003, scale 1:50,000.

Côté, F., Bérard, J., Roux, R. Cas de réactivité et de gonflement de remblais granulaires riches en shale pyriteux. Collection Environment et Géologie, APGGQ 1991. 12: 225-246. 93

Côté, F., Expansion de shales pyriteux. M.Sc. thesis, Département de genie mineral, École Polytechnique de Montréal, Montréal,Qué, 1990.

CSA A23.1-14/A23.2-14, Appendix P. "Concrete Materials and Methods of Concrete Construction/Test Methods and Standard Practices for Concrete," Canadian Standards Association, Mississauga, ON, Canada, 2014, pp.668.

Deer, W., Howie, R. and Zussman, J. (1992). An introduction to the rock-forming minerals. 2nd Edition. Pearson education limited, England, 696p.

Duchesne, J. and Fournier, B. (2011). Petrography of concrete deteriorated by weathering of sulphide minerals. *International Cement Microscopy Association Conference*, San Francisco, USA, April 2011. EN-12620 (2003) Aggregates for concrete.

Duchesne, J., Benoît, F., Deterioration of concrete by the oxidation of sulphide minerals in the aggregate. Journal of Civil Engineering and Architecture 2013. 7(8): 922-931.EN-12620 (2003) Aggregates for concrete.

Grattan-Bellew, P.E. and W.J. Eden. (1975). Concrete Deterioration and Floor Heave Due to Biogeochemical Weathering of Underlying Shale, *Canadian Geotechnical Journal*, Vol. 12, pp. 372–378.

Hawkins, A.B., and Pinches, G.M., Cause and significance of heave at Llandough Hospital, Cardiff—a case history of ground floor heave due to gypsum growth, Quarterly Journal of Engineering Geology and Hydrogeology, 20, 41-57, 1, 1987.

Hoover, S.E., and Lehmann, D., The expansive effects of concentrated pyritic zones within the Devonian Marcellus Shale Formation of North America, Quarterly Journal of Engineering Geology and Hydrogeology (2009) 42 (2): 157-164.

Jana, D., "Sample Preparation Techniques in Petrographic Examinations of Construction Materials: A State-of-the-art Review", *Proceedings of the 28th Conference on Cement Microscopy*, International Cement Microcopy Association, Denver, Colorado, pp. 23-70, 2006.

Jana, D., Concrete deterioration from pyrite staining, sewer gases, and chimney flue gases – Case studies showing microstructural similarities, Proc. of the 30th Conference on Cement Microscopy, International Cement Microscopy Association, Reno, Nevada, 2008.

Jana, D., DEF and ASR in Concrete – A Systematic Approach from Petrography, Proc. of the 30th Conference on Cement Microscopy, International Cement Microscopy Association, Reno, Nevada, 2008.

Jana, D., Pyrrhotite Epidemic in Eastern Connecticut – A Case Study (2017), www.cmc-concrete.com Case Studies page.

Jana, D., Pyrrhotite Epidemic in Eastern Connecticut – Diagnosis and Prevention, ACI Materials Journal, American Concrete Institute, accepted for publication, 2019.

Lee, H., Cody, R.D., Cody, A.M., Spry, P.G., The formation and role of ettringite in Iowa highway concrete deterioration. Cement and Concrete Research 2005. 35: 332-343.

Mahoney, J., Aggregates Containing Pyrrhotite, Executive Director, Connecticut Transportation Institute, PowerPoint Presentation.

Marcelino, A.P., Calixto, J.M., Gumieri, A.G., Ferreira, M.C., Caldeira C.L., Silva, M.V., and Costa A.L., Evaluation of pyrite and pyrrhotite in concretes, *Revista ibracon de estruturas e materials* (Ibracon Structures and Materials Journal), Vol. 9, No. 3, 2016.

Moum, J., Rosenqvist, I.Th.. 1959. Sulfate Attack on Concrete in the Oslo Region, *Journal of the American Concrete Institute*, 56-18, pp. 257-264.

Oliveira, I., Cavalaro, S.H.P., Aguado, A. (2014). Evolution of pyrrhotite oxidation in aggregates for concrete, *Materiales De Construccion*, Vo. 64, Issue 316, e038.

Penner, E., Eden, W.J., Grattan-Bellew, Expansion of pyritic shales, NRC Publication archive, Canadian Building Digest, CBD 152, 1972.

Quigley, R.M., Vogan, R.W., Black shale heaving at Ottawa, Canada. Canadian Geotechnical Journal 1970. 7(2): 106-112.

Rodgers, John, compiler, 1985. Bedrock Geological Map of Connecticut: Connecticut Geological and Natural History Survey. Hartford, Connecticut. 2 sheets, scale 125,000.

Rodrigues, A., Duchesne, J., Fournier, B. 2015. A new accelerated mortar bar test to assess the potential deleterious effect of sulfide-bearing aggregate in concrete. *Cement and Concrete Research*, 73: 96-110.

Rodrigues, A., Duchesne, J., Fournier, B. 2016 : Quantitative assessment of the oxidation potential of sulfide-bearing aggregates in concrete using an oxygen consumption test. *Cement and Concrete Composites*, 67: 93-100.

Rodrigues, A., Duchesne, J., Fournier, B. et al. 2012. Mineralogical and chemical assessment of concrete damaged by oxidation of sulphide-bearing aggregates. *Cement and Concrete Research*, 42: 1336-47.

Rodrigues, A., Duchesne, J., Fournier, B., Durand, B., Shehata, M., Rivard, P. 2016. Evaluation protocol for concrete aggregates containing iron sulfide minerals. *ACI Materials Journal*, 113 (3): 349-359.

Shayan, A., Deterioration of a concrete surface due to the oxidation of pyrite contained in pyritic aggregate. Cement and Concrete Research 1988. 18: 723-730.

Tagnit-Hamou, A., M. Saric-Coric and P. Rivard. (2005). Internal deterioration of concrete by oxidation of pyrrhotitic aggregates, Cement and Concrete Research, Vol. 35, p. 99–107.

Uytenbogaardt. W., Burke, E.A.J.. Tables for Microscopic Identification of Ore Minerals. Amsterdam, Netherlands: Elsevier Publishing Company. Pp. 139, 1971.

Wille, K. and Zhong, R. 2016. "Investigating the deterioration of basement walls made of concrete in CT." University of Connecticut, Storrs, CT 06269. 93 p.

✪ ✪ ✪ END OF TEXT ✪ ✪ ✪

# END OF REPORT[2]

[2] The CMC logo is made using a lapped polished section of a 1930's concrete from an underground tunnel in the U.S. Capitol.